“Oil structuring: polymer bridging mechanism for structuring soft materials using natural emulsions as templates”

Dissertation zur Erlangung des Grades

„Doktor der Naturwissenschaften“

im Promotionsfach Chemie

am Fachbereich Chemie, Pharmazie, Geographie und Geowissenschaften

der Johannes Gutenberg-Universität in Mainz

von

Juan Carlos Zambrano Solorzano

geb. in Guayaquil- Ecuador

Mainz, 2023

1. Berichstatter: Prof. Dr. Thomas A. Vilgis

Max Planck Institut für Polymerforschung, Mainz

2. Berichstatter: Prof. Dr. Gerald Gimpl

Johannes Gutenberg-Universität Mainz

Tag der mündlichen Prüfung: 5-04-2023

Preface

This thesis is not only the tangible physical results visible to the reader. This thesis represents an almost four and half year journey, which started with many expectations expressed in a single final goal. When reality clashed with my expectations and disappointments and unhappiness came, I realized that this journey never actually had a final destination but the journey itself. The process. As a result, expectations slowly started to dissolve, and the cup became empty. Many experiences and backgrounds behind this thesis make it challenging to quantify the added value these four years have brought to my life. Nevertheless, all good and bad things have, without a doubt, contributed to my overall personal growth. This is what made this journey a memorable one.

Table of Contents

Preface i

Acknowledgements ..... **Error! Bookmark not defined.**

List of figures viii

Abstract xiii

Zusammenfassung xv

1 Introduction 1

1.1 Introduction 3

2 Theoretical background 7

2.1 Oilseed processing 8

2.2 Oleosomes 8

2.2.1 Oleosome proteins 10

2.2.2 Phospholipids 11

2.2.3 Neutral lipids 12

2.2.4 Soybean oleosome extraction 12

2.2.5 Charge state of oleosomes 13

2.3 Polysaccharides 13

2.3.1 Sodium alginate 14

2.3.2 Xanthan gum 15

2.3.3 Iota-carrageenan 16

2.3.4 Polysaccharides in emulsions 17

2.4 Polymer bridging 18

2.4.1 Polymer- droplet concentration 18

2.4.2 Polymer characteristics 19

2.4.3 Dynamics aspects of bridging flocculation 22

3 Materials and methods 26

3.1 Sample preparation 27

3.2 Oscillatory rheology 28

3.2.1 Theoretical models describing gelation 30

3.3 Microscopy techniques 31

3.3.1 Optical microscopy 32

3.3.2 Confocal scanning laser microscopy 33

3.3.3 Scanning electron microscopy 35

3.4 Particle size measurements 36
3.5 Surface charge measurements 38
4 Influence of polysaccharide type and polysaccharide/oleosome ratio on polymer bridging-based structuring 41
4.1 Summary 43
4.2 Introduction 44
4.3 Materials and methods 45
4.3.1 Materials 45
4.3.2 Sample preparation 45
4.3.3 Demixing experiments 46
4.3.4 Particle size measurements 47
4.3.5 ζ-Potential measurements 47
4.3.6 Microscopic imaging 48
4.3.7 Rheology measurements 48
4.3.8 Characterization of polysaccharides 48
4.4 Results and discussions 49
4.4.1 Influence of pH on polysaccharides adsorption 49
4.4.2 Flocculation characterization of polysaccharide-oleosome mixtures 53
4.4.3 Characterization of compacted gels obtained upon densification of flocculated emulsions 66
4.5 Conclusions 70
5 Effect of polysaccharide architecture on polymer-bridging based structuring 72
5.1 Summary 74
5.2 Introduction 75
5.3 Materials and methods 78
5.3.1 Materials 78
5.3.2 Sample preparation 78
5.3.3 Demixing experiments 79
5.3.4 Particle size measurements 80
5.3.5 ζ-Potential measurements 80
5.3.6 Microscopic imaging 80
5.3.7 Bridging efficacy of polysaccharides 81
5.3.8 Rheological measurements 81
5.3.9 Characterization of polysaccharides 82
5.3.10 Theoretical models describing gelation 82
5.4 Results and discussions 83

5.4.1 Flocculation characterization of polysaccharide-oleosome mixtures 83
5.4.2 Bridging flocculation characterization 91
5.4.3 Effect of pH on polysaccharides adsorption 93
5.4.4 Rheological characterization of bridging-flocculated emulsions at different oleosome contents 95
5.4.5 Microstructural properties of flocculated emulsions 99
5.5 Conclusions 103
6 Compacted polymer bridging gels. Mechanical properties at large deformations 105
This chapter is based on the following manuscript: 106
6.1 Summary 107
6.2 Introduction 108
6.3 Materials and methods 109
6.3.1 Materials 109
6.3.2 Sample preparation 110
6.3.3 Preparation of bridging flocculated gels 110
6.3.4 Rheological measurements 111
6.3.5 Microstructural observation 111
6.4 Results and discussions 111
6.4.1 Visual appearance of polymer bridged gels 111
6.4.2 Microstructure of polymer bridged gels 112
6.4.3 Rheological characterization of polymer-bridged gels 113
6.4.4 Final discussion 120
6.5 Conclusion 122
7 Outlook and recommendations 124
Bibliography 127

List of figures

Fig. 2. 1 Schematic of a single oleosome droplet from soybean indicating the three major components: protein, phospholipids and triacylgyclerides. On the right, it shows a closer look to oleosome monolayer in which oleosin contains a large hydrophobic domain described as a hairpin connected via a proline knob motif (on yellow). The outer amphipathic domains may contain α-helices in which positively charged amino acids (on red) interact with negatively charged head groups of phospholipids via electrostatic interactions. Adapted from [32]. 9
Fig. 2. 2 Molecular structures with their respective schematic model of a) Alginate showing its block structures b) Iota carrageenan, and c) Xanthan gum showing its backbone with its trisaccharide side chain. Adapted from [51]..... 15
Fig. 2. 3 Schematic reflecting bridging flocculation by polymers. The double layer thickness is estimated as reciprocal Debye length, k^{-1}. Small polymers do not link adjacent droplets. Polymer who relax quickly and remain coiled also are not effective for bridging. Polymers that have flattened on the surface before linking to another droplet also lose their bridging ability. According to [67]. 21
Fig. 2. 4 Diagram showing a general schematic of the process of bridging flocculation: mixing, adsorption and flocculation occurring when an adsorbing polysaccharide molecule is added to an oleosome suspension. Adapted from [65]. 23
Fig. 3. 1 General schematic representation of the sample preparation process to induce bridging flocculation between an oleosome dispersion and polysaccharide molecules. 27

Fig. 3. 2 a) A typical graph of amplitude sweep measurement b) A parallel plate geometry where the sample is confined within the gap of height H between the two parallel plates, is sheared by rotation of the plates at angular velocity ω with a torque M_d measured in the inner cylinder (bob), r is the distance from the rotation axis. Adapted from [75]. 29
Fig. 3. 3 Schematic of general set-ups of microscopes a) bright field light microscope, b) confocal scanning laser microscopy. Adapted from [87]. 32
Fig. 3. 4 a) Particle size analyzer based on laser diffraction, b) optical system of the particle size analyzer. Adapter from [99]. 37
Fig. 3. 5 a) Schematic showing the ionic concentration and potential difference as a function of distance from the charged surface of a particle suspended in a dispersion medium b) Typical plot of zeta potential versus pH. Adapted from [100]..... 39

Fig. 4. 1 Influence of pH on the ζ-potential of polysaccharide/oleosome mixtures a) 0.2 wt% Oleosome-Sodium alginate, b) 0.2 wt% Olesome- Xanthan gum. 50
Fig. 4. 2 Flexible alginate chains gain more energy when adsorbing on oppositely charged surfaces as compared to semi-flexible, practically stiff xanthan molecules. Xanthan adsorbs with much lower probability, (free) energy and entropy are off balance due to high internal stiffness of the xanthan molecules. 52
Fig. 4. 3 Demixing experiments of 5 wt% Oleosome with different polysaccharide concentrations after being adjusted to pH 4. a) Visual appearance of alginate-containing mixtures b) Visual appearance of Xanthan-containing mixtures c) Plot of network height, *h(t)*, versus time of alginate-containing mixtures d) Plot of network height, *h(t)*, versus time of xanthan-containing mixtures..... 54
Fig. 4. 4 Optical microscopy images Oleosome 5 wt% - Alginate after being adjusted to pH 4 combined with Particle size distributions of the same sample. a) 5 wt% Oleo- 0 wt% Alg b) 5 wt% Oleo- 0.0025 wt%

Alg c) 5 wt% Oleo- 0.025 wt% Alg d) 5 wt% Oleo- 0.01 wt% Alg e) 5 wt% Oleo- 0.125 wt% Alg f) 5 wt% Oleo- 0.175 wt % Alg. 55
Fig. 4. 5 Plot of network contraction rate, *v*, extracted from demixing experiments plots versus polysaccharide concentration. 56
Fig. 4. 6 CLSM images of a) 5 wt% Oleosome with 0.025 wt% Alginate b) z-scan surface plot of sample 5 wt% Oleosome- 0.025 wt% Alginate. To visualize droplet aggregates for CLSM, samples were stained with Nile Red which dyes the oil core. 58
Fig. 4. 7 The bridging flocculation at 0.025 wt% alginate 5% Oleosome. (a) The oleosomes are coated partly by the negative charged blocks of the polymer. Entanglement formation between oleosomes become more likely, when chains are sufficiently long, i.e., by the high molecular weight fraction. (b) Oleosome aggregated are able to form larger clusters, which are able to join to a soft oleosome particle gel (c). 58
Fig. 4. 8 Optical microscopy images Oleosome 5 wt% - Xanthan gum after being adjusted to pH 4.00 combined with Particle size distributions of the same sample. a) 5 wt% Oleo- 0 wt% Xanthan b) 5 wt% Oleo- 0.0025 wt% Xanthan c) 5 wt% Oleo- 0.025 wt% Xanthan d) 5 wt% Oleo- 0.01 wt% Xanthan e) 5 wt% Oleo- 0.125 wt% Xanthan f) 5 wt% Oleo- 0.175 wt% Xanthan..... 60
Fig. 4. 9 Confocal micrographs of a) 5 wt% Oleosome- 0.05 wt% Xanthan. White arrows indicate presence of oil bodies at the interface of xanthan molecules b) 3D Project of sample 5 wt% Oleosome- 0.05 wt% Xanthan. 61
Fig. 4. 10 a) Mean particle size (d_{43}) as a function of Alginate concentration at three different Oleosome concentrations, b) plot showing alginate concentration (wt %) at maximum aggregation as function of oleosome (wt %) and an insert showing linear fitting and its parameters, c) mean particle size (d_{43}) from a expressed as a function of Polysaccharide/Oleosome mass ratio at three different Oleosome concentrations. 64
Fig. 4. 11 Mean particle size (d_{43}) as a function of Xanthan concentration at three different Oleosome concentrations. 65
Fig. 4. 12 Small droplets in between xanthan form loosely bound aggregates (a). Only a small number of xanthan molecules can adsorb on the oleosome surfaces. The aggregates are not stable at larger size, therefore a depletion flocculation occurs (b). 66
Fig. 4. 13 a) Plots of *G*' at 1% strain as a function of mass ratio for 5 wt% Oleosome b) Before (5 wt % Oleosome) and after Centrifugation (45 wt %) of 0.005 g/g Alginate showing a compact self-supporting gel..... 67
Fig. 4. 14 Polysaccharide- oleosome mixtures at different ratios upon centrifugation which depicts the separation between supernatant and a compacted cream network. 67
Fig. 4. 15 Oscillatory amplitude sweeps of compacted gels Oleosome content 46 wt% at two fixed polysaccharide/oleosome ratios 0.005 g /g (●) and 0.025 g/g (▲) of a) alginate and b) xanthan. *G'*: filled symbols, *G''*: open symbols. 70

Fig. 5. 1 Demixing experiments of 5 wt% Oleosome with different polysaccharide concentrations after being adjusted to pH 4.00. a) Plot of network height, *h(t)*, versus time of alginate-containing mixtures b) Plot of network height, *h(t)*, versus time of carrageenan-containing mixtures c) Visual appearance of alginate-containing mixtures after 150 min d) Visual appearance of carrageenan-containing mixtures after 150 min. 84
Fig. 5. 2 Comparison of network height versus time at two ratios of alginate and carrageenan. a) 0.005 g polysaccharide/ g oleosome b) 0.01 g polysaccharide/g oleosome. c) Network contraction rates (*v*) extracted from Fig. 5.1a, b. 85

Fig. 5. 3 Optical microscopy images Oleosome 5 wt% at different polysaccharide concentrations after being adjusted to pH 4.0 combined with particle size distributions. In a-e, emulsions contained different concentrations of Alginate. I f-j, emulsions contained different concentrations of ι-carrageenan. Scale bar: 100 µm. 87
Fig. 5. 4 Simple models of the physical properties of alginate and carrageenan. In alginate only the guluronic blocks (shown in blue) can be charged, the polar blocks behave as flexible chains in good solvents. Carrageenans are weakly charged polyelectrolytes in good solvents, illustrated in a simple blob-model based on scaling ideas [115]. 88
Fig. 5. 5 Alginate and ι-Carrageenan adsorb differently on the oleosome surface (drawn not to scale). Carrageenan gains most energy, when the chain of blobs bends according to the oleosome surface, without losing much entropy. 89
Fig. 5. 6 Conformation of chains in alginate and □-carrageenan solutions. Alginate chains are assumed to be able to form entanglements (red circles) at the polar, flexible blocks in concentrated (calcium free) solutions. The negative charges (visualised by the electrostatic blob diameter) prevent the formation of entanglements in Carrageenan. The closer the blobs come, the stronger is the Coulomb repulsion between the charges. 90
Fig. 5. 7 Mean particle size (d_{43}) as a function of polysaccharide/oleosome ratios at three oleosome concentrations. a) carrageenan-containing mixture b) alginate-containing mixture c) Plots of polysaccharide concentration (wt%) versus oleosome content (wt%) showing the concentration at which maximum bridging occurred. 92
Fig. 5. 8 Bridging performance of alginate (light gray bars) and carrageenan (dark grey bars) on oleosome droplets expressed as concentration of oleosomes after centrifugation recovery (wt%) at: a) 0.005 g Polysaccharide/g Oleosome b) 0.01 g Polysaccharide/g Oleosome. 93
Fig. 5. 9 a) Zeta potential plots versus pH of 0.2 wt% Oleosome with different alginate and carrageenan concentrations b) the change in ζ between bare oleosome and polysaccharide-adsorbed oleosome at each pH was quantified and expressed as $\Delta\zeta$. 95
Fig. 5. 10 Oscillatory rheology measurements of polysaccharide/oleosome mixtures at different oleosome contents and fixed at two polysaccharide/oleosome ratios. a) 0.005 g carrageenan/g oleosome, b) 0.005 g alginate/g oleosome, c) 0.01 g carrageenan/g oleosome, d) 0.01 g alginate/g oleosome. 96
Fig. 5. 11 Double logarithmic plot of $G'Pa\ vs\ (c - cp\ )t$ 97
Fig. 5. 12 Confocal laser scanning microscopy (CLSM) images from the different bridging flocculated emulsions with alginate and carrageenan at two fixed ratios, 0.005 – 0.01 g/g, at two 5% and 20% Oleosome content. Scale bar: 50 µm. 100
Fig. 5. 13 Schematics of typical oleosome clusters. Alginate binds oleosomes very differently as Carrageenan. 101
Fig. 5. 14 Comparison of the cluster distribution between the samples containing alginate (at 0.005 g/g) and ι-carrageenan (at 0.01 g/g). The different color intensities indicate as guide to the eye the cluster size. The clusters have been extracted from the corresponding CLSM results, Fig. 5.12. Representative weak links are indicated by arrows. 102

Fig. 6. 1 Visual appearance of polymer bridged gels of alginate and carrageenan-oleosome mixtures. Samples from the top correspond to samples before centrifugation, and samples from the bottom correspond to the same samples after centrifugation. a, c, e, g, corresponded to carrageenan, and b, f, d, h corresponded to alginate. 112
Fig. 6. 2 SEM images of polymer-bridged gels upon densification 45 wt% Oleosome fixed at 0.005 g /g. a-c) carrageenan b-d) alginate. Scale bars: 10 µm. 113

Fig. 6. 3 Oscillatory strain sweeps of polymer-bridged gels after centrifugation at different oleosome contents and fixed at two polysaccharide/oleosome ratios. a) 0.005 g carrageenan /g oleosome, b) 0.005 g alginate/g oleosome, c) 0.01 g carrageenan /g oleosome, d) 0.01 g alginate/g oleosome..... 114
Fig. 6. 4 Oscillatory strain sweeps of same samples as Fig.6.3 but expressed as shear stress, σ, as a function of strain (%). Black arrows highlight the first yielding γ_1 and the second yielding point γ_2, which represents the stress overshoot at large strains that is clearly prominent across the different oleosome contents. a) 0.005 g carrageenan/g oleosome, b) 0.005 g alginate/g oleosome, c) 0.01 g carrageenan/g oleosome, d) 0.01 g alginate/g oleosome..... 115
Fig. 6. 5 Plots of γ_1 and γ_2 as a function of oleosome content (wt%) of alginate and carrageenan at two fixed polysaccharide/oleosome rations. γ_1 and γ_2 were extracted from Fig. 6.4 as indicated by black arrows. Lines are guide for the eye..... 117
Fig. 6. 6 Schemes representing the different structures of oleosomes at high densities. The cages (polygons in dashed lines) limits motion, in addition alginate chains form entanglements (shown in black color)..... 120
Fig. 6. 7 Schematic representing oleogels cage under shear. a) ι-Carrageenan-oleosomes b) Alginate-oleosomes..... 121

Abstract

Using a bridging flocculation mechanism in the design of oleogels materials constitutes an alternative framework to achieve desired rheological properties of oil-in-water emulsions. Aggregation by polymer bridging generates a droplet network linked together by firmly bound polymer bridges. In this dissertation, we used negatively charged polysaccharides, sodium alginate, xanthan gum, and ι-carrageenan as the structuring agents and soybean oleosomes as the template. Bridging flocculation between polysaccharides and oleosomes was induced by mixing and adjusting the pH to values where both are oppositely charged, leading to electrostatic-driven interactions. Our results indicate that polysaccharides with flexible polymer chains, such as sodium alginate and ι-carrageenan, are effective bridging flocculants.

In contrast, polysaccharides with a more rigid backbone, such as xanthan gum, resulted in depletion flocculation characterized by phase separation between oleosome droplets and xanthan molecules. Bridging flocculation is more effective at an optimum dosage between polysaccharides and oleosomes, expressed as a mass ratio (g polysaccharide/g oleosome) or as an equivalent per droplet surface area (mg/m2). Sodium alginate presented a higher bridging ability than ι-carrageenan, with its optimum bridging ratio at 0.005 g/g and ι-carrageenan at 0.01 g/g. This was confirmed by quantitative analysis of oleosome content upon centrifugation recovery, where sodium alginate yielded more compact and concentrated gels than ι-carrageenan. Differences in structural conformations between sodium alginate and ι-carrageenan account for the difference in bridging ability. Sodium alginate presents a co-block arrangement of alternating charged and uncharged parts. The negatively charged blocks adsorb strongly onto the oleosome interface at several charged units. At the same time, the uncharged parts impart a high degree of flexibility, allowing the polymer chains to bridge several droplets together.

On the other hand, ι-carrageenan is less flexible than alginate, making the individual carrageenan chains more effective for oleosome surface coating but less effective for bridging neighboring droplets. This difference in bridging ability between sodium alginate and ι-carrageenan will influence the structure of the aggregated network and, as a result, will be responsible for the mechanical behavior in rheological measurements. Sodium alginate produced more heterogeneous and interconnected structures, while ι-

carrageenan produced smaller and less interconnected clusters. This difference in microstructure and the effect of the structural conformations in the polysaccharide chains becomes relevant at medium and large deformations in amplitude sweeps oscillatory rheology. At deformations between 3- 100%, sodium alginate presented steeper slopes in the moduli *G'*, indicating sudden microstructure fracture.

In contrast, ι-carrageenan presented less steep slopes indicating yielding rather than fracture behavior in the decrease of the moduli *G'*. At deformations between 200- 300%, the moduli presented an overshoot indicating a "cage effect" where individual droplets are immobilized due to crowding by surrounding droplets. This effect was more clearly prominent in conditions leading to the densest structures, such as in the compacted gels upon centrifugation performed at the optimum bridging ratios for sodium alginate (0.005 g/g) and ι-carrageenan (0.01 g/g). This study offers many perspectives on how to construct the macroscopic functional properties of oleogels in accordance with their application using the molecular architecture of polysaccharides.

Zusammenfassung

Die Verwendung eines verbrückenden Flockungsmechanismus bei der Entwicklung von Oleogelen stellt eine Alternative dar, um die gewünschten rheologischen Eigenschaften von Öl-in-Wasser-Emulsionen zu erreichen. Die Aggregation durch Polymerverbrückung erzeugt ein Tröpfchennetzwerk, das durch fest gebundene Polymerbrücken miteinander verbunden ist. In dieser Dissertation wurden negativ geladene Polysaccharide, Natriumalginat, Xanthangummi und ι-Carrageenan als Strukturierungsmittel und Sojaoleosomen als Vorlage verwendet. Die Ausflockung zwischen Polysacchariden und Oleosomen wurde durch Mischen und Einstellen des pH-Werts auf Werte induziert, bei denen beide entgegengesetzt geladen sind, was zu elektrostatisch bedingten Wechselwirkungen führt. Unsere Ergebnisse zeigen, dass Polysaccharide mit flexiblen Polymerketten, wie Natriumalginat und ι-Carrageenan, wirksame Brückenflockungsmittel sind.

Im Gegensatz dazu führten Polysaccharide mit einem steiferen Rückgrat, wie Xanthan, zu einer Verarmungsflockung, die durch eine Phasentrennung zwischen Oleosomentröpfchen und Xanthanmolekülen gekennzeichnet war. Die überbrückende Ausflockung ist bei einer optimalen Dosierung zwischen Polysacchariden und Oleosomen, ausgedrückt als Massenverhältnis (g Polysaccharid/g Oleosom) oder als Äquivalent pro Tröpfchenoberfläche (mg/m^2), effektiver. Natriumalginat wies eine höhere Verbrückungsfähigkeit auf als ι-Carrageenan, wobei das optimale Verbrückungsverhältnis bei 0.005 g/g und ι-Carrageenan bei 0.01 g/g lag. Dies wurde durch eine quantitative Analyse des Oleosomengehalts bei der Zentrifugationsrückgewinnung bestätigt, wobei Natriumalginat kompaktere und konzentriertere Gele als ι-Carrageenan ergab. Die Unterschiede in den strukturellen Konformationen von Natriumalginat und ι-Carrageenan sind für die unterschiedliche Überbrückungsfähigkeit verantwortlich. Natriumalginat weist eine Co-Block-Anordnung aus abwechselnd geladenen und ungeladenen Teilen auf. Die negativ geladenen Blöcke adsorbieren stark an der Oleosomen-Grenzfläche an mehreren geladenen Einheiten. Gleichzeitig

verleihen die ungeladenen Teile ein hohes Maß an Flexibilität, so dass die Polymerketten mehrere Tröpfchen miteinander verbinden können.

Andererseits ist ι-Carrageenan weniger flexibel als Alginat, so dass die einzelnen Carrageenan-Ketten zwar die Oleosomen-Oberfläche besser beschichten, aber weniger gut benachbarte Tröpfchen überbrücken können. Dieser Unterschied in der Überbrückungsfähigkeit zwischen Natriumalginat und ι-Carrageenan beeinflusst die Struktur des aggregierten Netzwerks und ist folglich für das mechanische Verhalten bei rheologischen Messungen verantwortlich. Natriumalginat führte zu heterogeneren und vernetzten Strukturen, während ι-Carrageenan kleinere und weniger vernetzte Cluster bildete. Dieser Unterschied in der Mikrostruktur und die Auswirkungen der strukturellen Konformationen in den Polysaccharidketten werden bei mittleren und großen Verformungen in der Amplituden-Sweeps-Oszillationsrheologie relevant. Bei Verformungen zwischen 3 und 100 % wies Natriumalginat steilere Steigungen in den Modulen *G'* auf, was auf einen plötzlichen Bruch der Mikrostruktur hinweist.

Im Gegensatz dazu wies ι-Carrageenan weniger steile Steigungen auf, was auf eine nachgiebige Abnahme der Moduli *G'* hinweist. Bei Verformungen zwischen 200 und 300 % zeigten die Moduli ein Überschwingen, was auf einen "Käfigeffekt" hindeutet, bei dem einzelne Tröpfchen aufgrund der Verdrängung durch umliegende Tröpfchen immobilisiert werden. Dieser Effekt war bei Bedingungen, die zu den dichtesten Strukturen führten, deutlicher ausgeprägt, wie z. B. bei den kompaktierten Gelen nach der Zentrifugation, die bei den optimalen Verbrückungsverhältnissen für Natriumalginat (0.005 g/g) und ι-Carrageenan (0.01 g/g) durchgeführt wurden. Diese Studie bietet viele Perspektiven, wie die makroskopischen funktionellen Eigenschaften von Oleogelen in Übereinstimmung mit ihrer Anwendung unter Verwendung der molekularen Architektur von Polysacchariden konstruiert werden können.

1 Introduction

1.1 Introduction

The use of solid fats in the food industry has brought health concerns to the consumer due to its high content of saturated and *trans* fats, which tend to raise “bad” (LDL) cholesterol levels in the blood, which may increase the risk of developing cardiovascular diseases (CVD) [1]. Therefore, substituting saturated fats with unsaturated fats has been advised to reduce the risk of developing CVD [2]. However, unsaturated fats (liquid oils) lack the functionality that saturated fats (solid fats) provide in food products, such as texture characteristics which, for instance, are responsible for the typical hardness and creaminess in everyday food products, such as sausages, and cream fillings. Nevertheless, there is a way to get around this. Liquid oils can be incorporated into a structured network provided by structurants to offer solid-like characteristics. This alternate method of oil structuring, known as "oleogelation," has received much attention over the past twenty years [3, 4] . Since then, a large and varied range of methodologies has emerged in research, causing this field to flourish exponentially. Examples of the different methodologies are using dispersed phases or oil gelators. These oil gelators have been classified into low molecular weight compounds (LMWOG). Within the category of LMWOG some molecules will form either crystalline networks, such as fatty alcohols [5], monoglycerides [6], wax esters [7], or fibrous network structures, such as phytosterol and oryzanol [8], lecithins [9], or even combination of these systems [10-12]. These oil gelators self-assemble to create a three-dimensional network and scaffold liquid oil. A sponge is a good metaphor for this process. Nevertheless, despite the impressive expansion in this field, most of these oil gelators might fall short of consumers' expectations, who might mistake some of these gelators for "chemicals."

Oil-in-water emulsions can be structured into oleogels in addition to LMWOG-based oleogels because they offer the functionality of oil phases. However, in these oleogels, oil is not immobilized by gelators but rather compartmentalized in stabilized oil droplets, which are then packed closely together and have viscoelastic qualities once the continuous water phase is evaporated. In several studies, this method has been known as the emulsion-templated approach, where several surface-active and non-surface-active food polymers, such as proteins and polysaccharides, have been used either alone or in combination [13-15] as emulsifying agents to stabilize the oil droplets. The emulsion-templated approach, however, requires

multistep procedures in order to be prepared, which essentially includes: 1) preparing the emulsion by mixing the hydrophilic solution with the oil phase via high energy homogenization, in addition to finding the optimal preparation conditions such as the most suitable emulsifier, optimal emulsifier concentrations, or/and finding the optimum pH, and, 2) dehydration which depending on the water content can lead to longer drying times. As a result, the resource-use efficiency of the emulsion-templated approach technique is not very high (time, energy, and raw materials). Additionally, the extraction of liquid oil entails safety and environmental concerns since organic solvents like hexane and benzene are required for yielding oil from oilseeds.

Another alternative is using naturally available oil-in-water emulsions, so-called oleosomes or oil bodies, which may serve as building blocks to create and design oleogels with different mechanical properties. Like many food emulsions, oleosomes exhibit fluid-like behavior when subjected to shear stress, which defines their physicochemical properties such as texture and mouthfeel attributes. However, oleosomes with tuneable rheological characteristics can help to formulate a wide variety of food materials. Many techniques have been explored to make oleosome-based gels with controlled rheological characteristics. High internal phase emulsions (HIPEs) were created by extensively centrifuging a dispersion of sunflower oleosomes [13]. This approach resulted in a highly concentrated emulsion, which exhibited the rheological properties of quasi-solids. Another approach is to combine oleosome dispersions with biopolymer molecules such as polysaccharides or proteins. Different types of gels may result depending on the biopolymer's functionality and the preparation conditions. For instance, composite gels were created by dispersing oleosome droplets within a hydrogel matrix, e.g., gelatin [14] or κ-carrageenan [15]. The rheological properties will then depend on the gel matrix's properties and the interaction between droplets and the gel matrix.

Encapsulating oleosome droplets to yield soft solids can also be prepared by using polysaccharides. This process exploits electrostatic interactions between polysaccharides and oleosome surfaces. It can be followed by either a cross-linking step [16] or a water evaporation step [17] to yield a soft solid structure. One must ensure that the droplet surface is fully covered for this process to be effective and avoid

undesirable effects such as droplet coalescence. For the studies mentioned above, complete surface coverages corresponded to polysaccharide concentrations > 1.5 %.

A more cost-effective approach would be exploiting electrostatic interactions for oleogel structuring by using sufficiently low polysaccharides concentrations. Polysaccharides concentration below the saturation concentration will lead to bridging flocculation, where two or more droplets become linked by a polysaccharide chain leading to the formation of large and interconnected aggregates with solid-like properties. Using bridging flocculation as a structuring mechanism benefits from low polysaccharide concentrations ranging from 0.05 to 0.20 %. Therefore, bridging flocculation remains a less explored but promising approach to providing alternative options for the formulation of fat-based materials.

Besides their functionality as thickening, gelling, and encapsulating agents, polysaccharides can be used to structure gel networks. This thesis is concerned with extending polysaccharides' already remarkable versatile functionality by using them as a direct structuring agent in oleosome emulsions to form edible oleogels. This was explored by using bridging flocculation to modulate the rheological properties of soybean oleosomes. Using different types of food-grade polysaccharides as structuring elements provides flexibility in the formulation because they can provide numerous properties and be positively perceived by consumers. This thesis aimed to design and understand the gelation process by bridging flocculation using soybean oleosomes as templates and polysaccharides as structuring agents and understand the mechanical aspects of the resulting oleogels.

Chapter 2 will provide the theoretical background of the systems used in the thesis, such as soybean oleosomes, sodium alginate, ι-carrageenan, and xanthan gum, which will serve as the basis for the results outlined in the following chapters. It will also describe the process of bridging flocculation. Chapter 3 will provide background knowledge on the methodology and the techniques used in this project. Chapter 4 compares the effect of a flexible polysaccharide, sodium alginate, and a stiff polysaccharide, xanthan gum, on the flocculation behavior of soybean oleosomes. Their effect is compared as a function of different polysaccharide/oleosome ratios in terms of stability against demixing, network microstructure, surface charge, and rheology. Chapter 5 compares the bridging ability of sodium alginate with that of another

flexible polysaccharide, such as ι-carrageenan. Their difference is discussed in terms of microstructure formation using microscopic analysis coupled with rheological measurements to describe the network characteristics and deformation behavior at medium strains. Finally, Chapter 6 describes specific rheological features at large deformations of alginate and carrageenan polymer bridging gels upon centrifugation. These characteristics are described as a function of oleosome content and polysaccharide/oleosome ratio.

2 Theoretical background

2.1 Oilseed processing

Conventional ways in which vegetable oil is obtained deserve some reflection. Vegetable oil is currently extracted from oilseeds by an expeller pressing method followed by solvent extraction [18]. This conventional method has been aimed primarily at obtaining purified and refined oil rather than obtaining quality oil. Byproducts of oilseeds extraction involve oilseeds cakes or meals, which are a rich source of diverse ingredients, e.g., lipids, phenols, proteins, and carbohydrates which, if extracted in their native form, can provide ingredients with high functionality. However, during the solvent extraction process, most of these ingredients are degraded [19]. In addition, solvent extraction uses toxic and environmentally harmful organic solvents, which also provide a negative reputation among consumers [20]. Thus, the application of milder extraction processes appears necessary to obtain ingredients in which their native functionality is preserved. Among the different native components in oilseeds, oil bodies or oleosomes stand out as a remarkable ingredient with tremendous potential in food and cosmetic applications.

2.2 Oleosomes

Oleosomes are subcellular oil droplets present in eukaryotes and prokaryotes present as a way to store lipids in plant cells. Plants use these lipid reservoirs during early seedling development [21]. When oleosomes are extracted in their native form, they are present as a natural oil-in-water emulsion with remarkable physical and chemical stability [22, 23]. Natural emulsions have advantages over "manufactured" emulsions because they can be prepared without emulsifiers or high-pressure homogenization. In general, oleosomes comprise three significant components: neutral lipids, phospholipids, and proteins. Within the core, oleosome contain neutral lipids, mostly triacylglycerols (TAG), surrounded by a sophisticated membrane formed by proteins embedded within a monolayer of phospholipids (Fig. 2.1). The diameter of oleosomes ranges from 0.2-2.5 μm depending on the origin of the species. The size will depend on the availability of the oleosomes for the different functions the plant requires for its internal processes. For instance, diameters less than 0.2 μm would provide greater surface area for rapid oil mobilization during seedling growth.

On the other hand, larger oleosome diameters are found in species [24, 25], where oil is not to be mobilized for internal functions. These sizes have been positively related to the ratio between TAG and protein [26]. Table 2.1 shows theoretical values of oleosome diameters with the relative amount of their major components based on a model developed by Huang [27], which used a spherical TAG of a specific diameter particle surrounded by a shell of one layer of phospholipid embedded with proteins. Soybean oleosomes it has been reported in the literature [28] as containing 91.89 wt% neutral lipids, 5.42 wt% proteins, and 2.70 wt% phospholipids for a diameter size of around 0.350 µm. These values are consistent with the model from Huang. Soybean oleosomes have been reported to have the smallest diameter among the different species, which has also been positively correlated with excellent stability at different physical stresses [29]. Small angle neutron scattering (SANS) studies [30] revealed a shell thickness of 9 nm for soybean oleosomes, which corresponds to the layer of phospholipids and proteins (Fig. 2.1). The hydrophobic domain of the proteins is about 5 nm, indicating that the outer hydrophilic domain of the oleosome protein is about 3 nm (Fig. 2.1) [31].

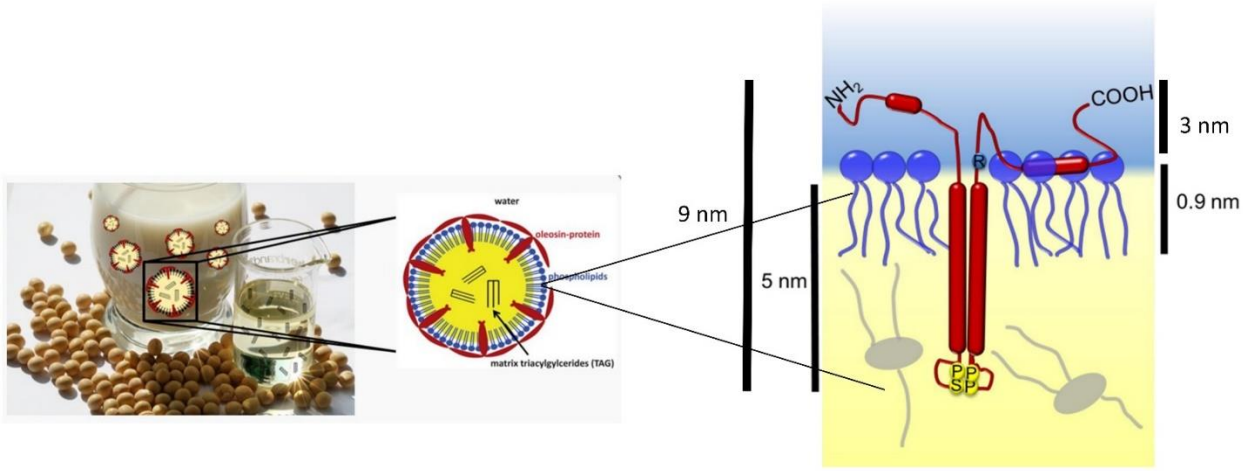

Fig. 2. 1 Schematic of a single oleosome droplet from soybean indicating the three major components: protein, phospholipids and triacylgyclerides. On the right, it shows a closer look to oleosome monolayer in which oleosin contains a large hydrophobic domain described as a hairpin connected via a proline knob motif (on yellow). The outer amphipathic domains may contain α-helices in which positively charged amino acids (on red) interact with negatively charged head groups of phospholipids via electrostatic interactions. Adapted from [32].

Table 2.1 Theoretical values of the concentration of the three main components of oleosomes in relation to the droplet size. Adapted from [27]

Diameter (μm)	TAG (%, w/w)	Phospholipids (%)	Proteins (%)	TAG/oleosin
0.1	74.1	10.0	15.9	85
0.2	85.1	5.8	9.1	170
0.5	93.5	2.5	4.0	425
1.0	96.6	1.3	2.1	836
1.5	97.7	0.9	1.4	1269
2.0	98.3	0.7	1.0	1787
2.5	98.6	0.5	0.8	2241
5.0	99.3	0.26	0.4	4514
10.0	99.7	0.13	0.2	9064

2.2.1 Oleosome proteins

Oleosins, caleosins, and steroleosins are the proteins found on the oleosome membrane. The most prevalent are oleosins, alkaline proteins with molecular weights of 15 to 20 kDa, depending on the plant species. Oleosin consists of three structural domains: a central hydrophobic domain, an amphipathic N-terminal domain, and a C-terminal amphipathic domain. The hydrophobic domain, consisting of 68-74 amino acids, is considered the most extended sequence found in any organism and is about 5 nm [33]. This hydrophobic domain is deeply anchored in the TAG core and forms a loop, the so-called ‘proline knot’ consisting of three proline and one serine residue. The secondary structure of the hydrophobic domain remains under

doubt because contradicting results have been reported where the domain could be formed by either two α-helices [34] or two β-sheets structures [35]. The hydrophilic N-terminal and C-terminal domains interact with the phospholipids head at the oleosome membrane via their charged amino acids, and their length can vary from 9 to 403 amino acids [36]. The secondary structure of the N- and C- terminal tend to be dominated by 'random coils' and β-sheets, but smaller α-helical portions are also possible [33] .

Caleosins have a similar three-domain structure to oleosin; however, it has been reported that it is smaller [37]. The proteins are between 25 and 35 kDa in size and have a half-calcium binding site that is likely accessible to the aqueous phase [38]. As a result, Ca^{2+} can alter the interfacial characteristics of caleosin and mediate the aggregation of oleosomes. Caleosin has a role in stabilizing oleosomes, as Chen et al. [39] demonstrated. The secondary structure contains amphipathic α-helices in its central hydrophobic domain, but the number of α-helices will depend on the polarity of the media [33].

Stereolosins are bigger proteins with molecular sizes of more than 35 kDa. Stereolosin also possesses a hydrophobic anchoring and hydrophilic domain that is equivalent to enzymes of the dehydrogenases/reductases type, which bind sterol. Stereoleosin may be involved in plant signal transduction processes regulated by various sterols [40]. Fig. 2.1 shows the oleosome monolayer showing the primary and secondary structure of oleosin embedded within the layer of phospholipids.

2.2.2 Phospholipids

The phospholipid layer has approximately 0.9 nm thickness (Fig. 2.1) and has their hydrophilic head groups exposed to the aqueous phase and the acyl moieties facing inwards to interact with TAGs. The most abundant phospholipids among different species are phosphatidylcholine, phosphatidylserine, phosphatidylethanolamine, phosphatidylinositol, and phosphatidic acid [33]. In soybean oleosomes, the major phospholipids found were phosphatidylcholine and phosphatidylethanolamine, followed by different contents of lysophosphatidylcholine [41]. Phospholipids interact with oleosins due to the charge and polarity distribution within the molecules. This interaction provides oleosome surface stability against

coalescence in part due to the oleosins, which provide not only charged-driven repulsion but also a steric hindrance.

2.2.3 Neutral lipids

TAG makes up most of the neutral lipids; diacylglycerols, sterol esters, and tocopherols are other minor neutral lipids constituents. The TAG compositions are highly species-specific, including their acyl components and acyl positional specificity. Even the extraction method and conditions of extraction will influence the composition of TAG. For soybean oleosomes, the primary fatty acids present were linoleic acid, oleic acid, palmitic acid, and α-linolenic at different recovery pHs [39]. TAGs are more or less randomly packed in the center of the oleosome, while sterol esters form several ordered shells below the surface of the phospholipid monolayer [33].

2.2.4 Soybean oleosome extraction

It is crucial to provide a simple extraction procedure that does not compromise the stability and membrane of the oleosome in order to boost their widespread use in several applications. The most appropriate methods reported for soybean oleosomes are aqueous extraction [23, 42] and enzymatic extraction [43, 44]. The aqueous extraction is a popular and effective technique. In general, soybeans are soaked, then ground and homogenized with deionized water, followed by washing steps, which include pH adjustment and centrifugation. Most aqueous extraction methods in literature have the same general steps with few modifications depending on the application [45]. For instance, oleosomes can be extracted as pure oleosomes or as mixtures of oleosomes and storage proteins. For the PhD project, pure soybean oleosomes were needed as they were intended for structuring building blocks. The method proposed by Waschatko [46] removes storage proteins, such as glycinin, β-conglycinin, lipoxygenase, and Gly m Bd 30 k, in which soybean oleosomes were extracted by incorporating washing steps with 20% sucrose and adjustment to pH 11. High alkaline conditions can remove enzymes responsible for lipid oxidation and oleosin proteases responsible for membrane deterioration [42]. Sucrose facilitates cream separation because by increasing water density, resulting in maximum oleosomes cream floating at the interface [45].

2.2.5 Charge state of oleosomes

The three types of charged molecules on the surface of oleosomes at neutral pH are oleosins, phospholipids, and free fatty acids. At neutral pH, oleosin carries positive charges, while phospholipids and free fatty acids carry negative charges. The oleosin protein's N- and C- terminal domains present positively charged residues, which are likely to interact with the anionic lipids of the monolayer. The charge interactions between the lipids and the oleosins result in a negatively charged oleosome surface at neutral pH. The oleosome is highly stable due to this negatively charged surface and the steric barrier offered by the numerous and firmly embedded oleosins. The isoelectric point (pI) of soybean oleosomes will depend primarily on the extraction method, but the values found in the literature range from pH 4.0 – 5.7 [23, 47, 48]. The electrostatically charged interfacial oleosome membrane can deposit oppositely charged polymers, such as polysaccharides, to form different structures.

2.3 Polysaccharides

Polysaccharides are the most prevalent complex polymers in nature. Polysaccharides are present in plants, bacteria, and fungi giving structural functions as they are part of their cell walls and serve as sources of energy for metabolism purposes. The basic structure of polysaccharides consists of several monosaccharides, D-glucose predominantly, linked together by inter-sugar glycosidic bonds[49]. Some polysaccharides have a linear structure, while others are branched. Most linear polysaccharides tend to form helical structures. Linear polysaccharides are the most abundant in the world because cellulose is ubiquitous in all plant cell walls as a structuring element. However, branched polysaccharides are the most numerous, occurring in numerous branched forms. The degree of ramification will influence physical properties such as water solubility, viscosity, and gelling behavior. Hydroxyl groups predominate in all polysaccharides and are often partially derivatized by esterification and present as acetate, sulfate, or phosphate or are etherified. A linear polysaccharide will produce much more viscous solutions than a branched polysaccharide of the same molecular weight. This is because of the stretched conformation in the solution of the linear polysaccharide, which gyrates on a much larger sphere [50]. As a result of the

much larger volume occupied by these linear polysaccharides, collisions between molecules frequently take up energy. Thus, the solution viscosity increases. Gyrating highly branched molecules of equivalent molecular weight will sweep out a much smaller volume and collide less frequently, thus contributing less viscosity to the solution.

Food polysaccharides are often used in the food industry as stabilizers, thickeners, and gelling agents [51]. As a stabilizer, polysaccharides help to control ice crystal formation in the case of frozen foods. Polysaccharides also often stabilize emulsions by preventing oil separation, as in the case of low-fat salad dressings. Polysaccharides also help to immobilize insoluble particles, which in the case of milk drinks, cause sedimentation. As thickeners, polysaccharides can thicken water, which in most cases improves the texture and mouthfeel of a wide range of food products. One of the critical features of polysaccharides is the ability to gel and solidify liquid products, for instance, to develop milk-gelled desserts. In this respect, gelling properties range from soft, elastic gels to hard and brittle gels, which have diverse application potential in the food industry.

2.3.1 Sodium alginate

Alginate is a high-molecular-weight polymer that occurs in brown algae's cell walls and intercellular spaces. The alginate molecules provide both flexibility and strength to the plants, and these properties are adapted as necessary for growing conditions in the sea. Alginates are salts of alginic acid with a degree of polymerization, usually in the range of 50-3000, corresponding to molecular weights of approximately 10 000-600 000 Da. Sodium alginate is predominantly used in foods because it dissolves well in cold or hot water to yield viscous solutions.

The alginate polymer is composed of two building blocks of monomeric units, namely β- D-mannuronopyranosyl and α-L-gulurunopyranosyl units. The ratio of D-mannuronic and L-guluronic acid components and their sequence predetermine alginate properties. Alginate is considered a true block copolymer in which the monomers are composed exclusively of one unit or another and referred to as *M*-blocks (polymannuronic acid) or *G*-blocks (polyguluronic acid) (Fig. 2.2a) [49]. They also occur in

alternating regions (*MG*-blocks) where the monomers are present in an approximately alternating sequence. The charge and bulk of the carboxylic acid groups give these different conformations differing degrees of extension and flexibility. It has been found that *M-G* is the most flexible conformation and *G-G* the most rigid arrangement (flexibility *MG* > *MM* >*GG*) [52].

In solution, alginate exhibits properties of a shear-thinning fluid. This is because of the long and highly charged polymer chains that provide rigidity to the molecule [51].

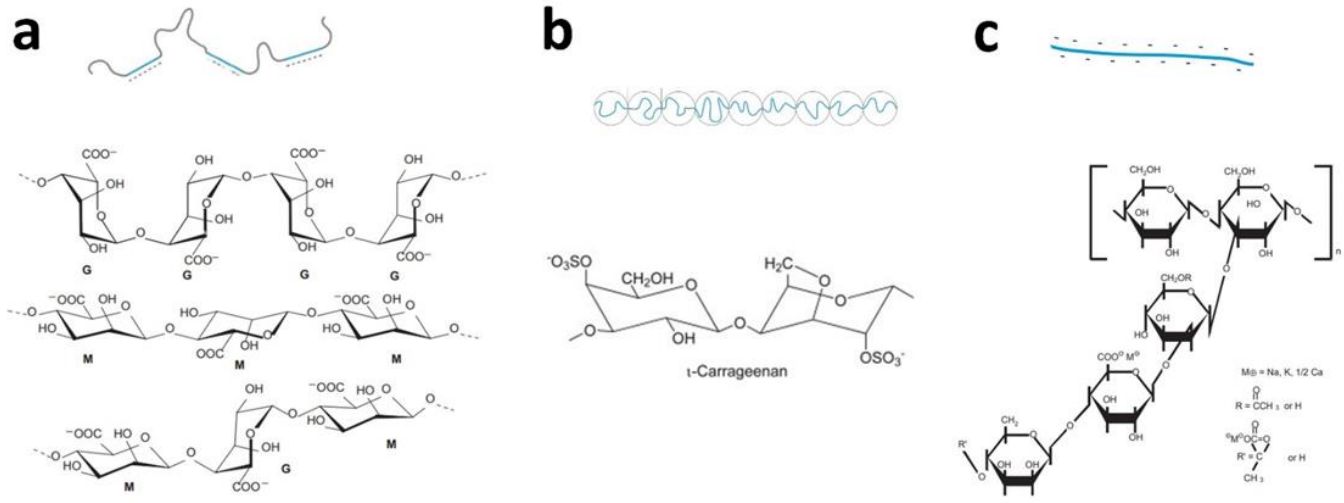

Fig. 2. 2 Molecular structures with their respective schematic model of a) Alginate showing its block structures b) Iota carrageenan, and c) Xanthan gum showing its backbone with its trisaccharide side chain. Adapted from [51]

2.3.2 Xanthan gum

Xanthan gum is a microbial-origin polysaccharide produced by *Xanthomonas campestris.* The polymer backbone consists of *β*-(1,4) linked D-glucopyranosyl units substituted on alternate D-glucoysl residues with a trisaccharide chain (Fig. 2.2c). The trisaccharide side chain comprises two mannose units separated by glucuronic acid. Approximately half the terminal mannose units are linked to a pyruvate group, and the non-terminal residue usually carries an acetyl group (Fig. 2.2c). The carboxyl groups on the side chains provide the negative charge on the polymer chain. The report estimates molecular weight ranges from 15

000 000 – 50 000 000 Da [50]. Some studies even report 300 000 Da in a strong dissociative environment [49].

This variance in reported molecular weight could be because xanthan is typically in an aggregate state consisting of several individual chains, which could be either single or dimeric helices. The solution conformation of xanthan has been suggested to be either rod-like, ordered conformation, or a worm-like chain with a low degree of flexibility [50]. One of the main properties of xanthan in solution is its viscosity, even at low concentrations. At very low shear rates, xanthan solutions exhibit Newtonian viscosity. Upon larger shear rates shear, xanthan presents a high degree of pseudo-plasticity, where the viscosity increases rapidly as the shear rate increases. In addition, xanthan presents a well-defined yield stress value, which is the shear stress required to start flow. At rest, xanthan solutions appear gel-like, yet they present low resistance to mixing or pumping. This feature results from an intermolecular association between polymer chains, forming a complex network of entangled rod-like molecules. These weekly bound xanthan aggregates are slowly disrupted under applied shear, thus the distinct pseudo-plasticity in the xanthan solutions [53]. This network of highly ordered entangled rigid molecules also explains the high yield stress value of xanthan.

2.3.3 Iota-carrageenan

Carrageenan is a naturally occurring polysaccharide in red seaweeds that fills the voids within the cellulose structure of the plant. Red seaweed from different species provides a sub-family of carrageenan extracts with different compositions and molecular conformations, which leads to different functionality. Carrageenan is a high-molecular-weight linear hydrophilic polysaccharide with molecular weights ranging between 200 000 and 800 000 Da. Carrageenan families have galactose backbone but differ in the proportion and location of ester sulfate groups and the proportion of 3, 6-anhydrogalactose. There are three primary types. Kappa carrageenan comprises approximately 22% ester sulfate and 33% 3,6-anhyfrogalactose, and iota carrageenan comprises 32% and 26%, respectively (Fig. 2.2b). Lambda carrageenan contains 37% ester sulphate with little or no 3,6-anhydrogalactose [51]. In its disordered form,

carrageenan is a random coil with an intrinsic chain flexibility similar to that of related polysaccharides. However, it is stretched due to polyelectrolyte effects, according to studies [54]. In its ordered conformation, iota carrageenan structure contains only a 3,6-anhydrous-D-galactopyranosyl unit, giving the molecule regularity and allowing for a helical tertiary structure. However, disaccharide units without the 3,6-anhydrous ring result in $^{1}C_{4}$ conformation, which provides 'kinks' to an otherwise regular helical strand [50]. At high temperatures, carrageenan chains exist as random coils, and the coil-to-helix transition temperature increases with increasing cations concentration. On the other hand, in the absence of added salt, the coil-to-helix transition is absent at low polymer concentrations.

2.3.4 Polysaccharides in emulsions

Polysaccharides can interact, via electrostatic interactions, at interfaces such as protein-stabilized oil-in-water emulsions forming a firm and stabilizing layer at the interface. This characteristic can be exploited to encapsulate emulsion droplets by forming multilayers, which improves the emulsion's stability to variations in external conditions such as low pH, thermal cycling, and freeze-thaw cycling [55]. This condition can only occur when the polysaccharide concentration has reached the amount to saturate and coat the emulsion interface thoroughly. Electrostatic interfacial complexation can also lead to the flocculation of the protein-stabilized emulsion droplets. Flocculation can occur in two ways: depletion flocculation and bridging flocculation. In depletion flocculation, the center of mass of the polysaccharide cannot reach the droplet surface closer than its radius of gyration (R_g) when the polysaccharide does not adsorb at the protein-stabilized interface. Therefore, a region near the droplet has a lower concentration of polysaccharide segments than the bulk fluid. The depleted zones and the bulk solution experience a different osmotic pressure due to the depletion effect. When two depletion zones overlap, this pressure difference causes an attracting force between the oil droplets[56]. The sum of the osmotic pressure (P_{OSM}) and the overlap volume ($V_{overlap}$) yields the interaction energy. These elements are related to the concentration of polysaccharides and the diameters of the droplets and the polysaccharide [57]. Above a minimal

polysaccharide concentration, when the attraction is strong enough to overcome the entropy of the emulsion droplets, the droplets flocculate.

Bridging flocculation occurs at low polysaccharide concentrations when flocs are produced by the adsorbed polymer chain, which bridges together adjacent emulsion droplets. Due to the visible cream separation in emulsion droplets, bridging flocculation has mostly been depicted as an instability affecting the emulsions' shelf-life [58]. However, it can also be exploited to create gel-like materials from emulsion dispersions.

2.4 Polymer bridging

Food colloids' structural, rheological, and textural characteristics are governed mainly by the state of aggregation of their component particles. Macromolecular bridging is one process that can lead to the aggregation of colloidal particles. Bridging flocculation occurs when the amount of adsorbing polymers is too low to cover the droplet interface and when oppositely charged molecules strongly interact. Single polysaccharide chains adsorb to the oil droplet interface and interconnect two or more emulsion droplets. The interaction between the polysaccharide and the droplet surface, frequently of electrostatic origin and about hundreds of k_BT, determines the attraction. As a result, the bonds created by bridging are strong and permanent. A micromechanics approach has studied the strength of bridging bonds [59], which showed that pulling apart bridging flocs requires forces of several hundred nN. The flexibility of bridging polymers may contribute to the strength of the flocs since some stretching could occur before actual rupture. As a result, depending on the degree of flocculation, the resulting structure consists of a highly cross-linked droplet network with gel-like characteristics. The extent and effectiveness of bridging flocculation will depend on the polymer and particle concentrations, the polymer's characteristics, and the influence of dynamics in bridging.

2.4.1 Polymer- droplet concentration

For bridging flocculation to occur, an optimum polysaccharide dosage should exist, which gives maximum flocculation effectiveness. La Mer [60] suggested that the optimum polymer dosage should coincide with the maximum rate of successful bridging encounters between particles. If the fractional surface coverage is

$\theta(1-\theta)$, then optimum bridging should occur when $\theta = 0.5$. This corresponds to the concentration at which half of the droplet interface is coated by polysaccharides. However, this theoretical value will depend significantly on the configuration of the adsorbed chains. For instance, high-adsorbed amount polymer chains are more crowded and occupy less surface area per chain [61]. This explains why certain studies have found that optimum bridging flocculation occurs at coverage significantly less than half surface coverage [62]. However, the concept of an ideal dosage for bridging flocculation prevails since higher amounts of polymer lead to re-stabilization or complete surface coverage of droplets [58]. Computer simulations revealed [63] that bridging flocculation strongly depends on the polymer/droplet ratio. At high polymer/droplet ratios, polysaccharide chains do not link clusters due to the lack of droplets and are the concentration regime where saturation of droplet surface occurs. On the other hand, low polymer/particle ratios will lead to a system composed of free droplets and small and separate clusters.

2.4.2 Polymer characteristics

From the standpoint of bridging flocculation, the essential characteristics of polysaccharides are their molecular weight (MW) and charge density. Bridging flocculation is more efficient with higher molecular weight polymers (Fig. 2.3). Polysaccharides with chains of large molecular weight occupy a larger volume in solution, increasing the probability of available dangling polymer segments allowing their chains to extend and interconnect several droplets. Lapoint and Barbeu (2020) [64] generated a summary among a wide variety of synthetic and natural polymers and reported that the adequate molecular weight for effective polymer bridging for anionic polymers was $> 10^5$ g/mol.

The charge density of a polysaccharide is a crucial factor in its bridging effectiveness. Charge density is responsible for the electrostatic interactions with the droplets and influences the extension of the polymer chains. Intermolecular charged segments along the polymer chain will generate charge repulsion between charged segments causing the chain to extend more or less depending on the charge density. Charge density depends on the proportion of ionized segments along the polymer chain. The degree of ionization depends on the solution pH for weekly ionizing groups, such as carboxylic and sulfuric acids. Charge density will

also be strongly influenced by ionic strength. At high ionic strengths, the presence of ions weakens the electrostatic repulsion between charged segments of the chain leading to a more coiled polysaccharide chain (Fig. 2.3) rather than a stretched polymer chain. At low ionic strengths, on the other hand, charged polysaccharides will tend to adsorb to oppositely charged surfaces in a flat conformation (Fig. 2.3). The ideal polymer conformation for bridging flocculation would be something in the middle between flat and coiled where sections of the polymer chains could stretch enough beyond droplet surface in order to adsorb on several other droplets[65, 66]. This is the concept of available chain segments for bridging (loops and tails) vs. unavailable chain portions already attached (train) onto droplets[67]. Adachi (1995) [68] described this concept in terms of nonequilibrium flocculation (tails and loops are still active for bridging) vs. equilibrium flocculation (flat configuration). The polysaccharide's charge density will determine the binding strength onto the droplet interface. This binding strength will have further consequences in the microstructure of the resulting floc. For instance, Dickinson (1991) [69] showed that compact and dense flocs with closer droplet-droplet separation are formed due to increasing adsorption strength. In this case, the bridges resemble a polymeric ‘glue’ between particle surfaces separated by no more than a few segment diameters.

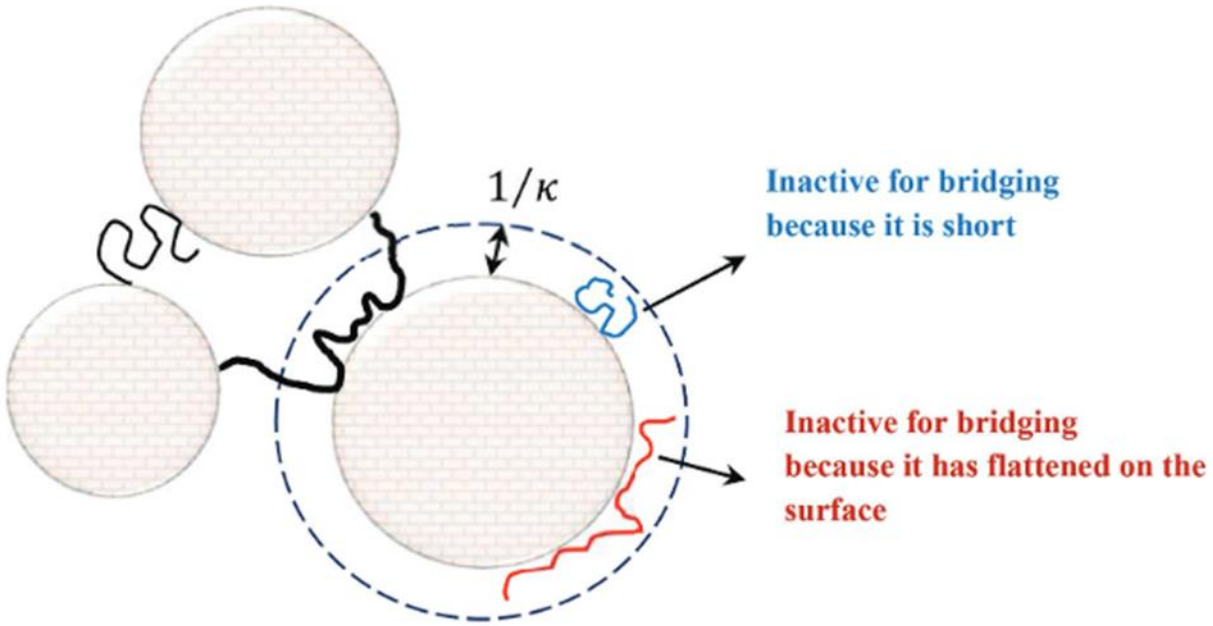

Fig. 2. 3 Schematic reflecting bridging flocculation by polymers. The double layer thickness is estimated as reciprocal Debye length, k^{-1}. Small polymers do not link adjacent droplets. Polymer who relax quickly and remain coiled also are not effective for bridging. Polymers that have flattened on the surface before linking to another droplet also lose their bridging ability. According to [70].

How the charges are distributed along the polymer chain also influences the bridging effectiveness. For instance, researchers found [71] that block cationic polymers, where charge moieties are concentrated in blocks, promote stronger adsorption onto the surfaces of colloidal particles. On the other hand, polymers with randomly distributed charges along the backbone may lead to the less efficient use of some charges on the backbone. Polysaccharides structural conformation will also influence the effective length of the polymer chain and as a result, the effectiveness of flocculation via interparticle bridging. For instance, polysaccharides with highly branched backbones and heteropolymolecular such as gum Arabic presented relatively weak bridging power compared to linear homopolymolecular polysaccharides, such as dextran, which presented stronger bridging power [72].

In bridging flocculation, the dynamics of chain relaxation are essential. For a polymer to act as an effective bridge between particles, it must remain extended beyond the double-layer thickness for a time greater than the average time between interparticle collisions (Fig. 2.3) [73]. Therefore, chains with greater molecular

weights, chains that occupy a larger volume in solution at a given molecular weight, and chains that relax relatively slowly will exhibit effective bridging flocculation (e.g., have monomers that show a relatively high degree of intrachain repulsion) [74]. Bridging flocculation is likely inefficient when the chain is relaxing quickly, while more efficient bridging flocculation occurs when relaxation is slow.

2.4.3 Dynamics aspects of bridging flocculation

Generally, a polymer is added to an emulsion dispersion under mixing conditions of shear flow to induce bridging flocculation. Mixing is critical to bridging flocculation because shear flow increases the rate of collisions between polymers and droplets and in-between droplets. The applied shear flow may also influence the adsorption of the polysaccharide chain on the oil droplets, which is an essential step for bridging flocculation to occur. The processes occurring during bridging flocculation must first be described to consider the dynamic aspects of bridging flocculation. Fig. 2.4 shows a very general schematic of the steps occurring during bridging flocculation and is based on Gregory (1988) [66]:

1. Mixing of the polysaccharide molecules with the droplets
2. Adsorption of polysaccharide chain on the droplets
3. Re-arrangement (re-conformation) of the adsorbed chains from their initial state to an eventual equilibrium configuration
4. Collisions between droplets having adsorbed polysaccharide form aggregates by bridging
5. Break-up of aggregates

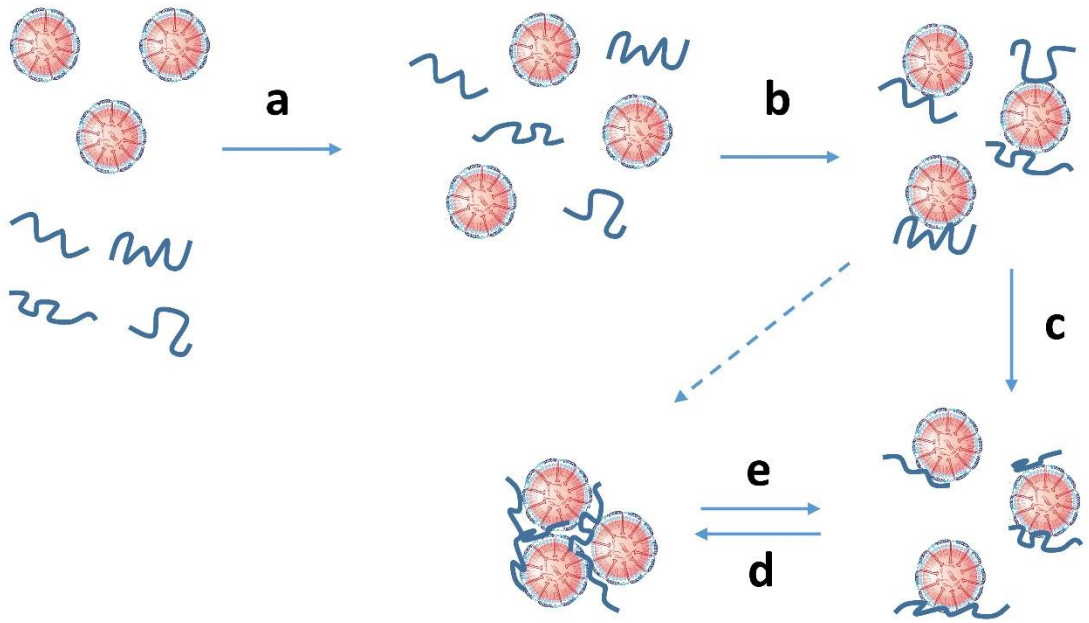

Fig. 2. 4 Diagram showing a general schematic of the process of bridging flocculation: mixing, adsorption and flocculation occurring when an adsorbing polysaccharide molecule is added to an oleosome suspension. Adapted from [66].

However, in practice, these processes do not occur in sequence but occur all at once, making the process very complicated. The rate at which these processes will depend on many factors, including those already described above.

Processes a to b (Fig. 2.4) describe the mixing between the oleosome dispersion and the polysaccharide molecules and the polysaccharide adsorption onto the oleosome surface due to electrostatic binding. The rate of polysaccharide adsorption as a result of stirring (shear-induced adsorption) should increase as the size of the polymer molecule increases. In contrast, at non-stirring conditions, the adsorption rate will decrease in polymers with higher molecular weights. Only in cases where polymer molecules are very small the polymer adsorption rate is higher in unstirred conditions than in stirring conditions. This is because diffusion processes (diffusion-controlled adsorption) take more relevance when polymer molecules are very small, as was shown by Gregory (1988) [66]. In this study, polymer molecules of (< 50 nm), presenting

high diffusion coefficients, lead to increased adsorption rates as determined by kinetic equations based on Smoluchowski expressions. In the above study, Smoluchowski expressions represented the adsorption rate or collision frequencies between polymer and particle, where perkinetic collisions define the adsorption rate at static conditions (diffusion-controlled), and orthokinetic collisions define the adsorption rate at shear conditions.

These expressions determined that polymer adsorption should take more than twice as compared as stirring conditions in unstirred conditions. In another study [75], shear flow increased the collision frequency between particles by 30 times higher than without mixing. In contrast, the collision frequency between polymer chains and particles is three times higher than without mixing. However, the approximations from these studies were rough and were based on simplistic models, but the main idea was to show rather qualitatively that polysaccharide adsorption rates could be significantly increased in sheared dispersions.

Processes c and d (Fig. 2.4) indicate the rate at which adsorbed polymer chains reach their equilibrium conformation and the subsequent floc formation. In bridging flocculation processes, the adsorbed polymer has relatively low surface coverage, indicating that re-conformation should take very fast compared to conditions where the polymer reaches complete surface coverage. At the latter, the re-conformation rate is prolonged (several hours) because the polymer chains hinder the re-conformation of neighboring polymer chains. The stirring speed may also influence the rapid dynamics of re-conformation occurring during bridging flocculation. Higher stirring speeds may accelerate droplet collisions, causing droplets to collide with each other before polymer chains can re-conform. This will cause the adsorbed polymer chains to extend further from the droplet surface (as indicated by the dashed line in Fig. 2.4), enhancing the opportunity for polymer bridging and the degree of flocculation, which will influence, for instance, the size of the resulting aggregates. Of course, the conformation of the polysaccharides will also influence the rate of re-conformation. For instance, polysaccharides with a rigid conformation will tend to adsorb with a relatively flat configuration on the droplet surface, decreasing the probability of extending further the polymer chains and bridging neighboring droplets.

Process e (Fig. 2.4) indicates the break-up of aggregates under the influence of a constant shear rate. The break-up of aggregates may occur due to subsequent stirring after the aggregates have reached a limiting size and no further flocculation occurs. The resulting size, therefore, may depend on the applied stirring speed and the strength of the aggregates. This could mean that the size of the aggregates is determined by the balance between the force of disruption of aggregates due to fluid motion and the strength of the bridging bonds between particles in the aggregates. Polymer bridging produces strong aggregates, which, if broken at high shear rates, may not easily re-form. This irreversibility may result from the re-conformation of chains during high shear and the strength of adsorption on the droplet surface, which is of electrostatic origin and on the order of hundreds of $k_B T$ [76].

Furthermore, polysaccharides are added to dispersions under shear conditions which are far from uniform, and the effects of turbulence need to be considered. Polymer molecules can be transported to a particle surface by turbulent eddies, depending on the sizes of particles and polymer in relation to the turbulence microscale, which depends, in turn, on the energy dissipation rate.

In summary, the stirring conditions (e.g., stirring speed, stirring type) will influence the extent of flocculation and the resulting characteristics of the aggregates, such as aggregate size and structure. Consequently, stirring conditions have been chosen carefully to provide reproducibility and clarity of data interpretation.

3 Materials and methods

3.1 Sample preparation

The oleosomes dispersions, extracted according to Waschatko et al. (2012) [77], were diluted with distilled water to different concentrations depending on the nature of the experiments. Subsequently, the initial pH of the oleosomes was adjusted to a value of 7.0 via dropwise addition of 1 N HCl. At this pH, the oleosome dispersion will be negatively charged. Polysaccharides (sodium alginate, ι-carrageenan, and xanthan gum) are added at pH 7.0, where both polysaccharides and oleosomes present a negative charge at different concentrations while keeping the same Polysaccharide/Oleosome ratio at the different oleosome concentrations. Fig. 3.1 shows a general schematic representation of the bridging flocculation process.

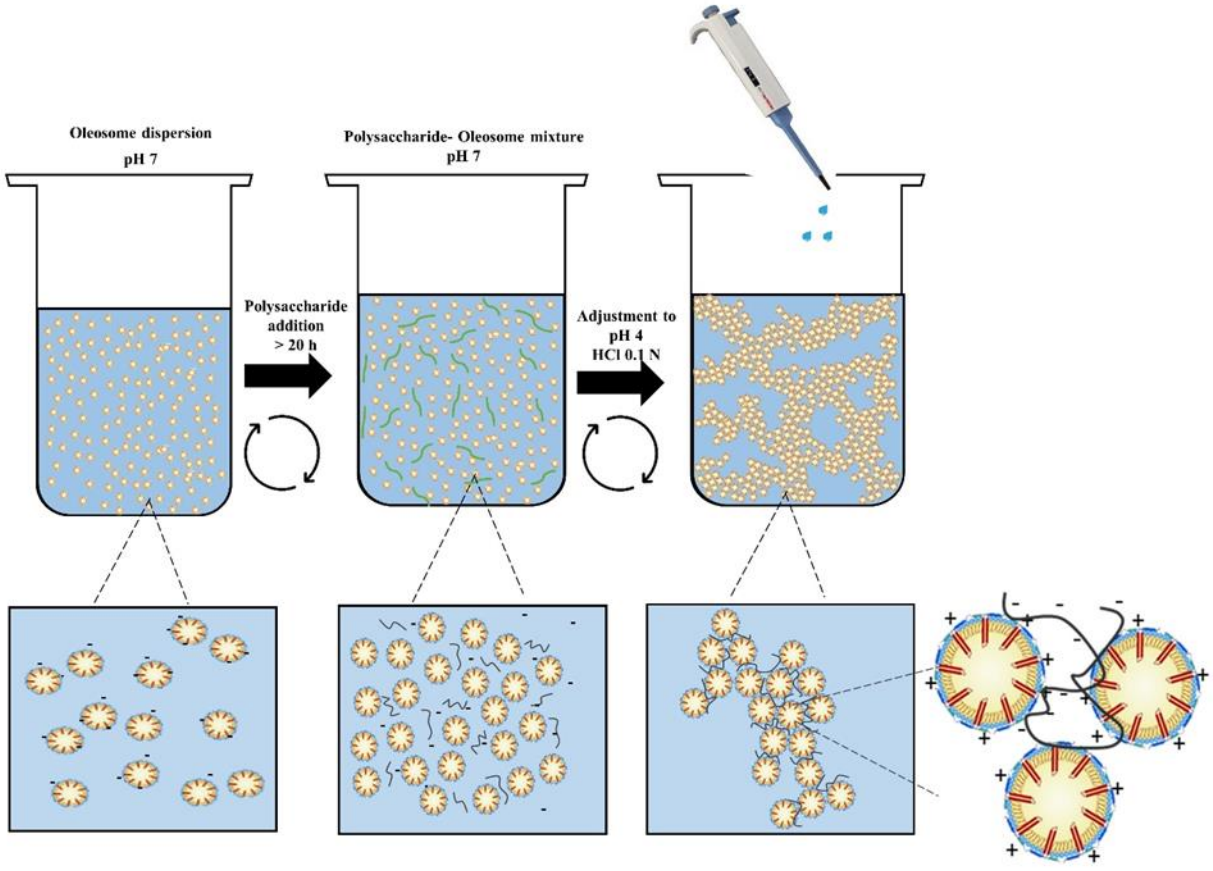

Fig. 3. 1 General schematic representation of the sample preparation process to induce bridging flocculation between an oleosome dispersion and polysaccharide molecules.

In order to induce bridging flocculation via electrostatic interactions, the pH of the polysaccharide-oleosome mixture was slowly adjusted to 4.0 (0.1 N HCl). Both polysaccharide (negative) and oleosome (positive) are oppositely charged at this pH. The stirring conditions like stirring speed (450 rpm), a stirring plate, and a stirring bar were kept constant with the different samples to minimize fluctuations in the flocculation process, as already indicated in Section 2.4.3. Following pH adjustment, the polysaccharide-oleosome mixtures will result in either more gel-like or viscous-like properties depending on which conditions, such as polysaccharide/oleosome ratio and the type of polysaccharide, lead to more efficient polymer bridging. This thesis builds upon this method, and the following techniques characterized the resulting properties.

3.2 Oscillatory rheology

Oscillatory rheological measurements determined the viscoelastic properties of the polymer-bridged gels. Amplitude sweep measurements were performed to study and compare the properties of the flocculated oleosome emulsions with the different polysaccharides alginate, xanthan, and ι-carrageenan at different polysaccharide/oleosome ratios and different oleosome concentrations. This section covers the basics of oscillatory rheology and physical models, which can be applied to understand the interactions occurring within the oleosome droplet network.

Rheology is defined as the study of the flow or deformation of matter as a result of applied stress. As for flow or deformation, it entails changes in the shape or dimension of the volume elements of the material. As for applied stresses, it means the contact force applied on the surface of a material (Force/Area) [78]. The rheological properties of materials can be considered as being between Newtonian viscous fluid and Hookean elastic solids, like, for example, rubber. However, most food colloids (gels, emulsions) exhibit both viscous and elastic mechanical properties. As a result, they are called viscoelastic.

When constant deformation occurs in viscoelastic materials, material stress relaxes over time and eventually disappears for viscoelastic liquids. The is so-called linear viscoelastic regime (LVR) is when the stress relaxation is proportionate to the strain. The apparent shear modulus becomes strain dependent over a

certain strain. This the so-called nonlinear viscoelastic regime. In general, interactions and microstructural changes in food colloids significantly impact the linear viscoelastic properties.

Small amplitude oscillatory shear is commonly used to investigate the linear viscoelastic behavior of materials. In amplitude sweeps, the strain is varied at a constant frequency. Up to a critic strain γ_L (Fig. 3.2a) in the LVR, the structure of the tested material remains stable, and G' as well as G'' is independent of the strain amplitude. At higher strains, the sample structure starts to break down, and when $G'' > G'$, the sample has the properties of a viscoelastic fluid (Fig. 3.2a).

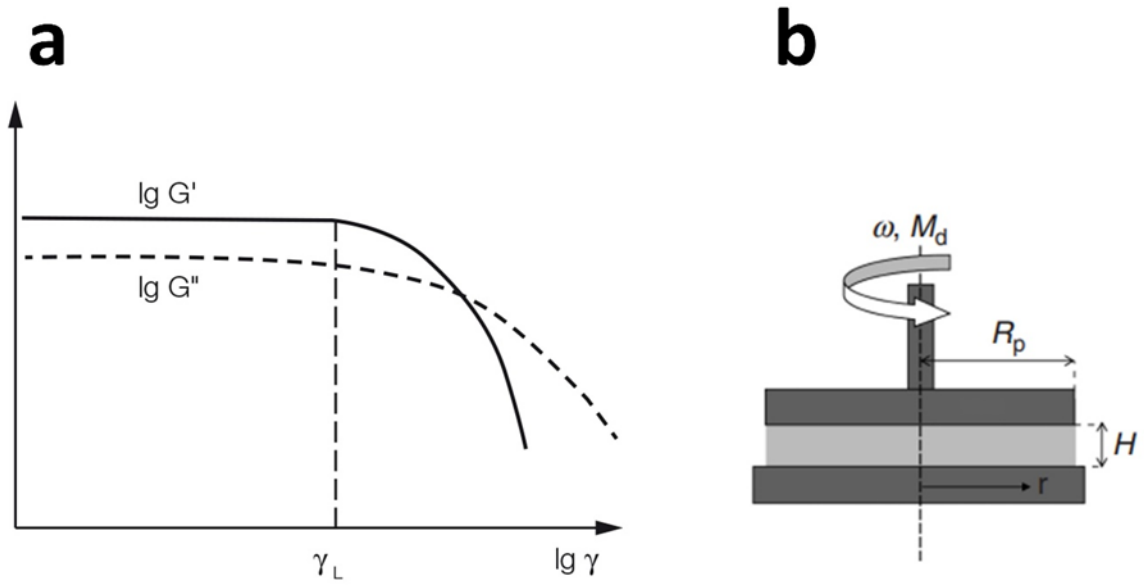

Fig. 3. 2 a) A typical graph of amplitude sweep measurement b) A parallel plate geometry where the sample is confined within the gap of height H between the two parallel plates, is sheared by rotation of the plates at angular velocity ω with a torque M_d measured in the inner cylinder (bob), r is the distance from the rotation axis. Adapted from [78].

Oscillatory rheology refers to the process in which the material is subjected to either a stress or frequency that varies harmonically with time. Typically, a sinusoidal strain is applied to the sample, causing stress to be transferred through the material. A sine curve is determined by its amplitude (maximum deflection) and oscillation period. The oscillation frequency is the reciprocal of the oscillation period. For a viscoelastic material, the sine curves of the preset parameter and the measuring result show a time lag for the response

signal. This lag is called the phase shift δ. It is always between 0°, and 90° δ is 0° for purely elastic materials (no phase lag) and 90° for purely viscous (out of phase due to viscous losses). The following equations describe the above:

$$\sigma = \sigma o \cos\delta \sin\omega + \sigma o \sin\delta \cos\omega t \quad (3.1)$$

Where σo is the shear stress amplitude and ω is the angular frequency. This allows for the following quantities to be defined:

$$G' = \frac{\sigma o \cos\delta}{\gamma O} \quad (3.2)$$

$$G'' = \frac{\sigma o \sin\delta}{\gamma O} \quad (3.3)$$

Therefore, the stress response can be written as follows:

$$\sigma = G' \gamma o \sin\omega t + G'' \gamma o \cos\omega t \quad (3.4)$$

Oscillatory rheological measurements are performed in rotational rheometers, in which the shear is generated between a fixed and a moving solid surface (Fig. 3.2b). A parallel-plate geometry was used, in which the sample is confined within a gap between two parallel plates. The resulting strain, strain rate, or shear rate is measured by applying a torque (rotational shear stress) to the upper plate. In parallel-plate measuring systems, calculations, and interpretation of rheological results are frequently based on the maximum shear rate value at the plate rim ($r = R_p$) (Fig. 3.2b). By using large gap heights, the parallel-plate measuring device enables measurements of suspensions with big particles.

On the other hand, the viscosity can be produced at comparatively high shear rates by working at small gaps. Additionally, errors brought on by edge effects and secondary flows can be reduced by using small gaps. Measurements at various gap heights can be used to correct wall slip effects.

3.2.1 Theoretical models describing gelation

It is possible to explain rheological data with theoretical models, which can give insight into the structural information of the resulting gel network. Branching, percolation, and fractal models [79-81] are used among

many different models. Percolation theories are based on the existence of a gelation threshold concentration c_p, which depends on the strength of interaction between the monomers that form the network and their morphology [82]. Below c_p, separate clusters are present, and above this concentration, an infinite cluster is present. The elasticity G' is described as follows:

$$G' \sim (c - c_p)^t \quad (3.5)$$

Where the scaling exponent t can describe the elastic energy of the network, when t is about 2 it is an indication of isotropic force percolation and a homogeneous network [83, 84]. If central forces between neighboring sites in the lattice are $t = 4.4 \pm 0.6$, a different university class is suggested [85]. In addition, Kantor and Webman [86] considered a model based on two contributions to elastic energy, a central force term, and a bending energy term. This model applies to macroscopically heterogeneous materials made of rigid and soft regions, where t lies between 2.85 and 3.55. The percolation model has been previously applied to protein gel systems [80, 87, 88] and bridging flocculated suspensions [82, 89].

In the fractal model, scaling of G' is given by:

$$G' \sim c^n \quad (3.6)$$

Where the exponent n is related to the fractal dimension D_f, Mellema et al. [81] developed a classification of the scaling exponent based on the fractal geometry of clusters. Here the scaling exponent is given by $n = \alpha/(3 - D_f)$, where the parameter α (between 1 and 4) depends on the amount of bending or stretching energy in the deformation of the bonds.

3.3 Microscopy techniques

Microscopy techniques have been used to visualize the structure of the bridging-flocculated emulsions and to observe the changes as a function of polysaccharide concentration. For this project, optical microscopy and confocal scanning laser microscopy techniques have been performed.

3.3.1 Optical microscopy

Optical microscopy, also known as light microscopy, uses visible light and a system of lenses to produce magnified images of samples. Light microscopy is one of the most traditional techniques to visualize samples at the microscopic scale. A microscope entails an imaging system that creates a magnified image of the light interacting with the sample, which may subsequently be viewed with the naked eye or a camera system, and an illumination system to illuminate the sample (Fig. 3.3a).

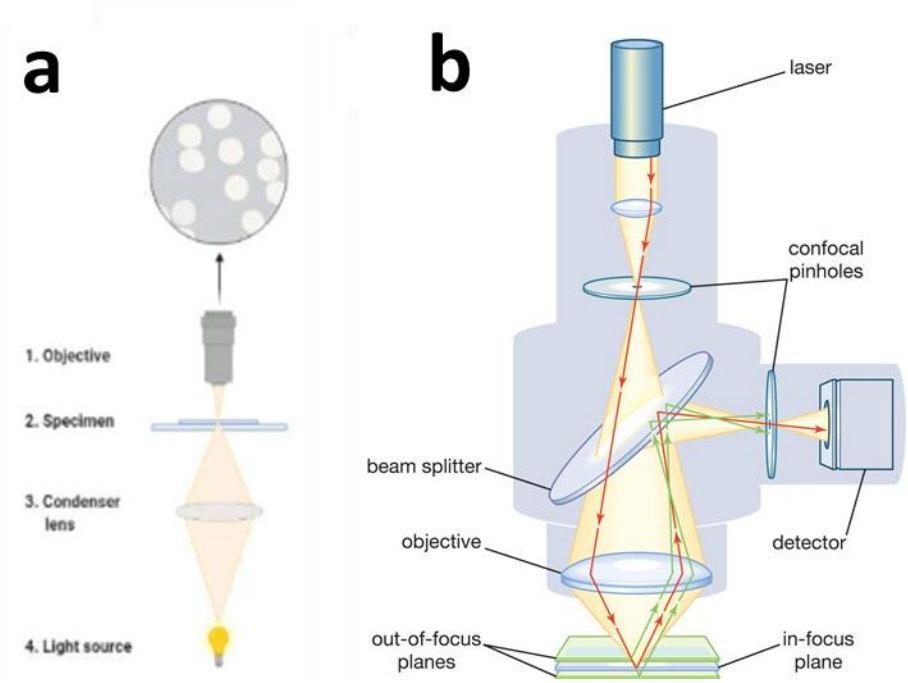

Fig. 3. 3 Schematic of general set-ups of microscopes a) bright field light microscope, b) confocal scanning laser microscopy. Adapted from [90].

The most elementary microscope is the simple microscope which uses a single lens (magnifying glass) and is limited to a maximum magnification of about 20X. The compound microscope consists of four components: a light source, condenser lens, objective lens, and eyepiece (ocular) (Fig. 3.3a) [91]. Their individual powers multiply to provide far higher magnifications than those possible with a simple microscope. The objective lens gathers light from the sample and is typically 40–100X magnification. The condenser collects light rays from the light source, which are focused onto the sample. The objective lens

(the lens nearest the sample) forms a real, magnified aerial image of the object in the intermediate image plane. The eyepiece further magnifies this actual image to form the final image, which can be viewed directly in the eyepiece or projected onto a camera. The sample can be illuminated from the bottom to observe transmitted light (Fig. 3.3a), or it can also be observed from the top as reflected light.

Light microscopy uses many different techniques, such as bright field, dark field, phase contrast, polarized light, or fluorescence microscopy. In bright-field microscopy (Fig. 3.3a), which was used for this project, most of the light from the condenser lens enters the objective lens after interacting with the sample to participate in image formation. This system generally results in an image with a bright field or background. The limitations of bright-field microscopy include the low contrast for samples, which contain several components such as food emulsions in which their components have similar refractive indices making them difficult to distinguish from each other. Nevertheless, it can offer valuable information about the size or structure of emulsions with larger droplets or flocculated emulsions [92].

3.3.2 Confocal scanning laser microscopy

Confocal scanning laser microscopy (CLSM) can reproduce images with a resolution equal to or superior to the conventional light microscope. CLSM offers optical sectioning of a thick sample, so it is possible to produce an image of a sample in three dimensions. CLSM can be used in transmission and reflection modes, but fluorescence imaging has been proven to be the most powerful microscopic technique in food materials. The main advantage of CLSM is using a pinhole aperture (Fig. 3.3b), ensuring that only light from the in-focus point is collected. This allows the exclusion of out-of-focus blur. Several apertures of varying diameter enable the operator to adjust pinhole size (and optical section thickness).

The working principle of CLSM is as follows (Fig. 3.3b): pinhole apertures are positioned in a conjugate plane (confocal) with a scanning point on the specimen and a second pinhole aperture in front of the detector, through which coherent light produced by the laser system (the excitation source) travels (a photomultiplier tube). Secondary fluorescence emitted from points on the specimen (in the same focal plane) passes back through the dichromatic mirror, which acts as a beam splitter. It is focused as a confocal

point at the detector pinhole aperture. The laser is reflected by a dichromatic mirror and scanned across the specimen in a defined focal plane [93]. In order to eliminate out-of-focus light, the fluorescence light produced by this excitation returns through the dichromatic mirror and is focused as a confocal point at the detector pinhole aperture. Three-dimensional images are obtained by focusing the laser beam at different vertical depths (*z*-plane) into the specimen and then scanning in the horizontal direction (*x*-*y* plane).

The crucial properties of a laser to be employed in CSLM are the emission wavelength and the minimum intensity requirements estimated for fluorescence microscopy. Factors including emission wavelengths, power at each wavelength, stability, and cost are among the most crucial when choosing a laser. Currently, a CSLM with four laser lines encompassing the spectrum from ultraviolet to infrared offers the most extensive range of applications (300-650 nm). Three main categories of continuous wave gas lasers are utilized commercially: 1) argon-ion, 2) helium-neon (He/Ne), and 3) helium-cadmium (He/Cd). Many manufacturers offer multi-line or single-line argon-ion lasers with lines in the visible spectrum from 454-528 nm, with powers ranging from a few mW to 10-20 W. Commercially, extended argon-ion laser lines in the UV, from 275 to 528, are also accessible. He/Ne lasers with emission at 543, 594, 612, and 632 nm and lines in the infrared with typical powers between 0.5 and 10 mW have been made available by several manufacturers. Three emission wavelengths (325, 354, and 442 nm) and power levels as high as several hundred mW are available in He/Cd lasers [94].

Observation of the microstructure of multicomponent systems is often facilitated by using the natural fluorescence of specific components or by using fluorescent dyes that bind selectively to specific components (e.g., proteins, fats, or carbohydrates) or that are more soluble in one phase than another (e.g., oil vs. water). Nile red is a dye showing the properties of a fluorescent hydrophobic probe. Therefore, Nile Red has been widely used in oil-in-water emulsions. Nile red is a benzophenoxazone. Depending upon the relative hydrophobicity of the solvent, the excitation and emission maxima of Nile red fluorescence can vary over a range of 60 nm; the fluorescence colors range from golden yellow to deep red [95].

CLSM has been enormously helpful in studying the structure of food emulsions. For instance, it has been used to determine the size, concentration, and organization of droplets in oil-in-water emulsions [96], to observe the microstructure of butter, margarine, and low-fat spreads [97], to control the creaming of oil droplets [98], or to visualize the structural organization and interactions of droplets in concentrated emulsions [99].

3.3.3 Scanning electron microscopy

Scanning Electron microscope (SEM) was used to analyze the microstructure the compacted polymer bridging gels upon centrifugation. SEM is a kind of electron microscope that scans a sample's surface with a focused beam of electrons to obtain images of the surface. The samples' surface topography and chemical composition are revealed by the signals created as a result of the electrons' interactions with the sample's atoms. An image is created by combining the position of the electron beam with the strength of the signal being detected while it is being scanned in a raster scan pattern. The main two of electrons utilized in SEM are secondary electrons (SE) and backscattered electrons (BSE)[100]. Both SE and BSE signals can be recorded with a variety of different detector systems as a function of electron beam position on the sample surface. The most common electron detector in SEM mode to find SEs released by excited atoms is the Everhart–Thornley detector [101]. In order to prevent air from stopping or simply scattering the electron beam off the axis of the electron path, there must be enough mean free path for the electrons to travel from the electron source down to the specimen. A vacuum is required in this microscope setup because of this.

There are various techniques for managing food samples for SEM analysis, including freezing the sample to low temperatures, coating it with impermeable films that prevent water from being dispersed into a vacuum, dehydrating the sample if water loss does not simply change the imaging expectations, and so on. These techniques prevent the sample from degaussing (i.e., changing its morphology and structure) when in a vacuum.

Samples must be electrically conductive in order for images to be formed. This is because of the interaction of the negatively charged electron beam with the sample (the sample will become negatively charged as the

incident electrons reach it, and the sample then repels the beam). The samples that are inherently non-conductive need to be coated with a thin layer of metal or carbon to make them conductive before they can be imaged in an SEM.

The scanning electron microscope (SEM) provides an advantage over the light microscope in three key areas:

1) Resolution at high magnification: Resolution can be defined as the least distance between two closely opposed points, at which they may be recognized as two separate entities. The best resolution possible in a light microscope is about 200 nm, whereas a typical SEM has a resolution of better than 10 nm (typically 5 nm).

2) Depth of field: This is the height of a specimen that appears in focus in an image - SEM has more than 300 times the depth of field compared to the light microscope. This means that great topographical detail can be obtained. For many users, the three-dimensional (3D) appearance of the specimen image is the most valuable feature of the SEM. This is because such images, even at low magnifications, can provide much more information about a specimen than is available using the LM.

3) Microanalysis: The analysis of sample composition, including information about the chemical composition, as well as crystallographic, magnetic, and electrical characteristics.

3.4 Particle size measurements

Particle size measurements on the oleosome emulsions were determined to analyze the effect of bridging flocculation by the different polysaccharides at different concentrations. For this project, a particle size analyzer based on laser diffraction was used (Fig. 3.4a). Particle size by laser diffraction uses the principle of static light scattering (SLS). Light scattering occurs when light "hits" a particle. As a result, it changes its direction. Light scattering depends on the light's wavelength and the particle's optical properties. A scattering pattern is formed by light intensity as a function of the scattering angle. In SLS, the average intensity of scattered light at multiple angles is measured by detectors (Fig. 3.4b). It is possible to determine

the size distribution for particles of a specific shape from the measured angular scattering intensity pattern if the relationships between scattering intensity, scattering angle, particle shape, and particle size are known. SLS is based on the scattering theories of Rayleigh, Fraunhofer, and Mie.

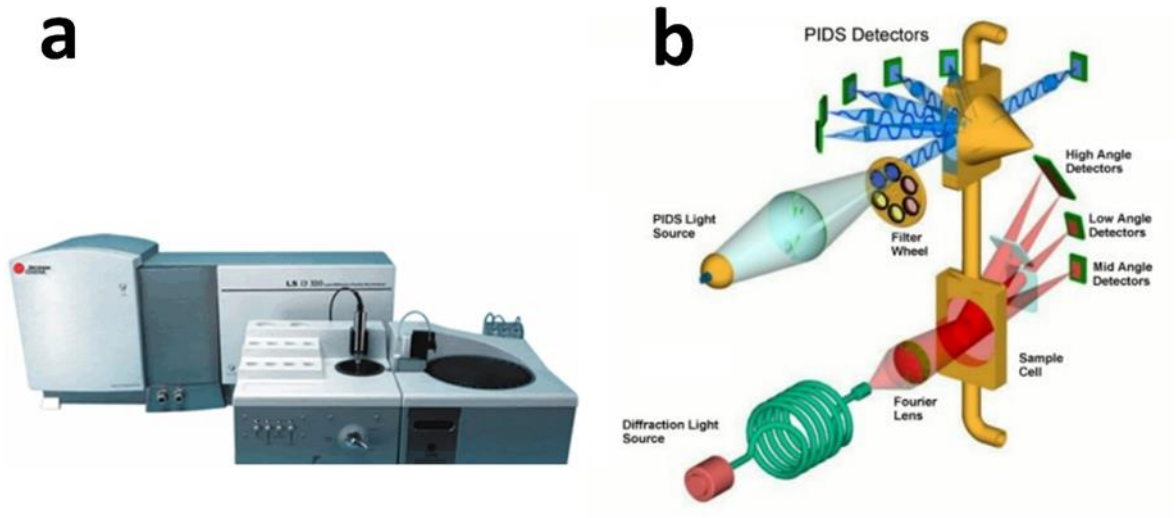

Fig. 3. 4 a) Particle size analyzer based on laser diffraction, b) optical system of the particle size analyzer. Adapter from [102].

Rayleigh scattering is seen in particles that are noticeably smaller than the wavelength of the incident beam ($D < 0.1\lambda$). No angular information can be collected for a laser diffraction experiment because the light is scattered equally in all directions in a Rayleigh scattering process. As a result, the Fraunhofer and Mie theories provide the foundation for most laser particle size analyzers. Mie scattering can be seen in particles with a particle size comparable to the wavelength of the incident light ($0.1\lambda < D < 10\lambda$). The Fraunhofer diffraction theory—which states that incident light is primarily diffracted at the outer edges of big spherical particles—is employed for large particles ($D > 10\lambda$). For extremely big particles, it can be roughly compared to Mie scattering with scattered intensities at small angles (for large particles, the scattering intensity is often focused in the forward direction at angles less than 10 degrees). For this reason, forward scattering is another name for Fraunhofer diffraction.

The particle size analyzer used for this project uses Polarization Intensity Differential Scattering (PIDS) technology (Fig. 3.4b). PIDS provides the primary size information for particles in the 0.017 µm to 0.4 µm range. Additionally, it improves the particle size distributions' resolution by up to 0.8 m. When the particles are less than 0.4 m in diameter, it is challenging to discern between particles of different sizes by diffraction patterns alone. The PIDS assembly uses an incandescent tungsten-halogen lamp and three sets of vertically and horizontally polarized filters to provide polarized monochromatic light at three different wavelengths: 450 nm (blue), 600 nm (orange), and 900 nm (near-infrared, invisible).

3.5 Surface charge measurements

Zeta (ζ) potential measurements were performed to analyze the effect of pH on the polysaccharide's adsorption to the oleosomes surface. A particle's ζ-potential is the charge that forms at the interface between a solid surface and its liquid medium. It depends on the types and concentrations of ions in the medium. The zeta potential of a sample is determined by the principle of Electrophoretic mobility, which is performed by performing an electrophoresis experiment on the sample and measuring the particle's velocity using Laser Doppler Velocimetry (LDV). The working principle of Zeta potential is depicted as follows.

When a particle in a liquid concentrates counterions at its interface due to a net charge at the particle surface, the liquid layer surrounding the particle occurs as two parts. Firstly, as an inner region (Stern layer), where the ions are firmly bound, and an outer region (Diffuse layer), where the ions are less firmly bound (Fig. 3.5a). As a result, an electrical double layer is present around each particle. A theoretical boundary within the diffuse layer where the ions and particles come together to form a stable entity. Zeta potential is called the potential that exists at the boundary (slipping plane) where ions, within the diffuse layer, move as a result of the movement of the particle, for instance, due to gravity (Fig. 3.5a).

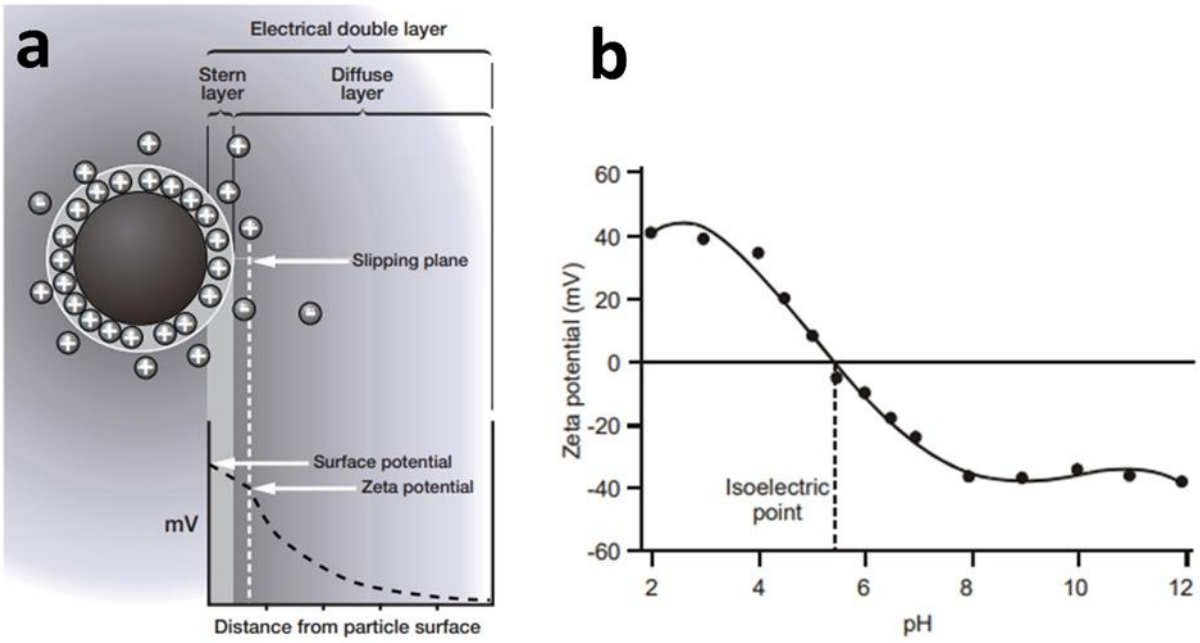

Fig. 3. 5 a) Schematic showing the ionic concentration and potential difference as a function of distance from the charged surface of a particle suspended in a dispersion medium b) Typical plot of zeta potential versus pH. Adapted from [103].

In electrophoresis, charged particles in a liquid are moved as a result of an application of an electric field, which moves the particles toward the electrode of opposite charge. Viscous forces typically resist the mobility of the particles. The particles move at a steady velocity until the balance between these two opposing forces has been attained. The particle's velocity depends on 1) the strength of the electric field or voltage gradient, 2) the dielectric constant of the medium, 3) the viscosity of the medium, and 4) the zeta potential. These parameters calculate zeta potential using the Henry equation [104]**.**

Electrophoretic mobility is measured in a cell with electrodes at either end to which an electric field is applied. LDV is responsible for measuring the velocity of the particles moving in the fluid towards the electrode of opposite charge.

The primary aspect that influences zeta potential in colloidal suspensions is pH. For instance, pH will decrease when acid is added to a negatively charged colloidal suspension, increasing positive charges on the particle surface. The point at which zero electrophoretic mobility occurs is called an isoelectric point

(Fig. 3.5b). Usually, the isoelectric point is where the colloidal system is the least stable in physical terms [105].

4 Influence of polysaccharide type and polysaccharide/oleosome ratio on polymer bridging-based structuring

This chapter is based on the following manuscript:

Tunable oleosome-based oleogels: influence of polysaccharide type for polymer bridging-based structuring

Juan C. Zambrano, Thomas A. Vilgis

Food Hydrocolloids 137 (2023): 108399

4.1 Summary

This chapter proposes a gelation approach based on bridging flocculation mechanism using soybean oleosomes as templates and polysaccharides as structuring agents. Two anionic polysaccharides, sodium alginate, and xanthan gum were investigated for their ability to induce bridging flocculation. Bridging flocculation occurs when flexible polysaccharides such as alginate strongly interact with oppositely charged oleosome particles in acidic pH ranges. In contrast, the more rigid xanthan leads to a different flocculation mechanism, which is not driven by strong electrostatic attractive interactions. In microscopy images, xanthan induced microscopic and macroscopic phase separation between oleosome droplets and xanthan, presenting large, irregular-shaped particles. The ratio between alginate chains and oleosome droplets is critical for optimum bridging, where 0.005 g/g (also expressed as an equivalent per droplet surface area 0.4 mg/m^2) induced extensive droplet flocculation. It is possible to obtain an interconnected droplet network at this optimum ratio. Upon densification at the optimum ratio, a compact and self-supporting gel of about 46 wt% starting from 5 wt% oleosome is obtained. Oscillatory rheology showed that gels at optimum bridging ratio have higher moduli (G') than those formed at a different ratio, confirming a highly cross-linked network. Bridging flocculation provides an alternative method to design gels with predictable rheological properties suitable for food and drug design and cosmetic applications.

4.2 Introduction

The addition of polysaccharides to charge-stabilized emulsions significantly affects the structural arrangement of emulsion droplets. For instance, polysaccharides can induce oil droplet aggregation by a bridging flocculation mechanism. Bridging flocculation occurs under a certain range of polysaccharide concentration, where single polymeric chains can link two or more neighboring oil droplets, eventually leading to a particle gel network [89, 106]. Furthermore, bridging flocculation takes place when polysaccharide molecules have a strong affinity for the droplet interface. This affinity generally results from attractive electrostatic interactions, as shown in protein-stabilized emulsions flocculated by polysaccharides [107, 108]. Bridging flocculation can be used as a structuring process to controlled design of soft materials. For instance, the molecular weight, charge density, and conformational structure of the chosen polysaccharide will influence the effectiveness of a polymer in inducing bridging flocculation [65, 107, 109]. The present research studies in detail the flocculation mechanism of sodium alginate and xanthan gum, which vary significantly in their structural configuration despite being both negatively charged. The polymeric chains of sodium alginate are composed of a random sequence of D-mannuronic acid (M), and L-guluronic acid (G) blocks combined with regions of alternating MG blocks. The occurrence and combination of these blocks influences the stiffness or flexibility of the polymer chain [110]. The structure of xanthan gum consists of repeating units of 1, 4-linked β-D-glucose with side chains containing two mannose units separated by guluronic acid. The negatively charged carboxyl groups on the side chains of the molecule are responsible for a very stiff, rod-like backbone that results in unusual and functional properties such as a high degree of solution pseudoplasticity [53]. Therefore, the structural differences between sodium alginate and xanthan gum will provide tunable physical properties of the flocculated emulsions and resulting oleogels.

For sustainable and economic reasons, using natural templates, such as oleosomes, for complexation with polysaccharides has emerged as a potential alternative to traditional 'artificial' emulsions. Oleosomes are naturally pre-emulsified oil droplets in oleaginous seeds and nuts such as soybeans, sunflowers, and hazelnuts. Because of the charged nature of its surface, it is possible to bind to oppositely charged

polysaccharides. Oleosin, the primary structural protein, is one of the endogenous surface proteins contributing to this charged nature. Oleosin comprises a hydrophilic N-terminal, a C-terminal facing the continuous water phase, and a lengthy hydrophobic domain firmly fixed in the triacylglycerols (TAGs) core [31]. Oleosins are deeply embedded within a monolayer membrane of phospholipids surrounding the inner core TAGs [31]. Although many previous studies have proved polysaccharides' complexation with oleosomes via electrostatic interactions [15, 30, 111], studies have yet to focus on the effect of anionic polysaccharides on bridging flocculation of oleosomes. Therefore, this study focuses on systems containing soybean oleosomes, sodium alginate, and xanthan gum under conditions favoring electrostatic interactions. For this purpose, the pH values will be gradually lowered to values where both oleosome and polysaccharide are opposite charged. As a result, the zeta potential was measured, the particle size was characterized, and the contraction rates of the network (v) were calculated during demixing experiments. These experiments have been combined with microscopy visualization and rheology.

4.3 Materials and methods

4.3.1 Materials

Commercially available soybeans was purchased from Rapunzel Naturkost GmbH (Legau, Germany) and were used for the extraction of oleosomes. Sodium alginate (TICA-algin 400 Powder) was provided by TIC Gums, Inc. (Belkamp, Md., USA). Xanthan gum extra pure was provided by Carl Roth (Karlsruhe, Germany). Distilled water was used for the preparations of all solutions.

4.3.2 Sample preparation

Soybean oleosomes extraction is based on the method described by Waschatko et al. 2012. Soybeans were soaked in distilled water at 4°C for at least 20 h. Then water was added to obtain a 10% soybean-to-water ratio, grounded in a Vorwerk Thermomix TM31 at 10.200 rpm for 90 s at 25°C. The resulting slurry was filtered through two layers of Kimtech wipes 21 x 11 cm (Kimberly Clark) to obtain raw milk. 25 wt% Sucrose was added to the raw milk and the pH was adjusted to 11.0 with 1 N NaOH (VWR Chemicals) solution. The solution was filled with 50 ml centrifuge tubes (Roth), which were centrifuged at 15000x*g* at

4°C for at least 5 h. The resulting floating fractions (cream layer) were collected with a small spoon and re-suspended in a new centrifuge tube in 45 ml of 20 wt% Sucrose in distilled water (pH 11.0). A new washing and centrifugation step (15000x*g*, 4°C, 5 h) was repeated, and the resulting oleosome cream was collected in a centrifuge tube. This method removes unspecific bounded soybean storage proteins (glycinin and β-conglycinin) and other allergenic proteins (Gly m BD 30K) from the surface of the oleosomes [77]**.** The final oleosome content was determined by a halogen dryer and ranged between 50 - 60 wt%. Since the precise composition of oleosomes is unknown, Huang's [27] theoretical values from a geometry-based model are described. This model calculates the amounts of approximately 3.3% (w/w) phospholipids, 5.2% (w/w) protein, and 91.5% (w/w) triglycerides for an oleosome with a 0.350 μm diameter.

Depending on the nature of the experiments, oleosomes emulsions were diluted with distilled water (w/w) to the desired concentration. The initial pH value was adjusted to 7.0 with 1 NaOH. Dried Sodium alginate and Xanthan gum samples were added directly to the oleosome emulsion at different concentrations to form different mass ratios (gr Polysaccharide/gr Oleosome). Polysaccharides-oleosome mixtures were stirred for a minimum of 20 h at 25°C to ensure proper hydration. Afterward, polysaccharides-oleosome mixtures were slowly adjusted to pH 4.0 via dropwise addition of HCl with varying concentrations (1.0, 0.5, 0.1, 0.01 N) at a constant stirring speed of 450 rpm. Samples were prepared in stock, some samples were used immediately for further experiments, and other sets of samples were centrifuged (at 5000 x *g*, 4°C, for 20 min) for separation and densification of flocculated oleosome droplets.

4.3.3 Demixing experiments

Immediately after being adjusted to pH 4.0, 5 wt% oleosome emulsions mixtures with alginate and xanthan containing various concentrations in the range 0- 0.125 wt% were stored quiescently in a sealed glass tube at 25 °C. Demixing was monitored over 18 days by visually following the height of the cream layer as it demixes out of a serum layer. The emulsion samples' initial height, H_0, was 10 ± 0.8 cm. The height of the contracting network at time t was defined as $h\,(t) = H\,(t)/H_0$. Parameters were obtained from the demixing curves. The rate at which the network contracts was determined by using $= \Delta H(t)/\Delta t$.

Permeability coefficient *B* was determined by Darcy's law $v = BP(\eta H_0)^{-1}$ [112], where η is the viscosity of the aqueous phase. The pressure (*P)* is the pressure exerted on the emulsion droplet network due to density difference is given by $P = \Delta\rho g H_0 \phi$ [76], where $\Delta\rho$ is the density difference between the oil and aqueous phase, g is the acceleration due to gravity and ϕ is the volume fraction of oil. Delay time, $t_{delay,}$ is defined as the time when network compression starts.

4.3.4 Particle size measurements

Freshly pH-adjusted emulsions were diluted in a ratio of 1:10 to obtain a final droplet concentration of 5 wt% using buffer solution (same pH 4.0 as the sample being analyzed) to avoid multiple scattering effects. The particle size distribution of the emulsions was determined as differential volume by using a laser diffraction particle analyzer (LS 13320 Beckmann Coulter, California, USA). Measurements were performed using a laser diode with λ= 780 nm and three Polarization Intensity Differential Scanning (PIDS) wavelengths at λ = 450, 600, and 900 nm. The data were analyzed using the instrument software applying Mie theory [113] and using refracting indexes as follows: refractive indexes soybean oil and water 1.47 and 1.33, respectively. A few drops of emulsion were placed into the sample chamber of the instrument and then recirculated through the optical measurement cell. The mean particle size was reported as the volume-weighted value, d_{43}. Results were reported as the average of three measurements.

4.3.5 ζ-Potential measurements

Oleosome emulsions from concentrated stock were diluted to a concentration of 0.2 wt%, and the same procedure as 4.3.2 was repeated (polysaccharide addition, pH adjustment to 4.0) while maintaining the same oleosome-polysaccharide mass ratios from the other experiments. Diluted emulsions were injected directly into the measurement chamber of a particle electrophoresis instrument (Malvern Zetasizer Nano Z) that measures the direction and velocity of droplet movement in the applied electric field. An individual ζ-potential measurement was determined from the average of 3 readings taken on the same sample.

4.3.6 Microscopic imaging

Freshly pH-adjusted 5 wt% polysaccharides-oleosomes mixtures were observed by optical microscopy using a Carl Zeiss Axio Scope.A1 microscope (Carl Zeiss AG, Oberkochen, Germany). Images were captured using transmission bright field microscopy with the objective lenses magnifying 10× at 25°C. ImageJ software was used to insert the scale bar. A drop of the emulsion was placed on a microscope slide and then covered with a cover slip. Confocal laser scanning microscopy (CLSM) was used to analyze network structure of flocculated oleosome/polysaccharide mixtures. CLSM was performed using a Zeiss Axiovert 200M (Oberkochen, Germany)**.** A few drops of Nile Red, a fluorescent label excited at 543 nm with a Helium-Neon laser, were added to stain the oil core of the oleosome droplets. 500 μL of the different mixtures were placed inside 8 well-chambered borosilicate coverglass systems (Nunc Lab-Tek, Thermo Fisher Scientific, USA). The obtained CLSM images were analyzed using the "ImageJ" software package.

4.3.7 Rheology measurements

After centrifugation, oscillatory rheology was performed on the compacted flocculated polysaccharide-oleosome mixtures to investigate their resulting viscoelastic properties. Measurements were performed with a Bohlin Instruments Gemini 200 rheometer (Malvern Panalytical Ltd., Malvern, UK) equipped with a 25-mm parallel plate geometry. The gap size was adjusted stepwise to the thickness of the gels until the load in the force was detected, leading to gap sizes between 1000 – 1500 μm. After loading, a 5-minute waiting period at 25°C was used to allow the sample's structure to relax before the measuring process began. Oscillatory amplitude sweeps were performed by increasing the strain logarithmically from 0.01 to 1000% at 1 Hz. All measurements were performed in triplicate at 25°C from different batches of gels, and all samples were prepared individually.

4.3.8 Characterization of polysaccharides

The molecular conformation of Sodium alginate and Xanthan gum was determined by gel permeation chromatography combined with multi-angle light scattering (GPC-MALLS). Polysaccharides were dissolved in 0.1 M $LiNO_3$ at 25°C. Measurements yielded distributions of molecular mass, $M_{w,}$ and radius

of gyration, R_g. In addition, ζ-potential values at pH 7.0 by dissolving both polysaccharides in a phosphate buffer. Averages are given in Table 1.

Table 4.1 Molecular characterization of alginate and xanthan. Surface charged expressed by zeta potential measurements at pH 7, R_g is the radius of gyration

Polysaccharide	**Surface charge (mV)**	***R_g (nm)***
Sodium alginate	-55.19± 8.29	62
Xanthan gum	-29.24± 8.97	150

4.4 Results and discussions

4.4.1 Influence of pH on polysaccharides adsorption

The interactions between the different polysaccharides and the oleosome surfaces were investigated by ζ-potential measurements. The surface charge of bare oleosome droplets changed from -46.07 mV to +39.07 mV when the pH was decreased from 7.0 to 3.0 (Fig. 4.1). The net charge was near zero somewhere between pH-values of 4.0 and 5.0, close to the isoelectric point (pI) of the oleosome-associated proteins being oleosin the predominant one [114]**.** Alginate and xanthan gum (Table 4.1), are considered anionic polysaccharides since they present negative charges at all the studied pH values considering their p*K*a values are above 3.0 [115].

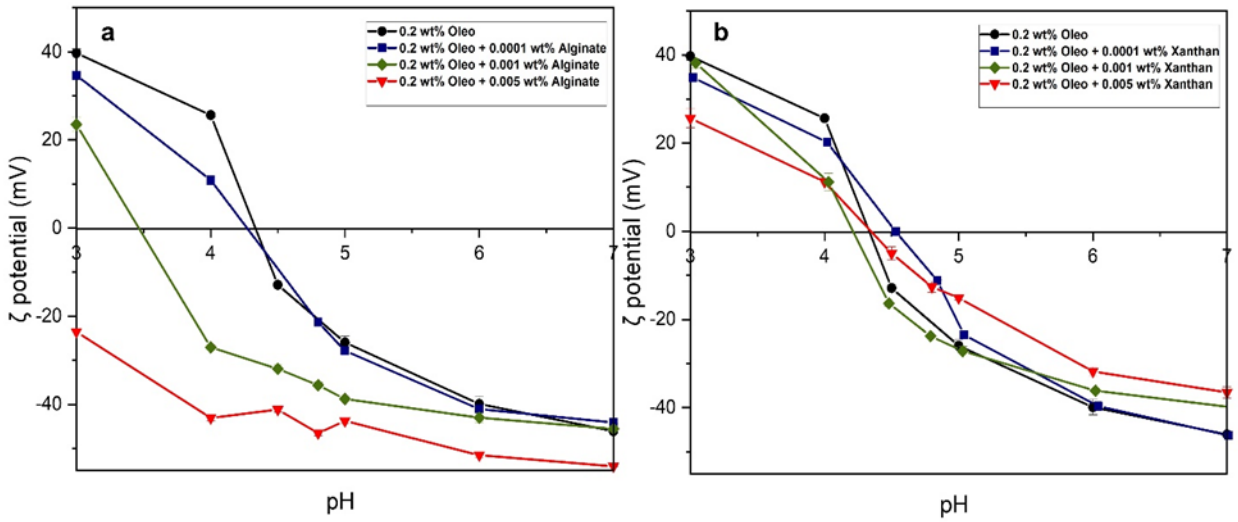

Fig. 4. 1 Influence of pH on the ζ-potential of polysaccharide/oleosome mixtures a) 0.2 wt% Oleosome- Sodium alginate, b) 0.2 wt% Olesome- Xanthan gum.

Adding polysaccharides to the oleosome droplets caused a change in charge density depending on whether alginate or xanthan gum was added. At pH values between 5.0-7.0 and a low concentration of polysaccharide (0.0001 wt%), alginate and xanthan had no significant effect on the oleosome net charge. Both polysaccharides and oleosome droplets are negatively charged at these higher pH values. In addition, a low amount of polymer chains was available to bind the droplet surface, preventing a significant change in the oleosome charge density. However, at pH 4.0 (where both polysaccharides and oleosomes are oppositely charged), a slight decrease in oleosome net charge starts with 0.0001 wt% alginate (from +25.63 mV to +10 mV).

On the contrary, xanthan does not significantly reduce oleosome net charge in these conditions. This observation suggests that alginate molecules can coat oleosomes, even at small concentrations, whereas xanthan molecules cannot. The relatively rigid xanthan molecules are unable to bend sufficiently to coat oleosomes and neutralize surface charges, as will be discussed in more detail later. Consequently, the gain in energy by adsorption cannot compensate for the entropy loss. In contrast, the uncharged blocks of alginate show high flexibility, and the distant charged blocks along the contour can adsorb partially on the surfaces of the oleosomes.

At higher concentrations of polysaccharide (0.005 wt%), alginate significantly affected the oleosome net charge, which increased from -46.07 to -54.03 mV at pH 7.0. Despite presenting similar charges at neutral conditions, polysaccharide molecules seem to adsorb to the oleosome surface. This can be explained by electrostatic interactions between anionic carboxylate groups (-CO_2-) on the alginate molecules and local cationic amino acid groups on the oleosome-associated proteins. A similar electrostatic interaction has been reported between anionic polysaccharides of high charge density and oil-in-water emulsions [116]**.** The most significant change occurred at pH 4.0 where charge reversal of oleosome net charge followed (from +25.63 to -43.06 mV). The ability of anionic polysaccharides to bind to the surface of oppositely charged colloidal particles and cause charge reversal is well established in the literature [117]**.** Consequently, alginate molecules strongly bind to numerous binding sites in the oleosome droplet interface via electrostatic interactions at higher alginate concentrations. The ratio between the chain length, flexibility, and surface curvature, determined by the oleosome radius, substantially influences polymer chain conformation to the surface of the oleosomes. The diameter of the oleosomes averages about 350 nm, as recently confirmed by small-angle neutron scattering [30]. As stated in Table 4.1, the squared average of the radius of gyration of alginate is about R_g = 62 nm. It is assumed that alginate chains are in a good solvent, $R_g \approx bN^{3/5}$, where b describes a statistic segment, and N corresponds to the degree of polymerization [118]. This assumption is based on the absence of detailed information about the distribution of charged guluronic and uncharged mannuronic acids. Considering the guluron and mannuron monomers of the alginate, it can be assumed that b is on the order of 5 nm, indicating values of N of the order of 70 and an average chain length of 360 nm. Comparing the chain length with the diameter of the oleosome shows that the average chain can adsorb at the surface at more than one charged block.

On the other hand, xanthan at 0.005 wt% only slightly decreased oleosome net charge to +11.23 mV at pH 4.00. This suggests that xanthan adsorption to the oleosome droplet surface occurred to a small extent and was not significant enough to cause charge reversal of the oleosome net charge. In several studies, xanthan gum is considered a non-adsorbing polysaccharide, which does not bind to protein-stabilized

droplet surfaces despite having negative charges along its chain [119, 120]. The physical reasons for these observations are clear. As mentioned before, xanthan shows high chain rigidity and must be considered as stiff polyelectrolyte [121]. Its high bending energy is caused by steric and electrostatic reasons. Each monomer can dissociate a cation and becomes negatively charged. The charged monomers repel each other intensely, stiffening the chains electrostatically in addition to steric reasons [122].

Consequently, xanthan chains are far less flexible (and turn for energetic reasons into single helices) [123]. Their persistence length is, therefore, of the order of the total contour length. In practice, the measured gyration radius (Table 4.1) can be assumed to be that of stiff rods. The interaction range scales as $\exp(-r/\xi)/r$, where r is the distance between the charges, ξ is the electrostatic screening length, which depends on the total ionic strength. According to the previous expression, xanthan may adsorb only at a minimal number of monomers. As a result, the gain in electrostatic energy is low [124]. It cannot balance the loss in entropy of free semi-flexible polyelectrolytes in solution, as outlined in Fig. 4.2.

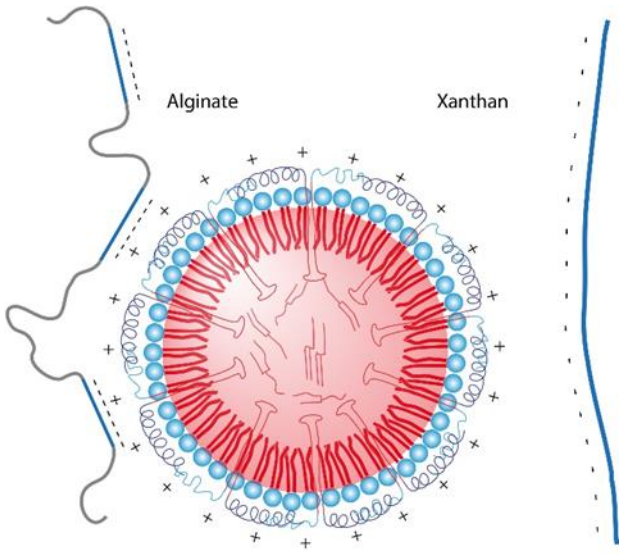

Fig. 4. 2 Flexible alginate chains gain more energy when adsorbing on oppositely charged surfaces as compared to semi-flexible, practically stiff xanthan molecules. Xanthan adsorbs with much lower probability, (free) energy and entropy are off balance due to high internal stiffness of the xanthan molecules.

Therefore, alginate has a stronger effect on the ζ-potential, even at low concentrations. The adsorption of the negatively charged guluron blocks neutralizes more of the positive charges of the oleosome surface proteins. On the contrary, xanthan has a lesser effect on adsorption. Interactions between xanthan gum and oleosomes may have taken place, but they seem not predominant enough, even under pH values where both xanthan and oleosome surface proteins are oppositely charged. Nevertheless, another study revealed [125] that attractive electrostatic interactions were present between xanthan gum and maize oleosomes. This can be easily explained with similar ideas. Maize oleosomes are, on average, larger [26, 126], which makes the curvature of the oleosome surfaces appears flatter. Therefore, the overall interaction is more significant since rigid xanthan molecules can adsorb easier when the curvature radius comes of the order of the xanthan persistence length. This behavior will be essential to interpret the flocculation experiments in more detail, as shown below.

4.4.2 Flocculation characterization of polysaccharide-oleosome mixtures

4.4.2.1 Demixing behavior and microstructural properties

The demixing kinetics of oleosome emulsions with alginate and xanthan gum were studied using plots showing the contraction of the network over time. Fig. 4.3a, b shows the visual appearance of oleosome at 5 wt% with different concentrations of alginate and xanthan (0.0025 wt%- 0.125 wt%) after being adjusted to pH 4.0. In the absence of polysaccharides (Fig. 4.3c), oleosome emulsion appears relatively stable until approximately 103 minutes, when the cream height decreases. Eventually, a steep decrease in cream height at 153 minutes occurs. In microscopy pictures (Fig. 4.4a), oleosome droplets appear homogenous with no signs of flocculation, with a small peak (0.350 μm) corresponding to intact oleosome droplets. However, a more prominent peak around 4.66 μm suggests the presence of single small flocs. It could be that single flocs where formed when the oleosome surface charge was reduced towards its isoelectric point (~pH 4.5). As a result, these small flocs slowly rise under gravity to the top of the emulsion, possibly dragging along most of the single unflocculated droplets and leaving behind a clear supernatant.

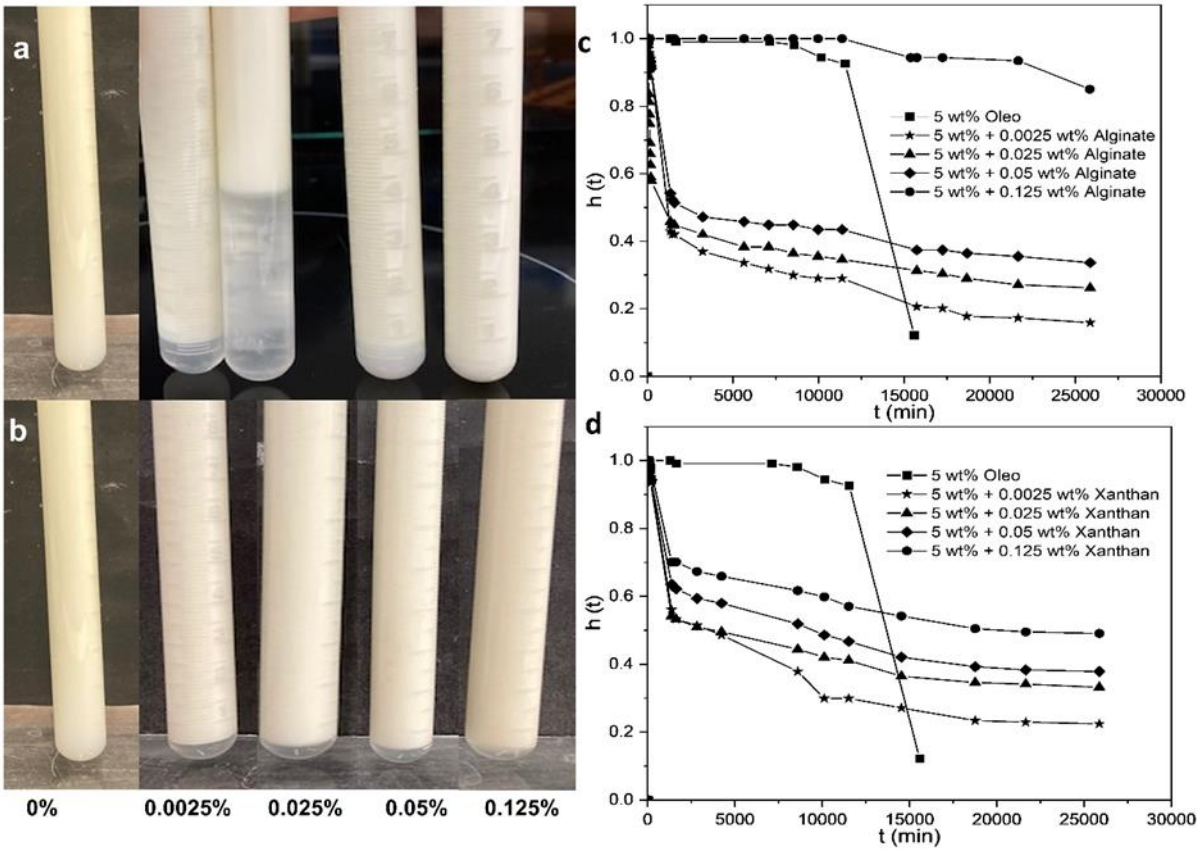

Fig. 4. 3 Demixing experiments of 5 wt% Oleosome with different polysaccharide concentrations after being adjusted to pH 4. a) Visual appearance of alginate-containing mixtures b) Visual appearance of Xanthan-containing mixtures c) Plot of network height, *h(t*), versus time of alginate-containing mixtures d) Plot of network height, *h(t)*, versus time of xanthan-containing mixtures.

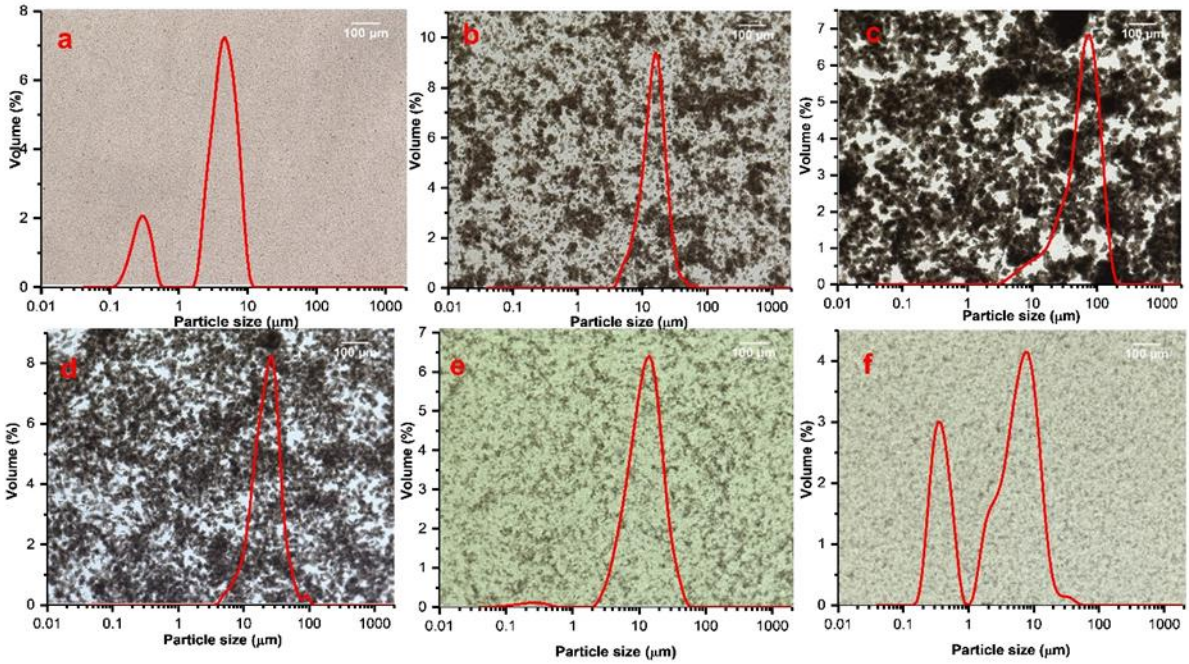

Fig. 4. 4 Optical microscopy images Oleosome 5 wt% - Alginate after being adjusted to pH 4 combined with Particle size distributions of the same sample. a) 5 wt% Oleo- 0 wt% Alg b) 5 wt% Oleo- 0.0025 wt% Alg c) 5 wt% Oleo- 0.025 wt% Alg d) 5 wt% Oleo- 0.01 wt% Alg e) 5 wt% Oleo- 0.125 wt% Alg f) 5 wt% Oleo- 0.175 wt % Alg.

When polysaccharides are added to oleosome emulsions, a characteristic change in demixing behavior can be observed. The addition of alginate leads to extensive demixing of oleosome emulsion to a concentration up to 0.025 wt%, which further re-stabilizes at higher concentrations (Fig. 4.3a). The rate of network contraction *v* was extracted from the demixing curves. Figure 4.5 shows a maximum in *v* (18.33 mm/h) at 0.025 wt% alginate. The maximum *v* indicates that extensive aggregation, *associated with polymer bridging*, already occurred during mixing and pH adjustment. This aggregation is likely to be driven by electrostatic interactions, as observed in Fig. 4.1a, where strong binding between alginate polymer chains and oleosome surface occurs at pH 4.00. Shortly after mixing, the rate of network contraction under gravity is mainly determined by the permeability of the network [76]. Table 4.2 shows permeability coefficient, *B*, where 0.025 wt% alginate, presents the highest *B*. Microscopic images in Fig. 4.4c show a droplet network

consisting of large and heterogeneous structures which may be responsible for large pores between the clusters and hence the higher initial permeability. Despite the high values for the rate *v*, the network height in 0.025 wt% alginate remained relatively unchanged at longer times (Fig. 4.3c). This indicates characteristics of a droplet network, which provides elastic resistance against the creaming of flocculated droplets. Several scans in the *z*-direction were conducted to verify the formation of an interconnected network. The resulting micrograph (Fig. 4.6) shows that oleosome aggregates formed a 3D network when alginate at 0.025 wt% was added. Alginate-mediated clusters can be interpreted and cartooned in Fig. 4.7, which shows the behavior on different scales.

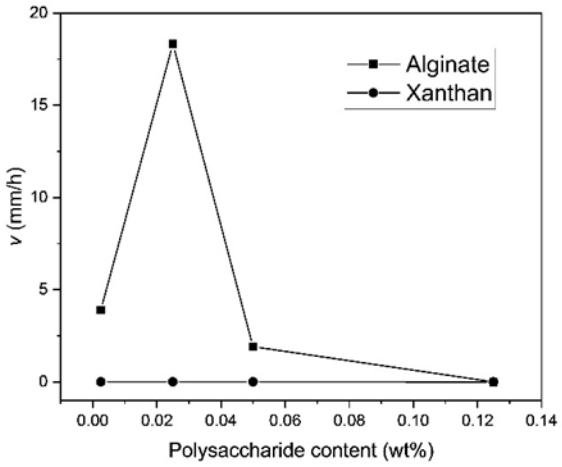

Fig. 4. 5 Plot of network contraction rate, *v*, extracted from demixing experiments plots versus polysaccharide concentration.

Table 4.2 Data parameters obtained from demixing plots. 5 wt% Oleosome. *B* is permeability coefficient and t_{delay} is delay time

Mixture Oleosome/ Polysaccharide	***B* (μm^2)**	**t_{delay}(min)**
Sodium alginate		
0.0025 wt%	1580.44	10
0.025 wt%	7429.42	5
0.05 wt%	773.64	100
0.125 wt%	0	15700
Xanthan gum		
0.0025 wt%	1105.20	20
0.025 wt%	1013.10	25
0.05 wt%	729.43	40
0.125 wt%	135.08	140

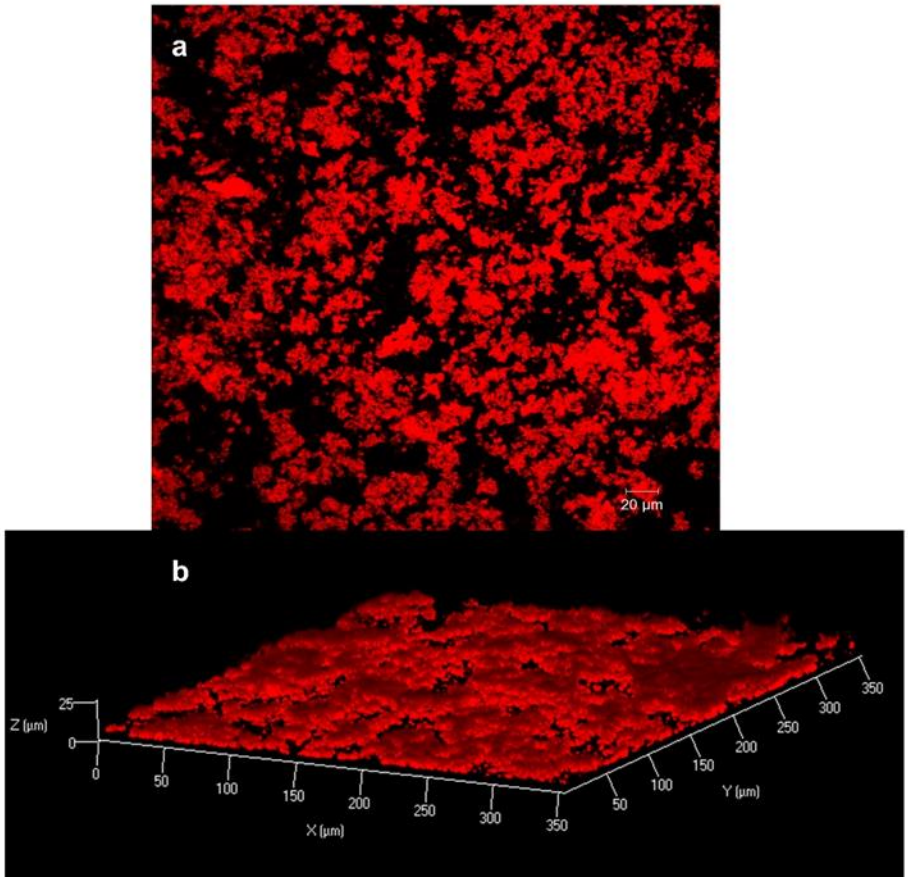

Fig. 4. 6 CLSM images of a) 5 wt% Oleosome with 0.025 wt% Alginate b) z-scan surface plot of sample 5 wt% Oleosome- 0.025 wt% Alginate. To visualize droplet aggregates for CLSM, samples were stained with Nile Red which dyes the oil core.

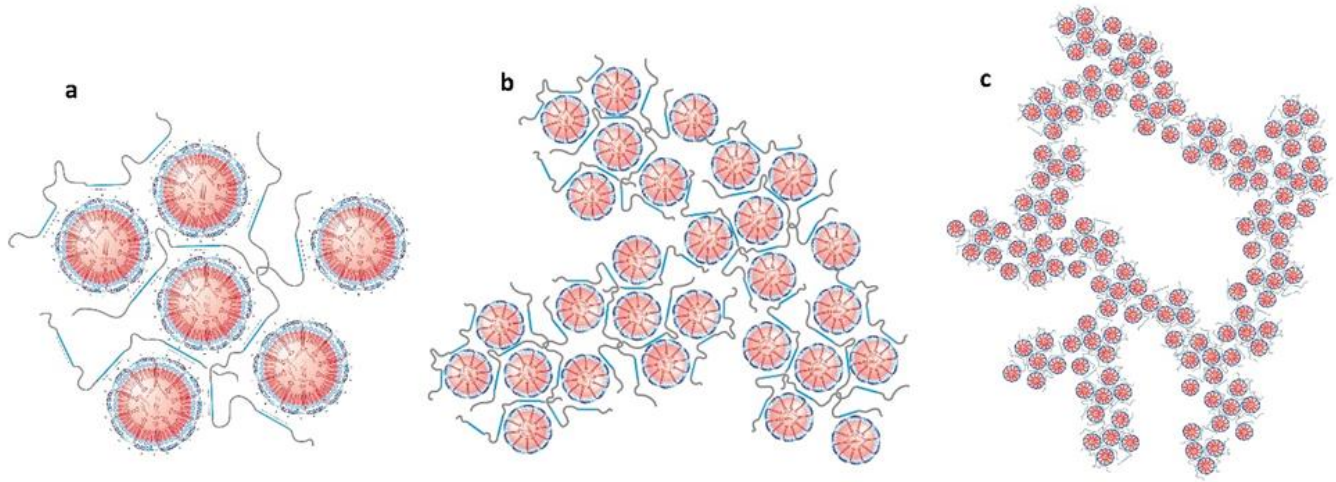

Fig. 4. 7 The bridging flocculation at 0.025 wt% alginate 5% Oleosome. (a) The oleosomes are coated partly by the negative charged blocks of the polymer. Entanglement formation between oleosomes become more likely, when chains are sufficiently long, i.e., by the high molecular weight fraction. (b) Oleosome aggregated are able to form larger clusters, which are able to join to a soft oleosome particle gel (c).

The estimates of the chain lengths and general properties of the molecular weight distribution of alginate [127, 128] indicate that longer alginate chains can join two or more oleosomes. This will depend on the chain and block lengths for the uncharged units at certain concentrations. The fraction of longer chains form entanglements and provides additional stability to the aggregates (Fig. 4.7a). These partially covered oleosomes can form small aggregates, which join into larger clusters (Fig 4.7b). Thus, the clusters can form alginate-mediated soft particle networks (Fig. 4.7c).

For >0.025 wt% alginate, microscopic images (Fig. 4.4 d-f) show that clusters become smaller as alginate content increases. Accordingly, the peak around 10 µm decreased, and the peak around 0.350 µm increased, which corresponds to intact oleosome droplets (Fig. 4.4f). The disappearance of these big clusters is also related to the decrease in *v* and *B*, and are visually reflected in the disappearance of transparent supernatant at 0.125 wt% alginate (Fig. 4.3a). This behavior suggests that oleosome droplets start to be re-stabilized by the increasing amount of alginate polymer chains. It is likely that at >0.125 wt% alginate, the concentration is sufficient to cover the droplet surfaces. This behavior is typical for interacting flexible polysaccharides which increase the stability of protein-coated oil droplets by forming protective interfacial multilayers [117].

Demixing in xanthan-oleosome mixtures presented a different behavior (Fig. 4.3b). At zero xanthan concentration, a homogeneous sample was observed (Fig. 4.8a), and no serum separation was observed within the first minutes. When xanthan was present at low concentrations, serum separation started early in the first minutes after preparation (Fig. 4.3b, d). In microscopy images, it can be observed that slightly flocculated oleosome droplets and the presence of large and irregularly shaped structures become more noticeable as xanthan content increases (Fig. 4.8c-f). In confocal microscopy pictures (Fig. 4.9a, b), xanthan 0.05 wt% showed similar irregularly shaped structures as observed in both 2D and 3D projection scans. It is well documented that xanthan induces microscopic and macroscopic phase separation when in combination with other colloidal systems [129, 130]**.** Depletion flocculation phenomena and geometric

incompatibility are possible mechanisms that could lead to phase separation [131-133]**.** Xanthan promotes flocculation by a depletion mechanism in which xanthan molecules are not entirely absorbed at the particle interface but are partially repelled from the region between the droplets. This causes the droplets to continue to approach each other, resulting in weak aggregation. However, interactions between the oleosome surface and the xanthan molecules occurred, albeit not extensively as observed in the ζ- potential values (Fig. 4.1b). Similarly, confocal microscopy images show that xanthan can interact with oleosome surfaces as observed by the white arrows in Fig. 4.9a. These arrows depict increased intensity in fluorescence, which may indicate oleosomes droplets on the borders of xanthan molecules.

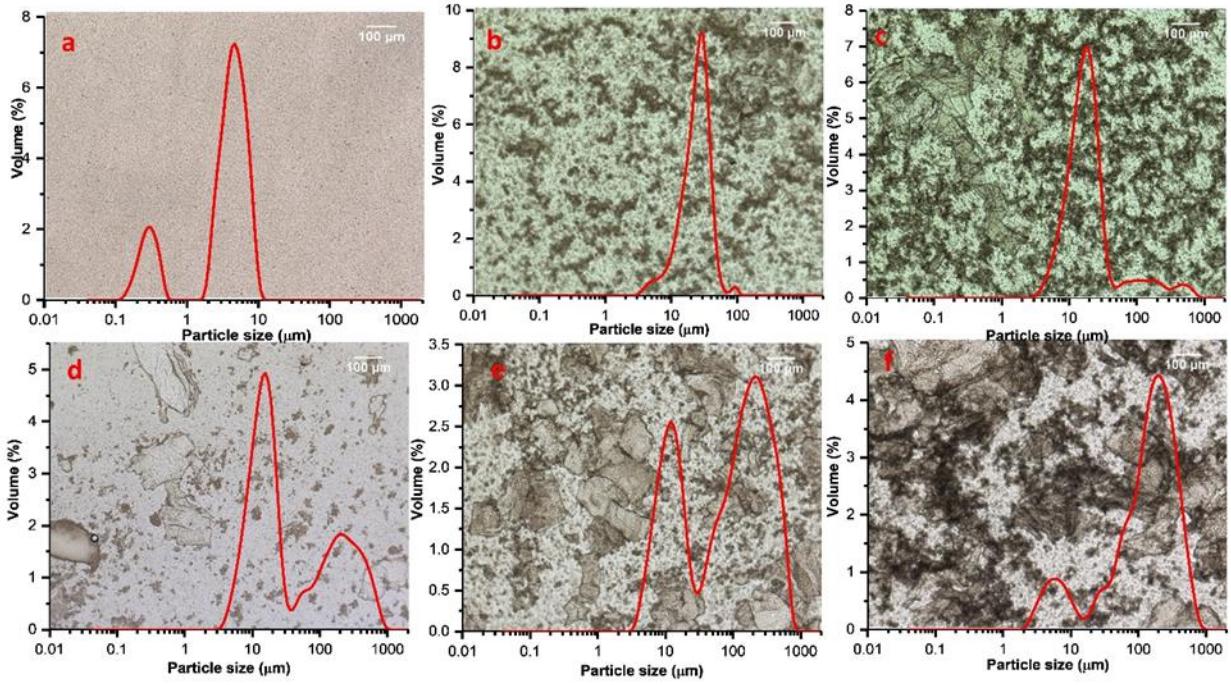

Fig. 4. 8 Optical microscopy images Oleosome 5 wt% - Xanthan gum after being adjusted to pH 4.00 combined with Particle size distributions of the same sample. a) 5 wt% Oleo- 0 wt% Xanthan b) 5 wt% Oleo- 0.0025 wt% Xanthan c) 5 wt% Oleo- 0.025 wt% Xanthan d) 5 wt% Oleo- 0.01 wt% Xanthan e) 5 wt% Oleo- 0.125 wt% Xanthan f) 5 wt% Oleo- 0.175 wt% Xanthan.

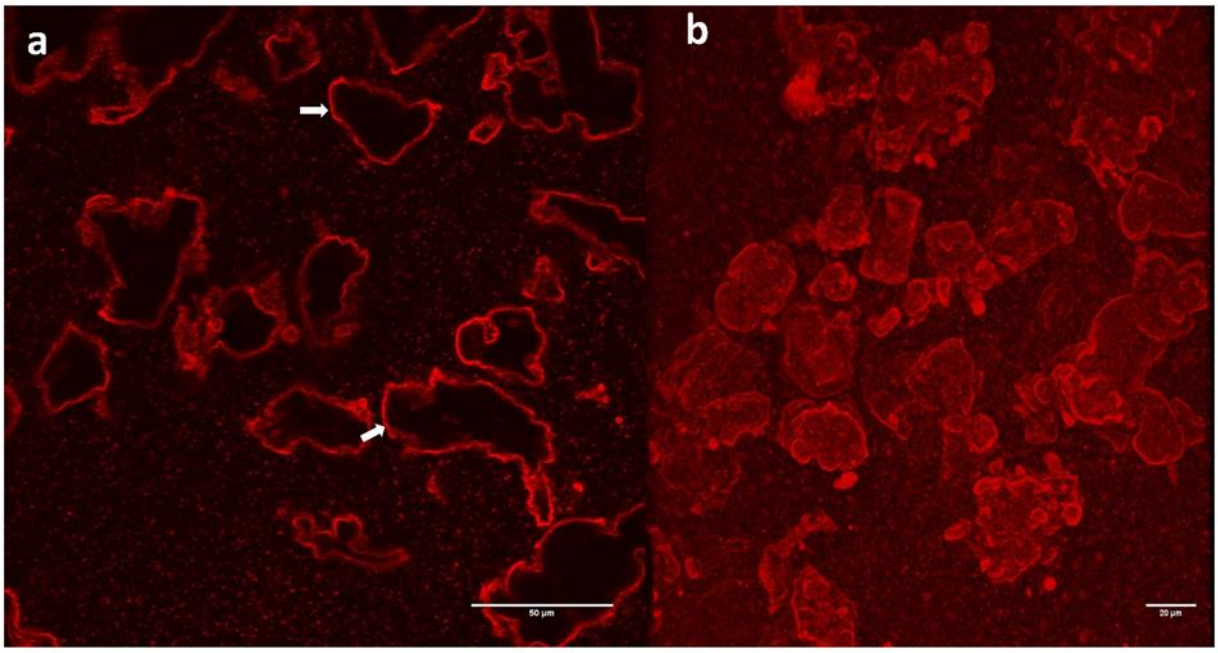

Fig. 4. 9 Confocal micrographs of a) 5 wt% Oleosome- 0.05 wt% Xanthan. White arrows indicate presence of oil bodies at the interface of xanthan molecules b) 3D Project of sample 5 wt% Oleosome- 0.05 wt% Xanthan.

This limited interaction between xanthan and oleosome droplets may discard depletion as the primary mechanism for flocculation in this system. It is more likely that xanthan gum induces phase separation due to geometric incompatibility. Phase separation can readily occur in a binary mixture of isotropic particles (such as spherical oleosome droplets) and anisotropic particles (such as rod-like xanthan molecules) [134]**.** This incompatibility becomes more favorable than electrostatic interactions and becomes more pronounced when the length-to-diameter ratio of the rods increases, as in the case of xanthan gum. Xanthan-induced-phase separation caused by geometric incompatibilities agrees with earlier theories [134]**.** However, the presence of loose oleosome aggregates in xanthan-containing mixtures questions whether this flocculation is due to depletion mechanisms to a certain extent. Usually, when particles are flocculated due to depletion by a polymer, a particle network is formed [56].

4.4.2.2 Efect of xanthan concentration on flocculation behavior

A delay time, $t_{delay,}$ in supernatant separation was present in xanthan-containing mixtures and it increased at increasing xanthan concentrations, as observed in Table 4.2. This behavior is consistent with previous studies where high xanthan concentrations delayed the creaming of oil droplets [129]. It is likely that the large xanthan molecules, as xanthan content increases, generate a viscosity increase in the aqueous phase.

Delay time in emulsions flocculated by non-adsorbing polysaccharides has been found to scale with the aqueous phase shear viscosity, the density difference between the oil and the aqueous phase, and permeability as $t_{delay} \sim B^{-1}\eta\Delta\rho^{-1}$ [89]. Therefore, the delay time in xanthan-containing mixtures is given by the combined effect of viscosity in the continuous phase and the permeability in the droplet network. The pores within the droplet network may be too small in the first minutes to allow supernatant separation. Eventually, the pores become wider by the effect of structural rearrangements driven by gravity. This is counteracted by the viscous drag of the aqueous phase, which hinders the upward movement of droplets, and it is in agreement with v, which decreases with xanthan content. Characteristic concentrations for xanthan are critical overlap concentration (c^*) of 0.007 wt% [53] and entanglement concentration c_e of 0.01 wt% [135]. As a result, it is likely that xanthan, at the conditions above, is in the overlap regime. Therefore, viscosity in the continuous phase plays a critical role in the phase separation dynamics of xanthan-containing mixtures. Compared with 0.0025 wt% alginate, which presents v 3.90 mm/h, 0.0025 wt% xanthan presents lower v, 0.0045 mm/h, while both present similar B, 1580.44 μm^2 and 1105.20 μm^2, respectively. This means that despite showing similar network porosity (due to droplet flocculation), the flocculation rate is slower in xanthan due to its influence in the higher viscosity of the continuous phase. This suggest that the effect of xanthan on the phase separation dynamics

arises from the competing effects xanthan concentration has on geometrical incompatibility and bulk viscosity. At low xanthan concentrations (0.0025 wt %- 0.05 wt %), flocculation dynamics are dominated by the effect of geometrical incompatibility, which causes microscopic and macroscopic phase separation. At higher xanthan concentrations (>0.125 wt %), macroscopic phase separation slows due to the slower droplet dynamics caused by the increasing viscosity of the xanthan-rich continuous phase.

4.4.2.3 Effect of alginate/oleosome ratio on bridging flocculation

Figure 4.10a shows a maximum in apparent d_{43} as a function of alginate concentration at three oleosome concentrations. This maximum value occurred at the alginate concentration, which induced maximum bridging flocculation. These maximum values are plotted as a function of oleosome concentration (Fig. 4.10b), resulting in an almost perfect linear relation. This linear relation indicates that the amount of alginate to induce maximum aggregation is proportional to the surface area of the oleosome. The plot slope is 0.005, indicating a relationship of $\%c_{Alg} = 0.005 \times \%c_{Oleo}$. Interestingly, d_{43} exhibits a sharp peak at 0.005 when plotted as a function of the polysaccharide/oleosome ratio (Fig. 4.10c), which is the same value as the slope of the linear fitting. Therefore, the alginate concentration for inducing maximum bridging flocculation is linearly dependent on the oleosome concentration making the ratio between alginate and oleosome a critical condition for inducing extensive flocculation. The dependence on the polymer and particle ratio for inducing maximum flocculation if the polymer is adsorptive to the particle is characteristic of bridging flocculation mechanism. The optimum ratio between alginate polymer chains and oleosome droplets for bridging flocculation corresponds to an interfacial coverage of approximately 0.4 mg/m^2. This value is similar to those found for other anionic polysaccharides that induced bridging flocculation in protein-coated oil droplets: approximately 1 mg/m^2 for carrageenan and carboxymethylcellulose [76, 116] and 0.2- 0.3 mg/m^2 for dextran sulfate [136]. The fact that optimum bridging in alginate was closer to the values reported for dextran sulfate suggests that charge density in polysaccharides plays a critical role in bridging flocculation. Dextran sulfate is a highly charged density polysaccharide that adsorbs to a protein-coated

surface even at neutral pH values. Similarly, as observed in Fig. 4.1a, alginate adsorbed to the oleosome surface at pH 6.00.

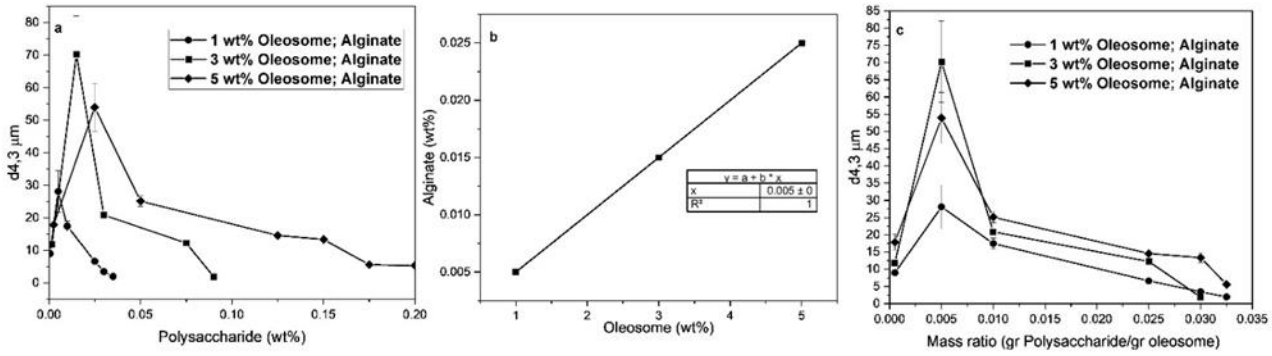

Fig. 4. 10 a) Mean particle size (d_{43}) as a function of Alginate concentration at three different Oleosome concentrations, b) plot showing alginate concentration (wt %) at maximum aggregation as function of oleosome (wt %) and an insert showing linear fitting and its parameters, c) mean particle size (d_{43}) from a expressed as a function of Polysaccharide/Oleosome mass ratio at three different Oleosome concentrations.

4.4.2.4 Xanthan-olesome flocculation mechanism

Xanthan, on the other hand, despite being an anionic polysaccharide, showed a different flocculation mechanism. As observed in the previous experiments, Fig. 4.11 shows a different flocculation mechanism in xanthan. Instead of showing a maximum particle size, it shows a gradual increase in d_{43} with an increasing concentration of xanthan (Fig. 4.11). This increase in d_{43} increase are in accordance to the large irregular structures observed in optical microscopy images (Fig. 4.8) which seem to become predominant as the xanthan content increases. It is proposed that these large structures, also observed in confocal images (Fig. 4.9), correspond to xanthan molecules that separate into local microdomains because it becomes more favorable than interacting with oleosome droplets.

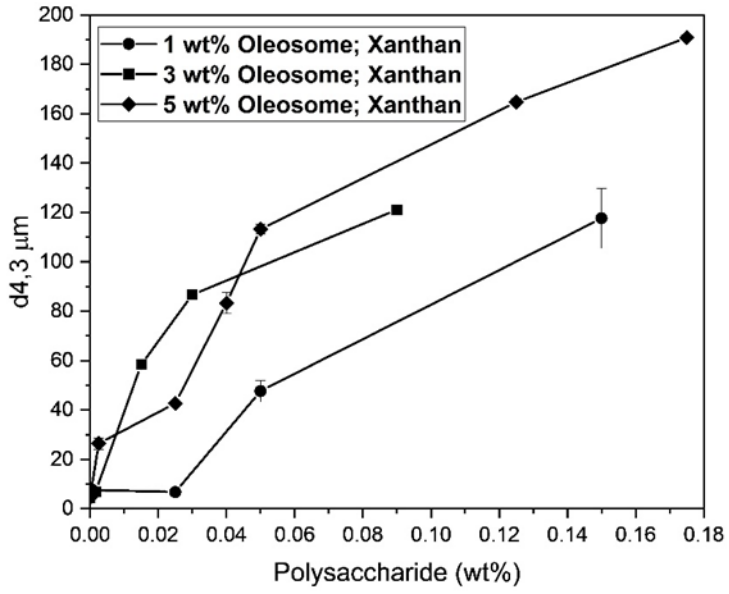

Fig. 4. 11 Mean particle size (d_{43}) as a function of Xanthan concentration at three different Oleosome concentrations.

The partial demixing in the xanthan-oleosome mixtures can be understood by considering two driving forces: Firstly, since xanthan is strongly electrostatically negatively charged, the strongly repulsive and rigid molecules can only assume very specific conformations in the dissolved state. Liquid crystalline structures are excluded because of the strong repulsion. Consequently, compromises have to be made because of the repulsion. Therefore, xanthan molecules orient themselves randomly to minimize electrostatic energy and maximize entropy *[137]*. The second point is the low adsorption tendency of the xanthan molecules on the surfaces of the oleosomes, already indicated in Fig. **4.**2, which is also due to the high chain rigidity.

As a consequence of the electrostatic attraction, xanthan-mediated aggregates of oleosomes can form, but these have a much poorer cohesion than those with alginate. Clustering, or even the formation of a particle network, as indicated in Fig. **4.**7, is largely excluded. For entropic and energetic reasons, only more narrowly confined domains of oleosome-xanthan phases remain stable, while the xanthan molecules not adsorbed (on oleosomes) separate from them, as shown in the red and black regions by confocal microscopy shown in Fig. **4.**9b. These considerations lead to the model shown in Fig. 4.12.

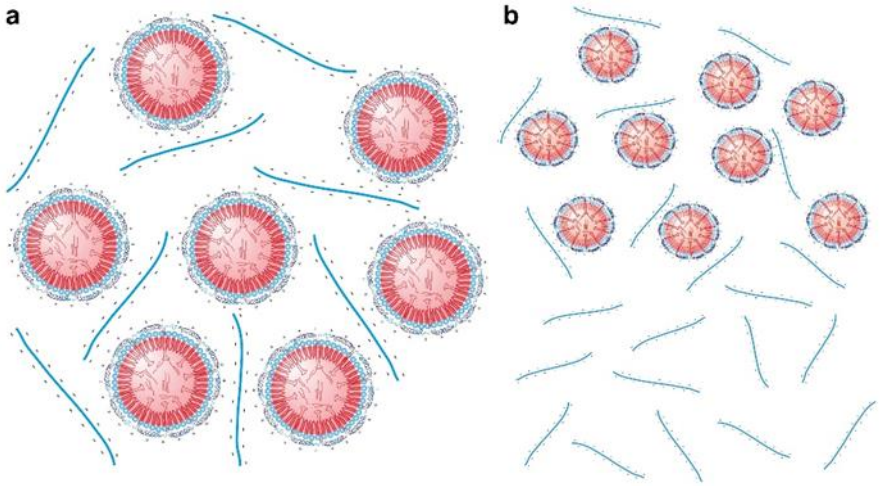

Fig. 4. 12 Small droplets in between xanthan form loosely bound aggregates (a). Only a small number of xanthan molecules can adsorb on the oleosome surfaces. The aggregates are not stable at larger size, therefore a depletion flocculation occurs (b).

An additional limiting factor in the size of the xanthan oleosome aggregate is their net surface charge, which depends on the local arrangement between xanthan and oleosomes. The larger the aggregates are, the larger becomes their net surface charge. Rayleigh instabilities will limit the size of the loosely bound aggregates [138, 139], another factor of provoking depletion flocculation.

4.4.3 Characterization of compacted gels obtained upon densification of flocculated emulsions

Flocculated polysaccharide-oleosome mixtures were centrifuged to compact the droplet network and analyze the resulting materials. As observed in Fig. 13b, alginate-containing mixtures at optimum bridging ratio (0.005 g/g) presented a compact and self-supporting gel upon centrifugation, which corresponds to an oleosome content of about 46 wt%. Figure 4.14 showed that higher and lower alginate/oleosome ratios resulted in either more turbid supernatant or lesser compact gels, which indicated that polymer bridging became less effective.

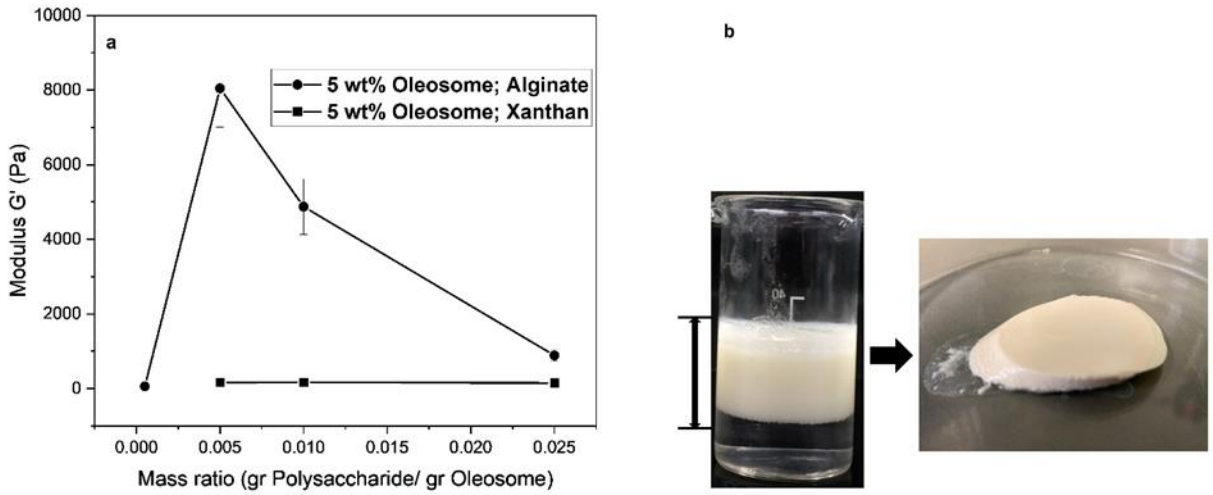

Fig. 4. 13 a) Plots of *G*' at 1% strain as a function of mass ratio for 5 wt% Oleosome b) Before (5 wt % Oleosome) and after Centrifugation (45 wt %) of 0.005 g/g Alginate showing a compact self-supporting gel.

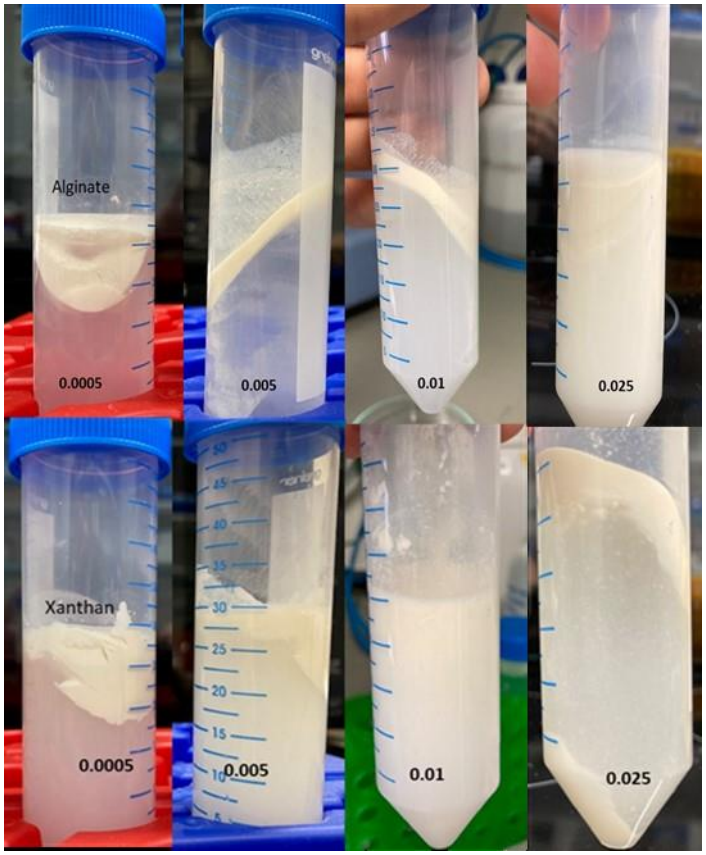

Fig. 4. 14 Polysaccharide- oleosome mixtures at different ratios upon centrifugation which depicts the separation between supernatant and a compacted cream network.

4.4.3.1 Rheological characterization of resulting materials

Figure 4.13a shows the dependence on polysaccharide/oleosome mass ratio of compacted gels with the storage modulus G' given by oscillatory rheological measurements. There is a steep increase in G' up to 8000 Pa at 0.005 g alginate/g oleosome followed by a drop at higher ratios. This maximum G' at optimum bridging ratio confirms that this ratio is fully consistent with forming a network of polymer cross-linked droplets. At increased alginate ratios, a re-stabilization occurs, and the system becomes less elastic. Figure 4.15 shows the amplitude sweep plots for compacted gels at the optimum bridging ratio (0.005 g/g) and 0.025 g/g, corresponding to the re-stabilization of oleosome droplets. At optimum bridging, the modulus is constant up to 10% strain and shows a sudden decrease at larger strains. This sudden decrease is indicative of a microscopic fracture of the gel, and it is typical of bridging-flocculated gels [89]**.** Although 0.025 g/g alginate shows a decrease of G'due to droplet re-stabilization, it still shows a gel-like response $G' > G''$suggesting the system might still present polysaccharide bridges. This indicates that the rheological properties of polymer-bridging gels can be tuned by varying alginate/oleosome ratios. Alginate/oleosome ratios close to optimum bridging (0.005 g/g) will yield compact and stiffer gels, while ratios far from the optimum ratio will yield less compact and softer gels as the number of polymer bridges may decrease.

On the other hand, the addition of xanthan did not present a transparent supernatant at any given ratio after centrifugation (Fig. 4.14)**.** When removed, the cream did not show a compact gel, but had the characteristics of a viscous cream. Rheological measurements of the collected cream suggest that the rheological response is most likely given by oleosome droplets alone since there was no significant difference in G'at the different xanthan/oleosome ratios (Fig.4.13a). This confirms that polysaccharide bridges are not present at a given xanthan content. This observation is supported in Fig. 4.14, where at 0.025 g/g can be observed the presence of sediment at the bottom of the tube. This sediment suggests that xanthan molecules were present in the continuous phase allowing them to be easily precipitated. This observation is consistent with the results of the previous sections that xanthan gum induces microscopic phase separation, with this effect becoming more pronounced with increasing xanthan concentration.

These results are strongly supported by the models presented so far. The linear modulus $\boldsymbol{G'}$ of the alginate-oleosome mixture at the optimum bridging flocculation ratio is about two orders of magnitude higher than the xanthan oleosome solution at the corresponding concentration. Moreover, Fig. 4.13a shows a higher concentration dependence for alginate than for xanthan. The high modulus for alginate-oleosome mixtures supports the idea of forming a particle-cluster network as drawn in Fig. 4.7c. The interconnected network, as confirmed by CLSM, carries stresses and shear up to 10 % deformation before the particle gel ruptures to sub-units. Then the storage modulus G' drops. It decreases as expected for larger ratios of the alginate–oleosome mixtures. Many oleosomes are already sufficiently covered with alginate; inter-oleosome bridging can no longer form on large scales. Therefore the network becomes weaker. Similar arguments explain the shorter linear viscoelastic (LVE) range for the higher concentrations. The weaker network disintegrates at lower deformations. The larger LVE range supports the presence of entanglements (compare Fig. 4.7a), which makes the densified samples more rubbery.

The relatively low modulus in xanthan-oleosome mixtures are also in line with the model proposed in Fig. 4.12. The cohesion of the clusters is significantly weaker, and the flocculated and densified solution does not support large deformation. Therefore, the LVE range becomes smaller compared to the alginate solutions. Likewise, the more pronounced hump in the loss modulus G'' is noticeable for deformations around 80% - 100% (Fig. 4.15b). Xanthan molecules become arrested in a randomly oriented state at higher concentrations and form a stable pseudo-gel [53]. Each highly stiff, rod-like molecule is stuck in a cage formed by the surrounding charged polymers and oleosomes, and only local motions and limited rotations are possible. Only higher shear deformations orient the molecules in the direction of the shear, and large-scale motion becomes possible. The slight increase of G'' can thus be attributed to the overcoming of the electrostatic energy of the cage. The almost parallel motion of the xanthan molecules requires only little energy and stress, the solution flows, and the loss modulus decreases further.

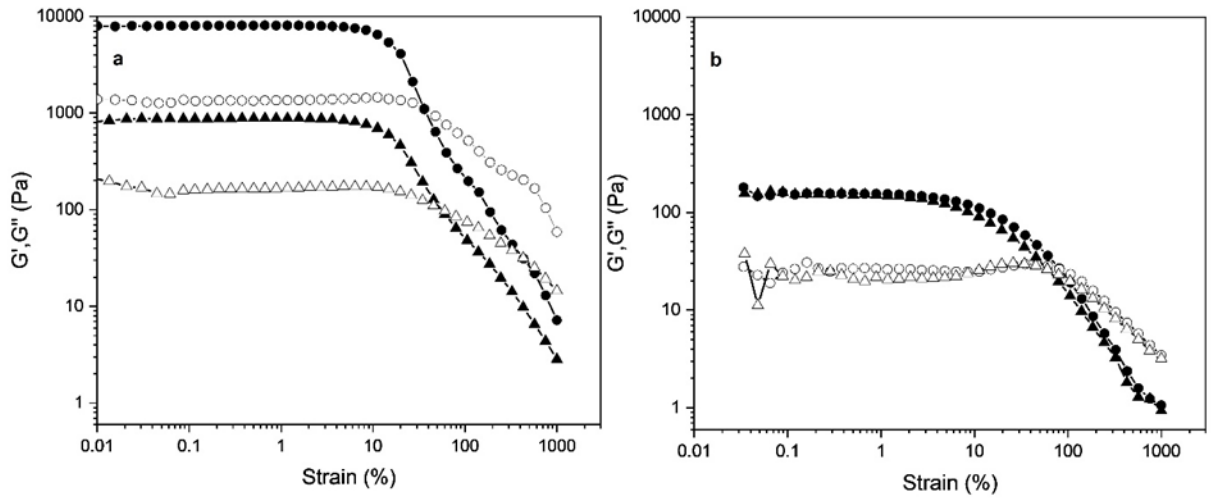

Fig. 4. 15 Oscillatory amplitude sweeps of compacted gels Oleosome content 46 wt% at two fixed polysaccharide/oleosome ratios 0.005 g /g (●) and 0.025 g/g (▲) of a) alginate and b) xanthan. *G'*: filled symbols, *G''*: open symbols.

4.5 Conclusions

This study reports the gelation of oleosome emulsions using bridging flocculation as a structuring mechanism. Polysaccharides' ability to induce bridging flocculation will depend on the configuration properties of the polymer chain, interaction strength between polysaccharide-oleosome, and the polysaccharide-oleosome concentration ratio. Polysaccharides with flexible polymer chains, such as alginate, will be effective for bridging since charged blocks of the chain will adsorb efficiently on the oleosome surface via strong electrostatic interactions. Polysaccharides with semi-flexible, almost stiff chains, such as xanthan, cannot effectively interact with the oleosome surface due to energy constraints given by its rigidity. As a result, xanthan leads to a depletion effect where phase separation occurs at different scales between xanthan and oleosomes. Alginate-driven bridging occurs efficiently at an optimum polysaccharide-oleosome concentration ratio, expressed as 0.005 g/g or 0.4 mg/m^2. This optimum ratio is characterized by an interconnected and dense droplet network, as confirmed by rheology and confocal microscopy measurements. Upon densification, bridging-flocculated emulsions lead to a compact and self-supporting soft gel characterized by fracture behavior at higher strains in oscillatory rheology. This densification process resulted in gels of about 46 wt% oleosome starting from 5 wt% oleosome. This diversity in varying oleosome concentrations and polysaccharide-oleosome ratios provides opportunities to

tune network structure and its resulting rheological properties. Generally overlooked as a gelation mechanism, bridging flocculation can be further exploited as a gelation method due to a straightforward preparation method that requires small amounts of polysaccharides and oleosome emulsion.

5 Effect of polysaccharide architecture on polymer-bridging based structuring

This chapter is based on the following manuscript:

Tunable oleosome-based oleogels: influence of polysaccharide architecture on polymer bridging-based structuring

Juan C. Zambrano, Thomas A. Vilgis

Physics of Fluids 35(2), 027131

5.1 Summary

In this chapter, we compare the bridging ability of sodium alginate with that of another flexible polysaccharide, such as ι-carrageenan, to produce polymer-bridged gels. Polymer bridging occurs over a range of polysaccharide/oleosome ratios where bridging ability is heavily influenced by the strength of binding between polysaccharide and the oleosome surface where sodium alginate presented higher bridging power than ι-carrageenan. These differences in bridging ability are associated with the different molecular architecture and physical differences between the two polysaccharides. Alginate has a co-block arrangement of charged and uncharged units. The charged units promote stronger adsorption in several parts of the oleosome surface, while flexible parts of the chain allow the bridging of several droplets. In contrast, the less flexible ι-carrageenan polymer chains are less able to bridge neighboring droplets. The difference in polymer bridging ability will influence the resulting microstructure and rheological properties. Confocal scanning laser microscopy showed that the difference in microstructure is mainly in the extent of heterogeneity over different length scales, where sodium alginate produced the most heterogeneous and largest structures. Bridging-flocculated emulsions showed the power-law scaling behavior of the storage modulus with the oleosome concentration, which was explained using percolation theory.

5.2 Introduction

Food emulsions are ubiquitous in many products, such as soft drinks, spreads, and ice cream. The oil droplets in emulsions significantly affect sensory perception of o/w emulsion-based foods since they provide, for instance, thickness and creaminess perceptions [140, 141]. Since rheological properties mainly define sensorial perceptions of o/w emulsions, it is interesting to expand the range of viscoelastic properties of emulsions. The benefits are manifold and include a broader range of possibilities in applications in the food industry, e.g., reduced-fat food products and novel formulations for non-animal-based foods. Gelation of food emulsions may result in the formation of distinct textures and can also be designed to control the release of flavor compounds by entrapping them into the oil droplets.

Using natural emulsions based on oil bodies, or so-called oleosomes, stands as an alternative to conventional methods for emulsion preparation. Oleosomes are natural particles that exist in oleaginous seeds already as pre-emulsified oil droplets. Extracted oleosomes benefits from environmentally friendly methods because they require gentle extraction by using water as the solvent medium instead of conventional oil-extracting organic solvents, such as hexane. This is also relevant to health concerns. Moreover, aqueous extraction yields oleosome particles with remarkable physical stability and sizes ranging from the nanoscale to a few μm [26], depending on the botanical origin.

From a soft matter point of view, emulsions are colloidal dispersions that can be assembled to create new colloidal structures, which may directly impact the macroscopic properties such as texture [142]. Emulsion self-assembly can be done, for instance, by modification of its surface properties that are given by a certain balance between repulsive and attractive forces. By manipulating these interparticle forces, the destabilization of an emulsion can lead to droplet aggregation, which modifies the rheological behavior of emulsions from viscous liquids to semi-solid products [92]. In conventional emulsions, it is essential to control the aggregation of oil droplets to create products with defined rheological properties. Several approaches have been previously accomplished on the controlled aggregation of emulsions: 1. *reduction of electrostatic repulsion* in protein-stabilized oil droplets by altering the pH or ionic strength to reduce the

charge on the droplets [143] ; 2. *Aggregation due to attractive hydrophobic interactions* in protein-stabilized droplets due to the effect of high temperatures on the structural conformation of globular proteins [144]; 3. *enzymatic induced aggregation* by either removing sections of the peptide chain of the proteins that leads to a reduction of steric hindrance or crosslinks between protein-stabilized oil droplets [145, 146].4. *hetero-aggregation of emulsion droplets* when two or more oppositely charged emulsions varying in droplet size, concentration, or charge density are mixed, and by the effect of electrostatic attractions, the result is the formation of micro-clusters of different rheological properties depending on the interaction strength between the oil droplets [147, 148]; 5. *aggregation by complexation of polyphenols molecules, e.g., proanthocyanidins with protein-stabilized oil droplets*, produces crosslinking of oil droplets as an effect of a broad range of specific interactions such as hydrogen bonds, hydrophobic interactions, π-π stacking, and covalent bonds [149].

Adding polysaccharides to colloidal dispersions is another effective method to control the assembly of emulsion droplets. Particles aggregate through polymer bridging if an adsorptive polysaccharide is added at concentrations below particle total surface coverage. Polymer bridging flocculation is a well-known mechanism in colloid science. It occurs when a polymer chain adsorbs on two or more particles, and attractive interactions mediate between the polymer and the particle surface, which is often electrostatic origin and of the order of hundred k_BT. As a result, a particle network is formed with relatively strong and irreversible bonds. Due to this, bridging-flocculated particles network can be exploited to design semi-soft materials that can have great flexibility to alter rheological properties. Zhao et al. previously showed the gelation of microspheres through a bridging mechanism induced by microgels [150]. However, bridging flocculation has received little attention as a gelation mechanism in food emulsions. Although studies have shown emulsions gelled by bridging flocculation produce strong gel networks [76], bridging flocculation has been referred to mainly as an instability phenomenon affecting emulsions' shelf life [92, 107].

Nevertheless, polymer bridging is a promising alternative to tailor the rheological properties of oleosomes as natural templates. In the previous chapter, it was shown that polysaccharides concentrations as low

as 0.025 wt% could produce compact self-supporting gels from oleosome concentrations of 5 wt%. Oleosomes are covered by a unique monolayer composed of phospholipids connected to a particular protein called oleosin. These proteins are unique because they have a long hydrophobic domain that is partly in contact with the oil core while deeply trapped within the phospholipids layer. The outer part of the protein is made of two amphipathic N- and C- terminals that protrude towards the aqueous phase and provide electrical charge characteristics. This charged nature of oleosomes allows them to adsorb onto their surface, charged polysaccharides from different characteristics, providing an opportunity to influence aggregation and design droplet networks with different structures and properties.

However, obtaining control over network formation is challenging. In polymer bridging flocculation, aggregate formation is determined by the interplay between the configuration properties of the polymer chains, the concentration of free polymer in the continuous phase, and the volume fraction of particles. Earlier publications [151, 152] showed that optimum bridging occurs at a certain ratio between the polymer content and oleosomes content. Structural factors in polymer chain conformation play an essential role in bridging flocculation efficiency. The above studies showed that polysaccharide surface charge is not the only factor influencing bridging flocculation but also polymer chain flexibility. Despite presenting a negative charge, xanthan gum could not induce bridging flocculation of soybean oleosomes, while alginate effectively induced bridging flocculation. This was attributed to the relative flexibility of alginate polymer chains instead of xanthan gum which is modeled as a stiff, rod-like structure.

The present study investigated the bridging mechanism of another anionic polysaccharide with flexible polymer chains, such as ι-carrageenan. It belongs to the Carrageenan family (kappa, iota, and lambda), and it is a high molecular weight polysaccharide formed by galactose units and 3, 6-anhydrous-D-galactopyransyl ring joined together by alternating glycosidic linkages. A previous study [153] found that ι-carrageenan was more effective at creating charged interfaces in soybean oleosomes than κ- and λ-carrageenan. This was attributed to the densely charged helical structure of ι-carrageenan favoring electrostatic interactions with oleosomes interface**.** It may thus be worthwhile to probe the bridging ability

of ι-carrageenan on soybean oleosomes and compare it with another anionic polysaccharide that proved effective in bridging flocculation, i.e., alginate. Both polysaccharides are similar in that they present similar molecular weight, are negatively charged, and present relatively flexible polymer chains. However, they differ in how their structural backbone is arranged, having ι-carrageenan as a repeating galactose unit, while alginate is arranged in a random sequence of blocks of D-mannuronic acid (M) and L-guluronic (G).

Therefore, the present study's focus is to compare the effect of two anionic polysaccharides with flexible chains on the bridging capacity of soybean oleosomes. In order to induce polymer bridging flocculation, electrostatic attractive interactions are triggered by gradually lowering the pH to values where both polysaccharide and oleosome become oppositely charged. The interactions between alginate, ι-carrageenan, and oleosomes over a range of pH values (3.00-8.00) are compared, followed by analyzing the effect of polymer/oleosome ratio and oleosome content on the rate of network contraction, particle size, and flocculation efficiency. Finally, confocal laser scanning microscopy (CLSM) will be used and compared to percolation gelation models. These considerations provide a consistent correlation between the rheological properties and the microstructures of the oleogels.

5.3 Materials and methods

5.3.1 Materials

Commercially available soybeans were acquired from Rapunzel Naturkost GmbH (Legau, Germany) and were used to extract oleosomes. TIC Gums, Inc (Belkamp, Md., USA) supplied sodium alginate (TICA-algin 400 Powder) for the experiments. Carl Roth (Karlsruhe, Germany) provided iota carrageenan. All solutions were prepared using distilled water.

5.3.2 Sample preparation

Soybean oleosomes extraction is based on an aqueous extraction method [77] that yields oleosomes cream free of soybean storage proteins (i.e., glycinin, β-conglycinin, Gly m BD 30K). Soybeans are ground (Vorwerk Thermomix TM31) in a 1:10 soybeans/water ratio at 10 2000 rpm for 90 s. The resulting slurry was filtered through two layers of Kimtech wipes 21 x 11 cm (Kimberly Clark), and soybean milk was

obtained. Following filtration, the pH of the milk was brought down to 11.0 with 1 N NaOH (VWR Chemicals), and 25 wt% Sucrose was added. 50 ml Roth centrifuge tubes were used to fill the solution, which was centrifuged at 15000 xg at 4 °C for at least 5 hours. The resulting oleosomes were present as an upper cream layer collected with a spoon and then re-dispersed in a 20 wt% Sucrose solution with pH adjustment (11.0). Two more washing and centrifugation steps (15000x*g*, 4°C, 5 h) were completed. The oleosome content of the resulting cream was determined by a halogen dryer and ranged between 50 - 60 wt%. The concentrated cream was used as stock to dilute emulsions. The theoretical values of the three major components of soybean oleosome were estimated according to a model developed by Huang [27]. The model calculates theoretical values of oleosome components according to the oleosome diameter size. Soybean oleosomes obtained from this protocol resulted in a 0.350 μm diameter size. As a result, the estimated amounts are as follows: 3.3% (w/w) phospholipids, 5.2% (w/w) protein, and 91.5% (w/w) triglycerides.

Oleosome emulsions were diluted with distilled water to create different concentrations (w/w), depending on the nature of the experiments. Starting from pH 7.0, dried sodium alginate and ι-carrageenan samples were added to the oleosome dispersions at different concentrations while keeping the same mass ratios (g Polysaccharide/g Oleosome). Polysaccharides/Oleosome mixtures were stirred for a minimum of 20 h at 25 °C to guarantee proper hydration. Next, the pH of the mixtures was gradually lowered to 4.0 via dropwise titration with HCl at 1.0, 0.5, 0.1, 0.01 N at a constant stirring speed (450 rpm) at 25 °C. Following pH adjustment, samples were either used immediately for further experiments or were centrifuged (5000 x*g*, 4°C, 20 min) for experiments described in 5.3.7.

5.3.3 Demixing experiments

5 wt% oleosome emulsions of alginate and carrageenan (0- 0.125 wt%) were left in sealed glass tubes at 25 °C to follow the demixing dynamics. Demixing was monitored over 18 days by visually following the cream's height as it separates from the supernatant. The emulsion samples' initial height, H_0, was 10 ± 0.8 cm. Change in cream height became more significant in the first 2 hours after preparation. As a result, data

points became less frequent after the first day. The height of the collapsing network at time t was defined $h\,(t) = H\,(t)/\mathrm{H}_0$. The rate at which the network contracts v was obtained from the demixing curves and established where the cream contraction was more significant (120 minutes). It was determined by $\Delta H(t)/\Delta t$.

5.3.4 Particle size measurements

Oleosome-polysaccharides mixtures were diluted from 5 wt% to approximately 0.5 wt% (that is, 1:10) using buffer solution (same pH 4.00 as the sample being analyzed) to avoid multiple scattering effects. The particle size distribution of the emulsions was determined using a laser diffraction particle analyzer (LS 13320 Beckmann Coulter, California, USA). Measurements were performed using a laser diode with λ= 780 nm and three Polarization Intensity Differential Scanning (PIDS) wavelengths at λ = 450, 600, and 900 nm. The data were analyzed using the instrument software applying Mie theory and using refracting indexes as follows: refractive indexes soybean oil and water 1.47 and 1.33, respectively. Four to five emulsion droplets were placed into the sampler chamber and then recirculated through the optical measurement cell. The mean particle size was reported as the volume-weighted value, d_{43}. Results were reported as the average of three measurements.

5.3.5 ζ-Potential measurements

Oleosome emulsions of 0.2 wt% were created by diluting concentrated cream stock, and the same procedure in 5.3.2 was repeated (polysaccharide addition, pH adjustment to 4.0) while maintaining the same ratios from the other experiments. Diluted emulsions were injected directly into the measurement chamber of a particle electrophoresis instrument (Malvern Zetasizer Nano Z) that measures the direction and velocity of droplet movement in the applied electric field. An individual ζ-potential measurement was determined from the average of 3 readings taken on the same sample.

5.3.6 Microscopic imaging

5 wt% polysaccharides-oleosomes mixtures from 5.3.4 were observed in parallel by optical microscopy using a Carl Zeiss Axio Scope.A1 microscope (Carl Zeiss AG, Oberkochen, Germany). Images were

captured by using transmission bright field microscopy with the objective lenses magnifying 10×. ImageJ software was used to insert the scale bar. A drop of the emulsion was placed on a microscope slide and then covered with a cover slip. Confocal laser scanning microscopy (CLSM) was used to analyze the microstructure of bridging flocculated emulsion for 20 wt% Oleosome. CLSM was performed using a Zeiss Axiovert 200M (Oberkochen, Germany). Nile Red at 1 mg/ml, a fluorescent label excited at 543 nm with a Helium-Neon laser, was added in a 1:2000 ratio to stain the oil core of the oleosome droplets. 500 µL of the different mixtures were placed inside 8 well-chambered borosilicate coverglass systems (Nunc Lab-Tek, Thermo Fisher Scientific, USA). The obtained CLSM images were analyzed using the "ImageJ" software package.

5.3.7 Bridging efficacy of polysaccharides

Polymer-bridged gels, upon densification, were collected and quantified to analyze the bridging efficacy of alginate and carrageenan. After centrifugation, the transparent supernatant was decanted, and the compacted cream gels were collected and immediately weighed for determination of the concentration in the gel. The concentration in the cream (oleosomes), C_g, is then given by

$$C_g = \frac{X1}{X2} C_e \qquad (5.1)$$

,where C_e is the initial concentration of oleosomes before centrifugation, X_1 is the amount in g of the initial oleosomes dispersion, and X_2 is the amount in g of the concentrated oleosomes cream after centrifugation.

5.3.8 Rheological measurements

In order to investigate their resulting viscoelastic properties, oscillatory rheology was performed on the bridged-flocculated emulsions from 10 - 40 wt% Oleosome. Measurements were performed with a Bohlin Instruments Gemini 200 rheometer (Malvern Panalytical Ltd., Malvern, UK) equipped with a 25-mm parallel plate geometry. The gap size was adjusted stepwise to the thickness of the gels until the load in the force was detected, leading to gap sizes between 1000 – 1500 µm. After loading, a 5-minute waiting period at 25°C was used to allow the sample's structure to relax before the measuring process began. Oscillatory

amplitude sweeps were performed by increasing the strain logarithmically from 0.01 to 1000% at 1 Hz. All measurements were performed in triplicate at 25°C from different batches, and all samples were prepared individually.

5.3.9 Characterization of polysaccharides

The molecular conformation of Sodium alginate and Iota Carrageenan was determined by gel permeation chromatography combined with multi angle light scattering (GPC-MALLS). Polysaccharides were dissolved in 0.1 M $LiNO_3$. Measurements yielded distributions of molecular mass, M_w and radius of gyration, R_g. The measurements also provide ζ-potential values at pH 7.0 by dissolving both polysaccharides in phosphate buffer. Averages are given in Table 5.1.

Table 5.1 Molecular characterization of alginate and carrageenan. M_w is the weight averaged molecular weight, surface charged expressed by zeta potential measurements at pH 7, R_g is the radius of gyration

Polysaccharide	**M_w (g/mol)**	**Surface charge (mV)**	***R_g (nm)***
Sodium alginate	250000	-55.19± 8.29	62
Iota Carrageenan	300000	-28.36± 10.49	63

5.3.10 Theoretical models describing gelation

Particle gels systems usually show a power-law scaling behavior between the storage modulus G' and the concentration, *c*, of dispersed particles *[81]*. Therefore, they can be described using different gelation models to give information on the type of deformation within the emulsion droplet network originating from the type of droplet-droplet interaction *[81, 154, 155]*. Percolation theory is known for its general applicability in particle gel systems e.g., colloidal particles, protein gel systems, and bridging-flocculated systems *[80, 87-89, 156]*. The percolation model shows a critical percolation threshold, c_p, which has been shown to be dependent on the polysaccharide type (e.g. charge distribution) and also to parameters that affect molecular interactions, e.g. pH, ionic strength *[80]*.

For random percolating systems the elastic shear modulus shows a scaling law as shown in Eq. (5.2)

$$G' \propto (c - c_p)^t \quad (5.2)$$

Where c is the oleosome concentration, c_p is the critical percolation threshold concentration and t an exponent. The exponent t depends on the type of forces between network elements that leads to the elastic rigidity of an irregular (particle) network where it can range from central stretching forces to bond-bending forces [89].

5.4 Results and discussions

5.4.1 Flocculation characterization of polysaccharide-oleosome mixtures

5.4.1.1 Demixing behavior and microstructural properties

Curves of the process of network contraction are shown in Fig. 5.1. In the absence of polysaccharides, the oleosome dispersion remains stable until 10^4 minutes, when the cream collapses. As suggested in Zambrano et al. 2023, this type of demixing indicates the gradual increase of the size of the flocs, which causes sufficiently large flocs to cream faster as a result of density difference according to Stokes law [157]. At 0.0025 wt%, alginate and carrageenan-containing mixtures present similar rates of network contraction, but network contracts to a greater extent in alginate-containing mixtures (Fig. 5.1a). Fig. 5.1c shows the presence of oil on top of the cream network indicating signs of droplet coalescence. Carrageenan-containing mixtures presented no signs of droplet coalescence, suggesting that a more stable droplet network is formed. Both carrageenan and alginate oleosome-containing mixtures present instant flocculation at 0.025 wt% shortly after pH adjustment to 4.0. This is reflected in the short time frames at which the network contracts in the first minutes after preparation (Fig. 5.1a, b). Optical microscopy images also show large and heterogenous aggregates for both polysaccharides at 0.025 wt% (Fig. 5.3 b,g). Intensive aggregation at 0.025 wt% alginate indicates polymer bridging, which corresponds to a mass ratio of 0.005 g/g (g polysaccharide/g oleosome). As observed previously [151, 152], 0.005 g/g corresponds to the ratio where optimum bridging occurs for alginate. Carrageenan induces a similar bridging mechanism, while the maximum bridging ratio also seems to be around 0.005 g/g. However, when comparing network contraction rates (v) (Fig. 5.2c), carrageenan showed lower v, 10.20 mm/h, than alginate, 18.33 mm/h indicating a

seemingly less intense aggregation in carrageenan. This observation is also reflected in Fig. 5.2, which shows a closer look at the gel heights over time at the two ratios that present intense aggregation, 0.005 g/g, and 0.01 g/g. It can be observed that the network compresses to a lesser extent in carrageenan-containing mixtures for both ratios, being more evident at 0.005 g/g, where there is a significant difference in network height between alginate and carrageenan-containing mixtures. At 0.01 g/g oleosome, on the other hand, *v* is higher in carrageenan-containing mixtures (4.80 mm/h) than in alginate-containing mixtures (1.91 mm/h), indicating a greater extent of aggregation.

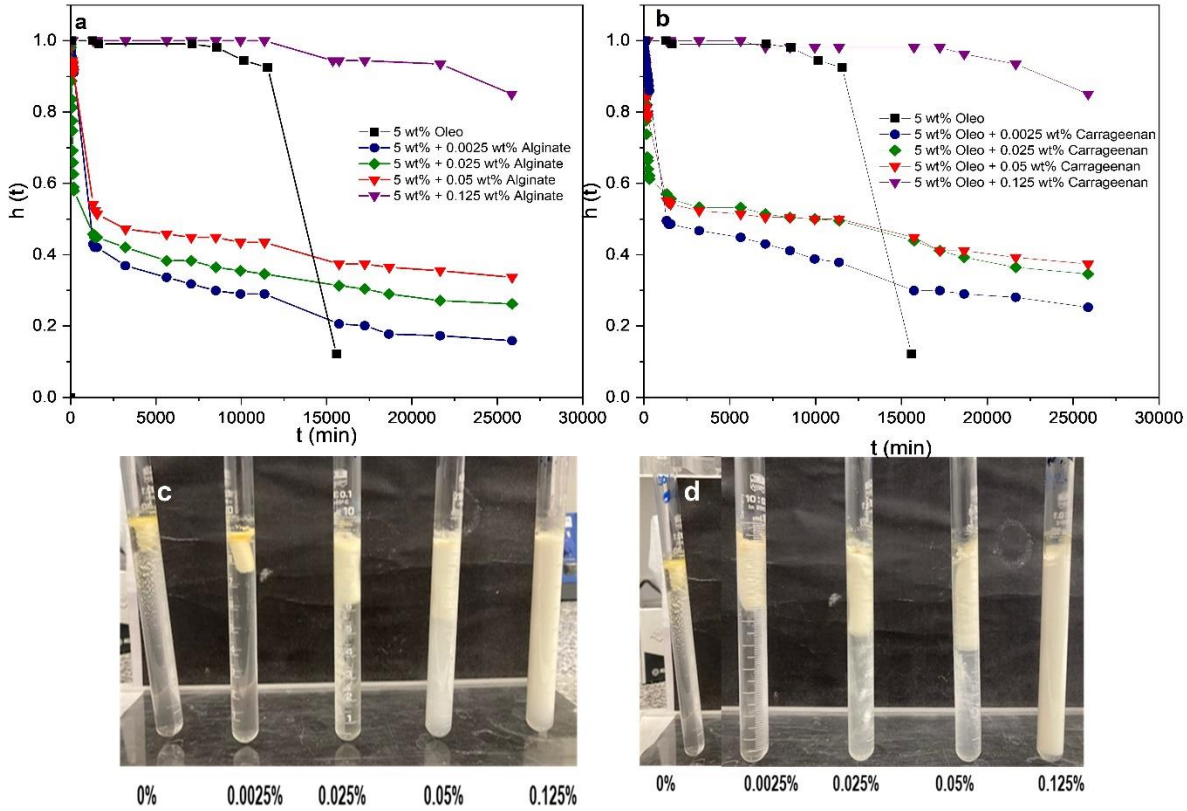

Fig. 5. 1 Demixing experiments of 5 wt% Oleosome with different polysaccharide concentrations after being adjusted to pH 4.00. a) Plot of network height, *h(t)*, versus time of alginate-containing mixtures b) Plot of network height, *h(t)*, versus time of carrageenan-containing mixtures c) Visual appearance of alginate-containing mixtures after 150 min d) Visual appearance of carrageenan-containing mixtures after 150 min.

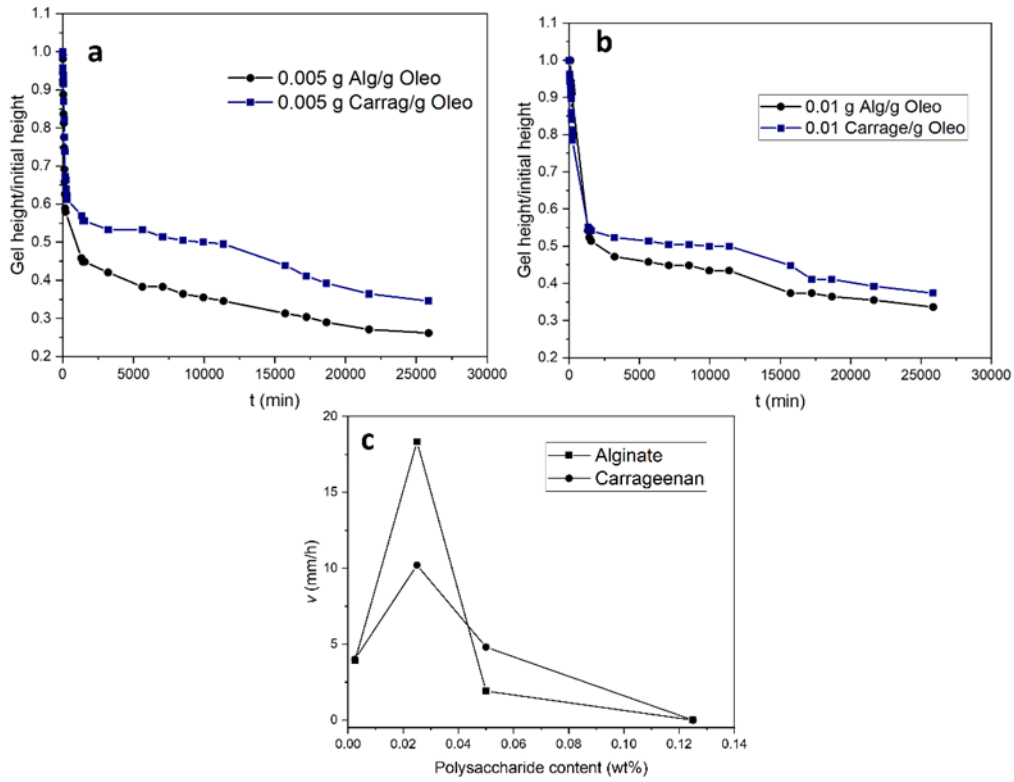

Fig. 5. 2 Comparison of network height versus time at two ratios of alginate and carrageenan. a) 0.005 g polysaccharide/ g oleosome b) 0.01 g polysaccharide/g oleosome. c) Network contraction rates (*v*) extracted from Fig. 5.1a, b.

This agrees with microscopy images where larger aggregates are observed for carrageenan-containing mixtures compared to alginate at 0.05 wt% (0.01 g/g) (Fig. 5.3c, h). Aggregates in alginate-containing mixtures instead start to be less dominant at >0.05 wt% (Fig. 5.3d-e). Figure 5.1c shows 0.05 wt% alginate presenting a turbid supernatant indicating that alginate polymer chains stabilize some oleosome droplets. In contrast, 0.05 wt% carrageenan presents a transparent supernatant suggesting that at this ratio, all oleosome droplets are still effectively bridged by the carrageenan polymer chains. This indicates that polymer bridging in alginate becomes less effective at 0.01 g/g, and carrageenan can still bridge oleosome droplets at 0.01 g/g. On the contrary, carrageenan seems more effective at stabilizing oleosome droplets as observed in Fig. 5.3i, where at 0.125 wt%, aggregates completely disappear. In comparison, alginate still shows the presence of separate clusters at 0.125 wt% (Fig. 5.3d). This is also observed in particle size distribution where the peak around 0.350 µm, indicating intact oleosome droplets, becomes more

predominant in carrageenan at earlier concentrations than in alginate 0.125 wt%, 0.175 wt% (Fig. 5.3e-d, i-h). This indicates that carrageenan is more effective at fully covering the oleosome surface at lower concentrations than alginate, despite presenting a decreased bridging ability compared to alginate. These results can be attributed to the different physical properties of the alginate and carrageenan chains.

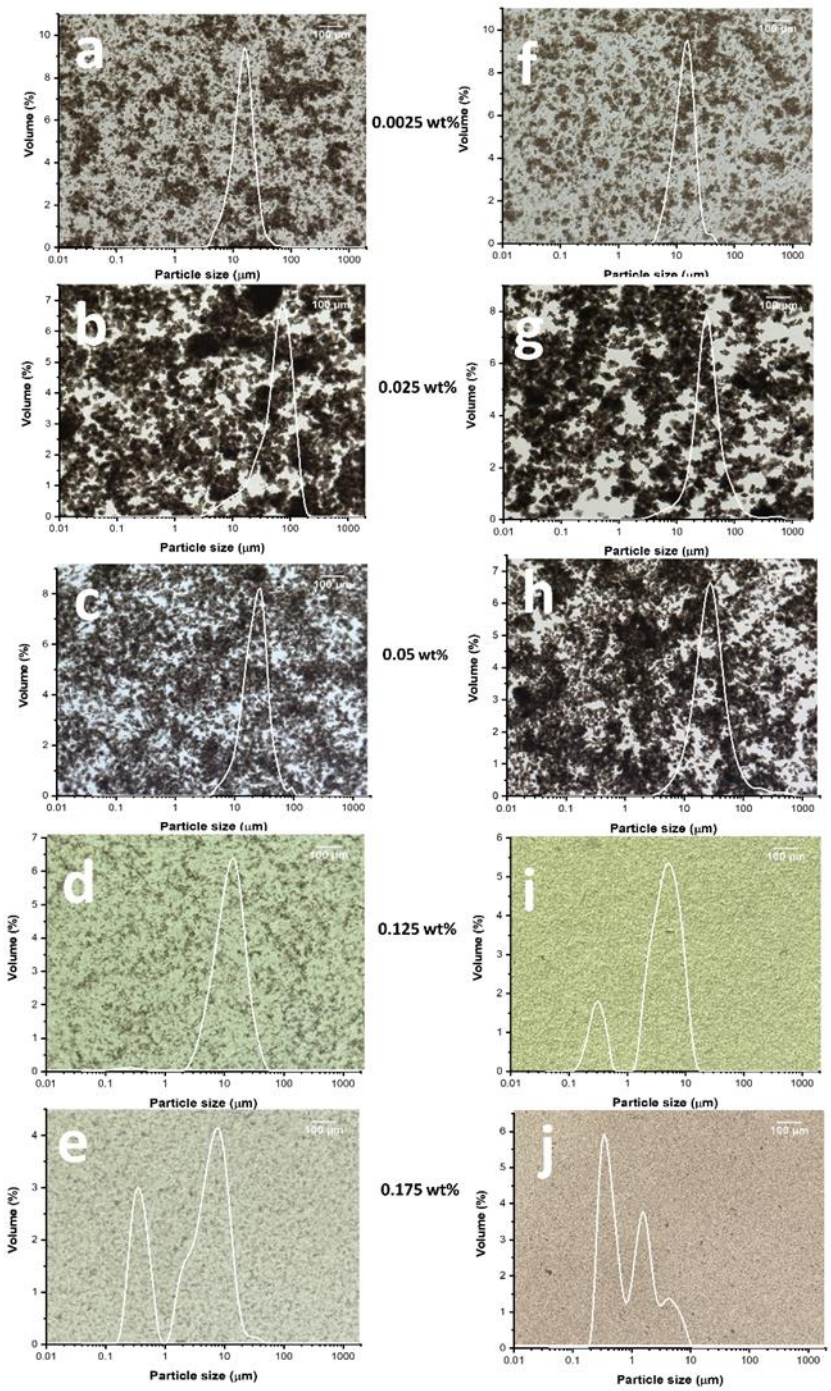

Fig. 5. 3 Optical microscopy images Oleosome 5 wt% at different polysaccharide concentrations after being adjusted to pH 4.0 combined with particle size distributions. In a-e, emulsions contained different concentrations of Alginate. I f-j, emulsions contained different concentrations of ι-carrageenan. Scale bar: 100 μm.

5.4.1.2 Polymer physics analysis

The structural differences between alginate and carrageenan chains require some attention. Alginate is a block polyelectrolyte composed of charged guluronic and polar mannuronic acids, whereas carrageenans are uniformly charged along their chains. The charged blocks in alginate, shown as blue zig-zag lines in Fig. 5.4, can be seen as relatively stiff due to the guluronic acid's chemical structure and bonds. The mannuronic and mixed (polar) blocks (shown as grey lines) are very flexible.

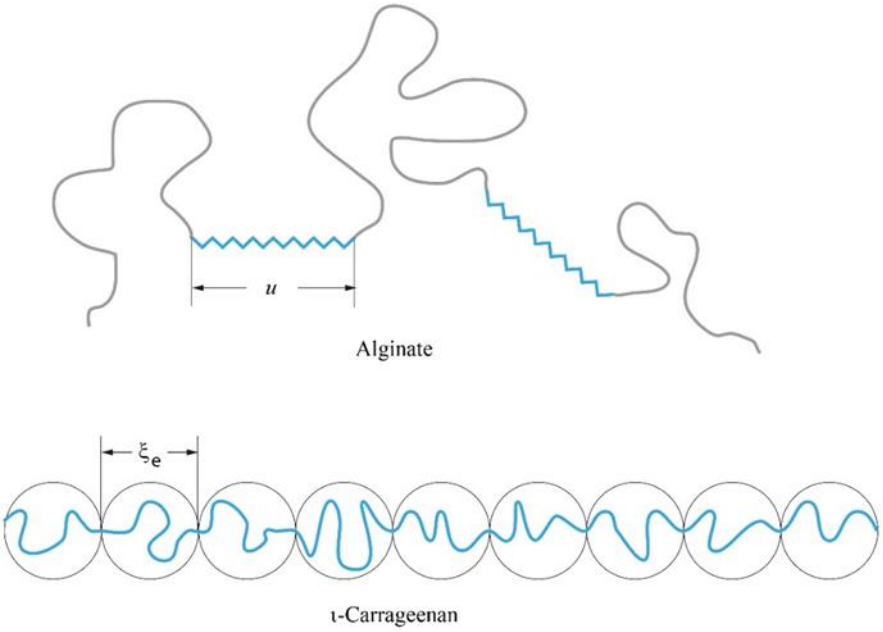

Fig. 5. 4 Simple models of the physical properties of alginate and carrageenan. In alginate only the guluronic blocks (shown in blue) can be charged, the polar blocks behave as flexible chains in good solvents. Carrageenans are weakly charged polyelectrolytes in good solvents, illustrated in a simple blob-model based on scaling ideas [118].

For the sake of simplicity, the conformation of carrageenan is described by simple models for polyelectrolytes, as suggested some time ago by de Gennes [118]. Not every monomer can release its counter ion, which means that the chain pieces between the charges are coiled for entropic reasons. The balance between the electrostatic repulsive forces and the entropy loss by stretching yields the blob model suggested in Fig. 5.4. The chains are stretched on large scales, whereas inside the blobs the chains are coiled. The electrostatic blob size ξ_e depends on the charge fraction f, the Bjerrum length l_B. Simple scaling

estimates suggest, for example, $\xi_e \cong \left(\frac{l_B f^2}{b}\right)^{-1/3}$, where b is the effective monomer size. The "chain of blobs" is consequently stretched, as shown in Fig. 5.4.

The primary mechanism of the adsorption of the different polysaccharides, as shown in Fig. 5.5, depends on their architecture and physical properties. Due to electrostatic interactions, the negatively charged alginate blocks adsorb strongly on the positively charged oleosome surfaces. The polar (uncharged) blocks, which separate the charged blocks allow for many degrees of freedom. The overall flexibility of alginate is thus high. According to Table 5.1, the mean molecular weight of carrageenan is about 300.000 g/mol, which yields about 300 monomer units, which implies chains around 20 electrostatic blobs in a very rough estimate, by assuming the Bjerrum length of about 0.7 µm and 0.9 µm (in water). The values shown in Table 5.1 suggest the blobs have a size of about 5 nm (assuming the Kuhn length is about 10 monomers). Of course, these estimates are very crude, but the results allow to understand the observer experimental differences between alginate and carrageenan more consistently.

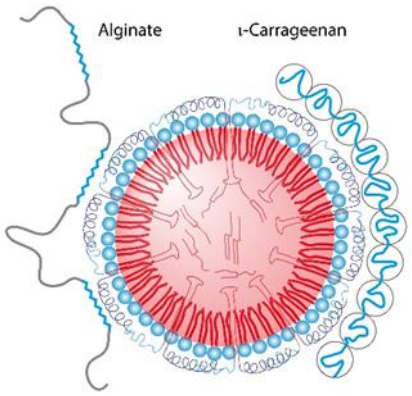

Fig. 5. 5 Alginate and ι-Carrageenan adsorb differently on the oleosome surface (drawn not to scale). Carrageenan gains most energy, when the chain of blobs bends according to the oleosome surface, without losing much entropy.

Carrageenan is represented as a chain of blobs but is less flexible on a larger scale, $r > \xi$. By bending according to the oleosome surface, it adsorbs strongly. As a result, it neutralizes parts of the oleosome charge, as illustrated in Fig. 5.5. Therefore, oleosomes can be easily coated in monolayers at appropriate

carrageenan concentrations but are bridged less effectively by carrageenan, especially when the chains are not sufficiently long. This naïve idea suggests a weaker tendency to form strong flocculated clusters, in contrast to alginate chains. Another consequence of the different basic structures is worth mentioning, which becomes important for the mechanical and rheological properties of solutions and gels containing these polymers and oleosomes. Because of the strong electrostatic repulsion, carrageenan chains will (at normal concentrations and without added monovalent salts) not be able to entangle at concentrations larger than the overlap concentration c^* [158, 159]. On the contrary, alginate chains can, especially within the neutral blocks [160, 161]. The viscoelastic properties of the solution will be different already at this simple level, as illustrated in Fig. 5.6.

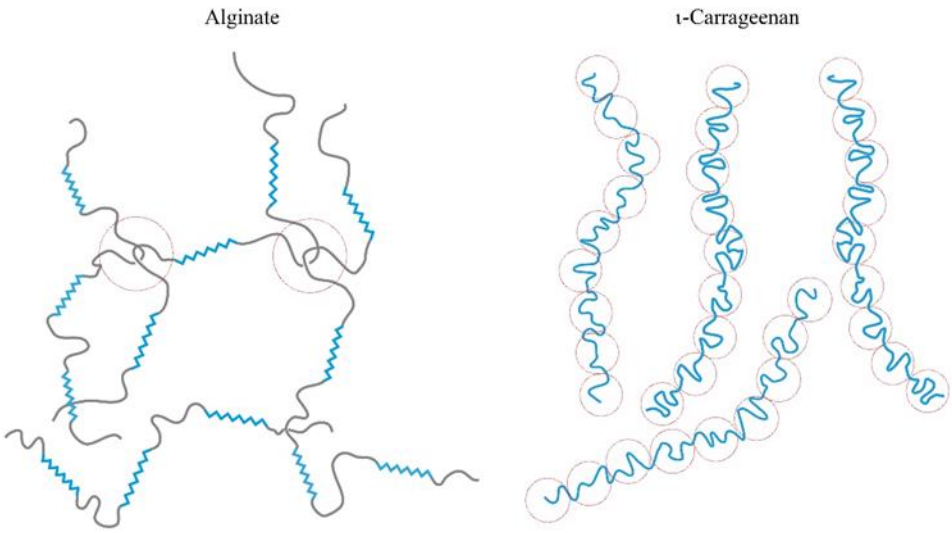

Fig. 5. 6 Conformation of chains in alginate and ι-carrageenan solutions. Alginate chains are assumed to be able to form entanglements (red circles) at the polar, flexible blocks in concentrated (calcium free) solutions. The negative charges (visualised by the electrostatic blob diameter) prevent the formation of entanglements in Carrageenan. The closer the blobs come, the stronger is the Coulomb repulsion between the charges.

Entanglements are topological restrictions. Thus they act at specific time scales and deformations as temporary crosslinks [162]. These points will become important, as it is demonstrated in the following sections.

5.4.2 Bridging flocculation characterization

Figure 5.7a, b shows the summary of mean particle sizes, d_{43}, as a function of polysaccharide/oleosome mass ratios at three different oleosome concentrations. The plots show prominent peaks in d_{43}, reflecting the ratio at which optimum bridging occurs, followed by a drop at higher polysaccharide/oleosome ratios indicating droplet re-stabilization. It can be observed that, in general, alginate-containing mixtures showed larger d_{43} values than carrageenan-containing mixtures. On the other hand, alginate-containing mixtures present three sharp peaks centered at 0.005 g/g, while the largest d_{43} in carrageenan-containing mixtures does not show a single peak centered at one specific ratio; instead is expanded between 0.005 and 0.01 g/g. This greater width of the flocculation peak in carrageenan indicates a weaker binding affinity of the carrageenan polymer chains with the oleosome interface. In previous studies [116, 163], it was also found that a broader flocculation peak by bridging polymers indicates weaker interfacial interaction between polysaccharide and droplet surface. These observations are aligned with previous demixing plots and indicate that carrageenan may produce less intense bridging than alginate. These issues are analyzed further in Fig. 5.7c, where the polysaccharide concentration plotted at which maximum aggregation occurred at the different oleosome concentrations. It can be clearly observed that alginate produces a perfect linear regression fit (R^2=1.0), while carrageenan presents a lower value (R^2=0.84). The relatively low value for carrageenan, however, is largely due to the limited amount of polysaccharide/oleosome ratios studied, rather than a true discrepancy. The slopes of the linear fitting result in 0.005 and 0.01 for alginate and carrageenan, respectively, agreeing with the polysaccharide/oleosome ratios discussed above. The difference in optimum ratios for bridging flocculation confirms that carrageenan is less efficient than alginate for polymer bridging, as more carrageenan polymer chains are needed to flocculate the same amount of oleosome droplets. These ratios correspond to an interfacial coverage of approximately 0.4 mg/m^2 and 0.8 mg/m^2 for alginate and carrageenan, respectively. These values for carrageenan are in agreement with other findings for bridging-flocculated emulsions [116], while for alginate, the value is closer to bridging-flocculated emulsions induced by highly charged polysaccharides such as dextran [136].

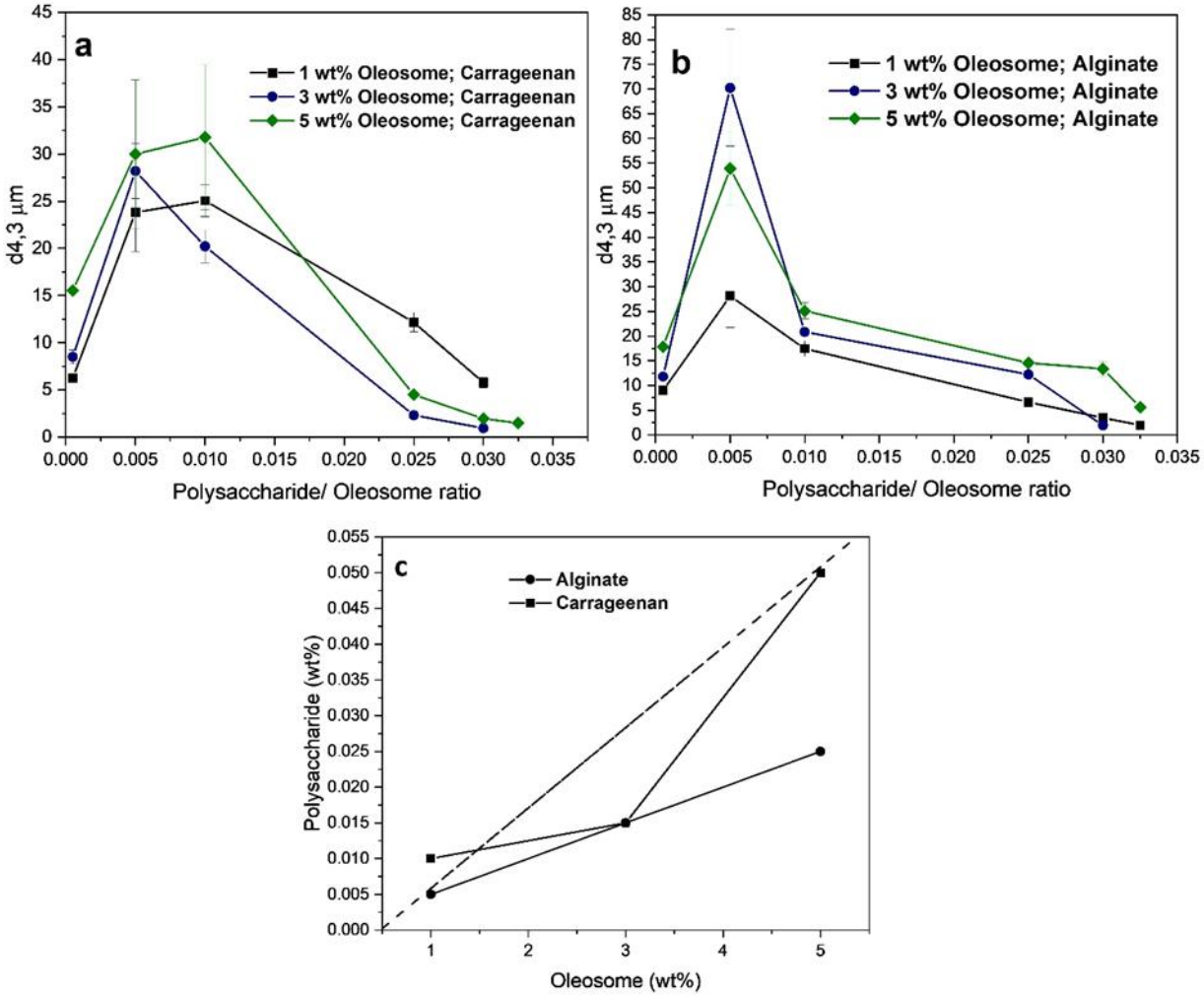

Fig. 5. 7 Mean particle size (d_{43}) as a function of polysaccharide/oleosome ratios at three oleosome concentrations. a) carrageenan-containing mixture b) alginate-containing mixture c) Plots of polysaccharide concentration (wt%) versus oleosome content (wt%) showing the concentration at which maximum bridging occurred.

5.4.2.1 Bridging flocculation efficiency of polysaccharides

A simple bridging efficiency test was performed to confirm whether carrageenan or alginate is more efficient for bridging. As bridging flocculation effectively separates the cream from the supernatant, the concentration after centrifugation is a good measure of how effectively a polysaccharide can bridge oleosome droplets. Bridging-flocculated emulsions at different initial oleosome contents were centrifuged and quantified according to Eq. 5.1. To this end, the higher the cream content (oleosomes) (wt%) after centrifugation, the more effective bridging es (Fig. 5.8). Here, the optimum bridging ratio between alginate and carrageenan ratios is compared.

At all oleosome contents, 0.005 g/g alginate yields the most concentrated gels. For example, starting at 40 wt% oleosome, alginate can yield gels of roughly 64 wt%, whereas carrageenan yields up to 57 wt%. Alginate-containing mixtures can be compacted to yield approximately 45 wt% starting at 5 wt% oleosome, while carrageenan produces about 42 wt% starting at 5 wt% oleosome. While this difference in bridging efficiency is more significant at the ratio alginate presents optimum bridging (0.005 g/g), it is less clear at 0.01 g/g as alginate becomes less efficient for bridging. The individual oleosomes are already coated, and the space for interconnecting chains is very much restricted. Carrageenan, at 0.01 g/g, yields more compact gels only at 20 wt% and 40 wt% oleosome resulting in 49 wt% and 60 wt%, respectively. Overall, alginate is more efficient in yielding more concentrated gels than carrageenan. This is expected since, as previously described, carrageenan adsorbs weaker than alginate on oleosome surfaces.

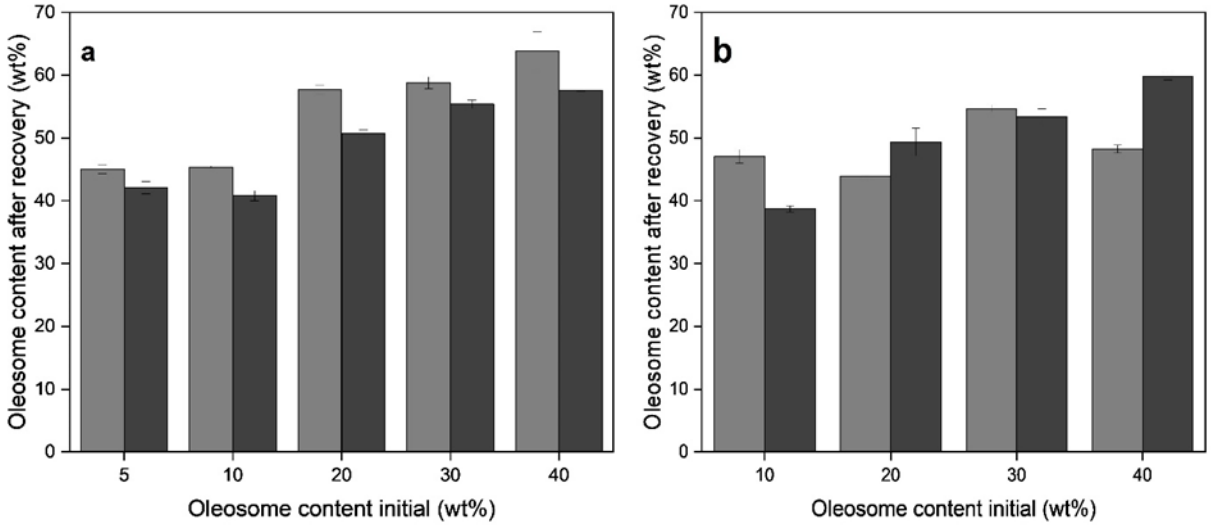

Fig. 5. 8 Bridging performance of alginate (light gray bars) and carrageenan (dark grey bars) on oleosome droplets expressed as concentration of oleosomes after centrifugation recovery (wt%) at: a) 0.005 g Polysaccharide/g Oleosome b) 0.01 g Polysaccharide/g Oleosome.

5.4.3 Effect of pH on polysaccharides adsorption

To better understand the nature of the interactions between alginate, carrageenan, and oleosomes ζ-potential measurements were performed. The addition of alginate and carrageenan to the oleosome droplets caused an appreciable change in the oleosome net charge depending on the pH and polysaccharide concentration

(Fig. 5.9a). The change in ζ- potential was calculated (Fig. 5.9b) at each pH: $\Delta\zeta = \zeta_2 - \zeta_1$, where ζ_2 and ζ_1 are the ζ - potentials of the polysaccharide-oleosome mixture and bare oleosome droplet, respectively. At pH> 6.00, the decrease in oleosome net charge is not significant as both polysaccharide and oleosome present negative charges and chances of electrostatic interactions are minor. However, it can be observed (Fig. 5.9b) that alginate decreased oleosome charge slightly more than carrageenan. Electrostatic interactions occurring at neutral pH are characteristic of highly charged polysaccharides where the polymer chains adsorb on a few positive charged patches on the oleosome-charged interface [136]. At pH 4.00, the change in oleosome charge density was appreciably more significant for both polysaccharides, which caused charge reversal of oleosome net charge from positive to negative charge density, especially for polysaccharides concentration > 0.0001 wt%. This indicates that electrostatic interactions strongly occur between polysaccharides and oleosome at the acidic range where both polysaccharides are oppositely charged. Nevertheless, alginate had the most significant overall change in oleosome net charge, as quantitatively shown in Fig. 5.9b. A significantly greater change in charge in alginate supports the idea of a considerably stronger electrostatic interaction between alginate and oleosomes when compared to carrageenan. This is consistent with the surface charge of the pure polysaccharide solutions, as alginate presented a higher charge density than the carrageenan solution (Table 5.1). Consequently, carrageenan can be considered a weakly charged polyelectrolyte [164]. However, it is essential to consider that zeta potential values are relative values that consider the electrokinetic potential at the slipping plane; therefore, it is not easy to conclude these values as the absolute surface charge of the molecules. These results show that electrostatic interactions and charge density are the driving factors that induce polymer bridging flocculation for both polysaccharides when combined with oppositely charged particles. In the presence of a pH decrease from 7.00 to 4.00, both polysaccharides interact with the oleosome interface more strongly.

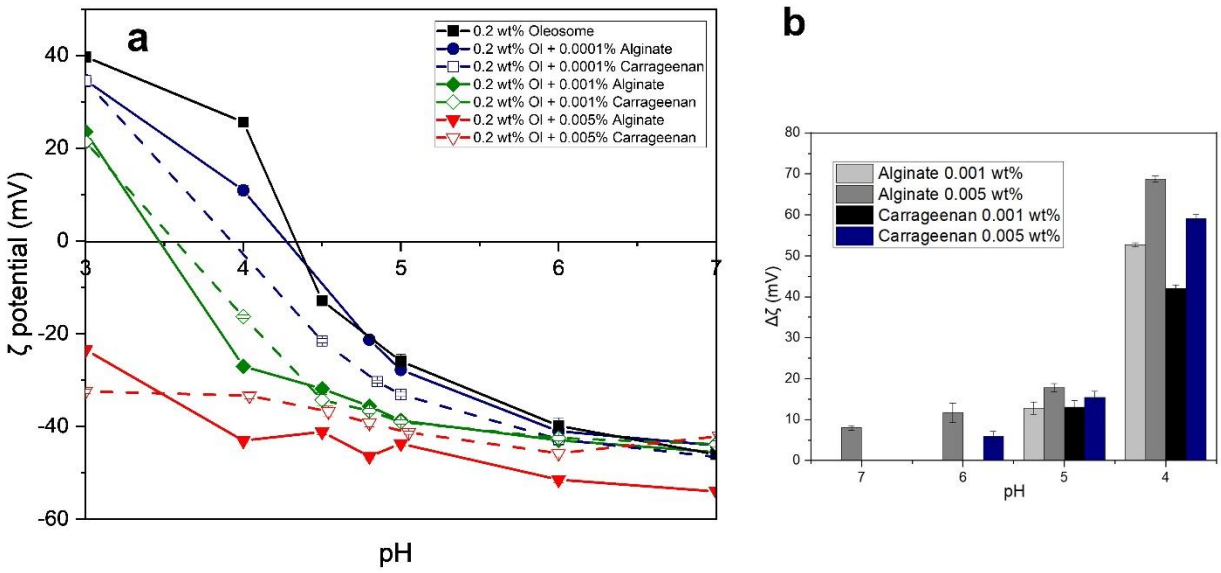

Fig. 5. 9 a) Zeta potential plots versus pH of 0.2 wt% Oleosome with different alginate and carrageenan concentrations b) the change in ζ between bare oleosome and polysaccharide-adsorbed oleosome at each pH was quantified and expressed as $\Delta\zeta$.

5.4.4 Rheological characterization of bridging-flocculated emulsions at different oleosome contents

The results of the oscillatory strain sweeps of the mixtures at different oleosome content and fixed polysaccharide/oleosome ratios are summarized in Fig. 5.10. All the samples show $G' > G''$at small strains ($\gamma <$ 20%), indicating solid-like character, and at larger strains ($\gamma >$ 20%) $G' < G''$ which indicates that the samples become a liquid-like material. The linear viscoelastic region (LVR) appeared to be independent of oleosome content presenting a critical strain (γ_0) of about 3% in all samples when considering the definition of a 10% deviation in G' from its maximum value. Overall, at $\gamma >$ 3% G' decreases faster than G'' in all samples, which is associated with the fracture behavior of a particle gel-like structure [151]. However, among the samples, G' and G'' will decrease either sharply or gradually depending on the polysaccharide type and the polysaccharide/oleosome ratio. To measure the steepness of the decrease in modulus, the slope was measured for the strain region between γ = 3 -100 % (Table 5.2). The parts that follow will go into greater detail about these findings.

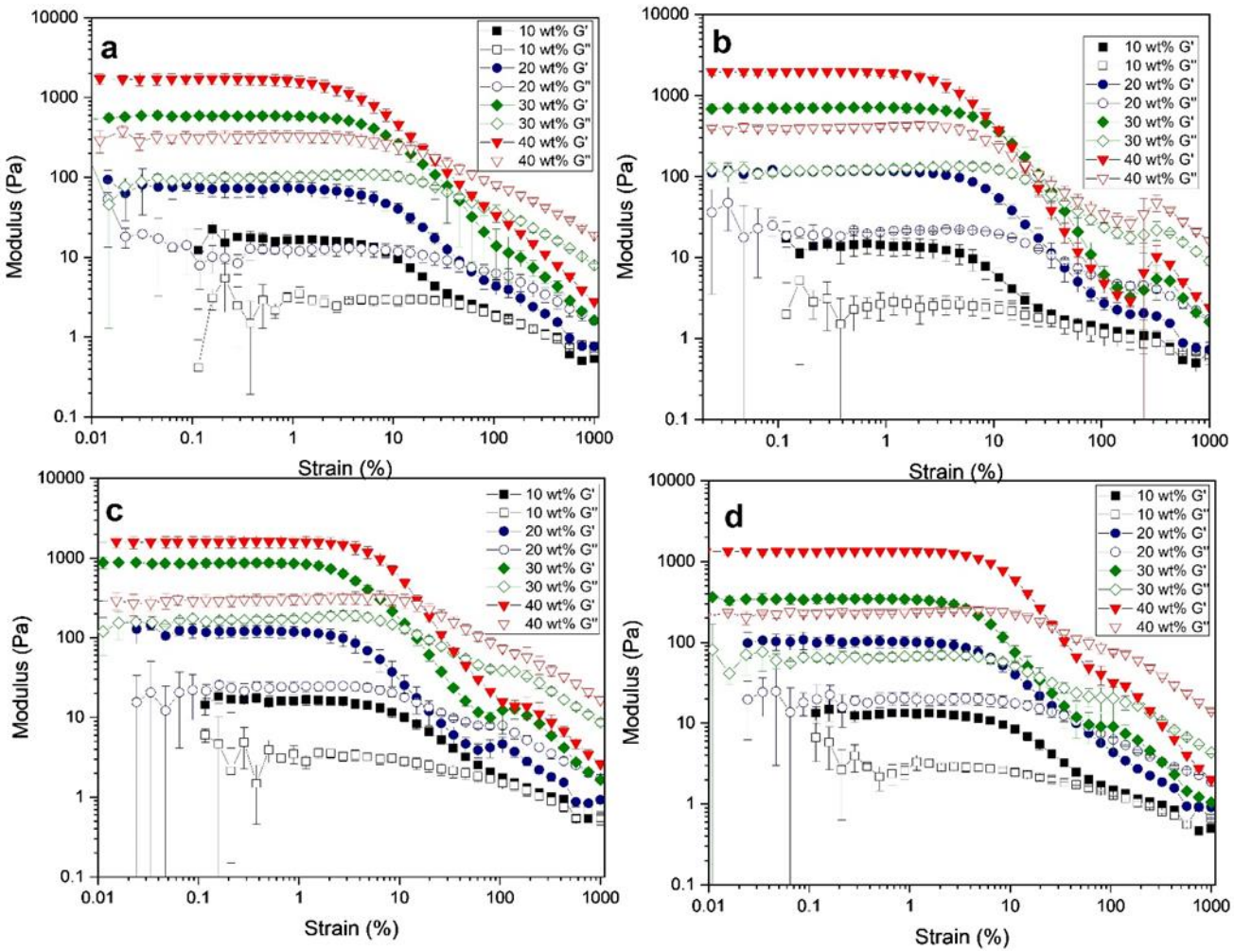

Fig. 5. 10 Oscillatory rheology measurements of polysaccharide/oleosome mixtures at different oleosome contents and fixed at two polysaccharide/oleosome ratios. a) 0.005 g carrageenan/g oleosome, b) 0.005 g alginate/g oleosome, c) 0.01 g carrageenan/g oleosome, d) 0.01 g alginate/g oleosome.

5.4.4.1 Percolation theory

In the LVR for all samples, G' (γ = 0.5%, ω = 10 rad s^{-1}) increases with oleosome content in a power law fashion, as shown in Fig. 5.11. By plotting G' against the oleosome concentration on a double logarithmic scale, it is tempting to apply a percolation model to fit the dependence of G' on oleosome concentration. The critical percolation concentration (c_p) and the scaling exponent (t), as defined in Eq. 5.2 were determined using a method described by van der Linden et al. [80]. This approach uses plots of $G'^{1/t}$ *vs c* to determine the exponent *t* (see eq.(5.2)) by providing arbitrary values that yield the best linear fits. From our results, the best fits were obtained for scaling exponent *t*, which yielded regression coefficients R^2 above

0.97, and an average c_p was determined. By using calculated c_p values, the actual *t* values could be obtained from the plots $G' vs\ (c - c_p)^t$. As shown in Table 5.3**,** c_p values were between 0.16 %- 0.40 %. These values are in agreement with those reported for protein gel systems (c_p = 0.3 ± 0.2%) [87]**,** (c_p = 0.45 ± 0.25%) [88], which presented stronger protein-protein attractions within the gel network due to increasing ionic strength values. In bridging-flocculated emulsions containing negatively charged Carboxymethyl-cellulose [89]**,** c_p was extrapolated to 0, attributed to the stronger bridging attraction between the oil droplets. Previous work from Segre et al. [165] related c_p to the magnitude of the attractive interaction, *U*, between the emulsion droplets, where c_p decreased with increasing attractive energy. Therefore our results further confirm that strong, attractive interactions drive flocculation in our systems. Furthermore, alginate presented the lowest c_p, 0.16 %, confirming that the strongest bridging interaction occurred at 0.005 g/g alginate, but as bridging becomes less effective at 0.01 g/g, c_p increases to 0.39 %.

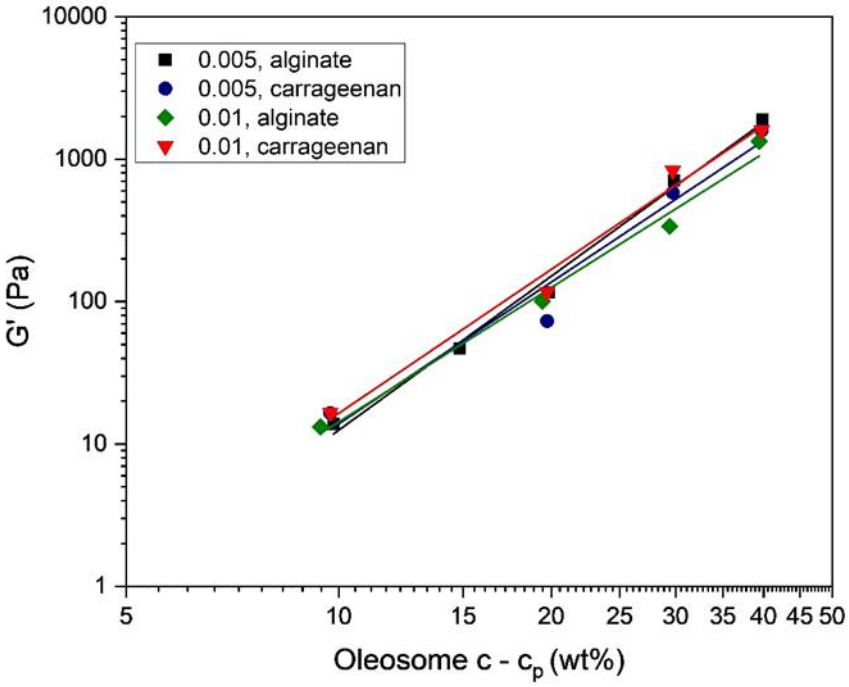

Fig. 5. 11 Double logarithmic plot of $G'(Pa)\ vs\ (c - c_p)^t$

Table 5.2. Slope parameters obtained from oscillatory amplitude sweep measurements for strain values between 3%- 100%. γ_1 = ~ 3% and γ_2 = ~100% were chosen as the coordinates of first and second point for all samples.

	0.01 Alginate		0.01 Carra		0.005 Alg		0.005 Carrag	
Oleosome	G'	G"	G'	G"	G'	G"	G'	G"
40%	-1.07±0.02	-0.35±0.00	-1.32±0.07	-0.43±0.02	-1.83±0.02	-0.82±0.02	-1.12±0.07	-0.44±0.03
30%	-0.98±0.15	-0.35±-0.09	-1.05±0.13	-0.40±0.06	-1.49±0.05	-0.56±0.01	-1.10±0.20	-0.33±0.10
20%	-0.83±0.04	-0.32±0.03	-0.80±0.07	-0.29±0.06	-1.08±0.06	-0.43±0.02	-0.80±0.04	-0.22±0.01
10%	-0.66±0.04	-0.25±0.13	-0.64±0.03	-0.25±0.03	-0.61±0.07	-0.22±0.02	-0.58±0.02	-0.08±0.03

Values are presented as the mean standard deviation ± of at least duplicate values

Table 5.3. Scaling exponents *n*, *t* and percolation threshold c_p for alginate and carrageenan containing bridging-flocculated emulsions at two mass ratios

	n	*t*	c_p
0.005 g/g, alginate	3.63±0.15	3.60 ± 0.15	0.15 ± 0.76
0.005 g/g, carrageenan	3.35±0.06	3.30 ± 0.06	0.24 ± 0.36
0.01 g/g, alginate	3.24±0.11	3.17 ± 0.11	0.39 ± 0.44
0.01 g/g, carrageenan	3.41±0.13	3.33 ± 0.12	0.40 ± 0.66

Values are presented as the mean standard deviation ± of at least duplicate values

The values for the scaling exponent *t* showed an average of 3.35, the highest at alginate 0.005 g/g (t = 3.60). The scaling exponent *t* is somewhat higher than predictions from the isotropic percolation model (t = 2.06 ± 0.6) [166], which was observed in diverse protein systems and describe their apparent homogeneous network architectures [80]. The higher *t* for our samples may indicate non-homogeneous network architectures, as similar values were reported for plant protein gels and pre-sheared systems, which are anticipated to be of this type [88, 166, 167]**.**

5.4.5 Microstructural properties of flocculated emulsions

The microstructure of the bridging flocculated emulsions was examined using CLSM (Fig. 5.12). From the length scales of the CLSM images (20 μm), the samples appear inhomogeneous to a different degree, where 0.005 g/g alginate at 5% and 20% oleosome presented the largest structures, therefore inhomogeneous up to a much larger degree compared to the other samples. This is also consistent with its largest scaling exponent (t = 3.60) among the other samples obtained from the percolation model. In addition, the interpretation of the scaling exponent *t* leads to information on the forces between network elements that leads to elastic rigidity. In gel networks where bond-bending forces are also present, *t* values have resulted in 3.75 ± 0.11 [168]**.** These higher *t* values have been reported elsewhere where structures were characteristic of heterogeneous systems [88, 166, 169], and according to Kantor and Webman [86]**,** when $2.9 < t < 3.6$, both bond-bending and bond-stretching forces are present in the gel network. These forces correspond to the bending energy of the polymers because they define mainly the stiffness of the clusters, apart from sterical and geometrical restrictions, which define the deformation properties of the clusters. The exponent suggests a mixed elastic behavior of the flocculated clusters. At local length scales, i.e., between two oleosomes, the different elastic stretching properties of the polymers play an essential role, whereas at larger scales, beyond the diameter of the oleosomes, steric hindrances between rigid oleosomes come into play.

Although percolation theory may be used to describe the network characteristics of the gels, the apparent structural heterogeneity of our samples coupled with the low c_p values may indicate that a fractal scaling model $G' \sim c^n$ (where c_p is zero) could be better suited [81]. The exponent *n* values observed in Table 5.3 are not significantly different from the exponent *t* values observed from percolation theory. This suggests that a fractal scaling approach could be better suited to describe the gel network of bridging-flocculated emulsions.

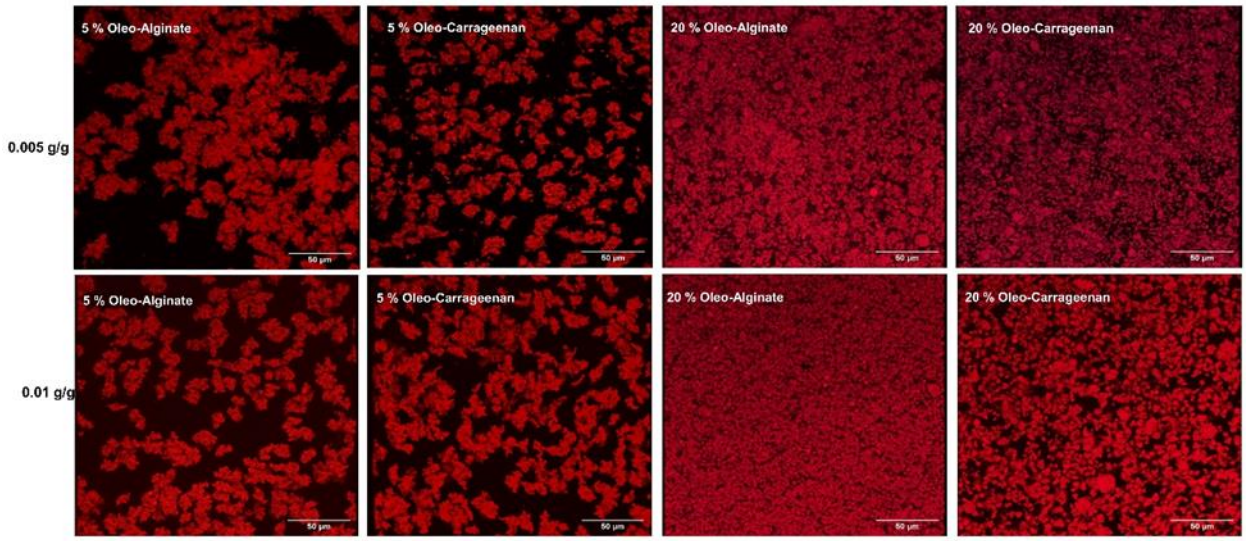

Fig. 5. 12 Confocal laser scanning microscopy (CLSM) images from the different bridging flocculated emulsions with alginate and carrageenan at two fixed ratios, 0.005 – 0.01 g/g, at two 5% and 20% Oleosome content. Scale bar: 50 µm.

Additionally, Fig. 5.12 shows the variation in microstructure between the different samples. In addition to the great degree of heterogeneity observed at 0.005 g/g alginate, the microstructure at 0.01 g/g alginate changes from a completely interconnected droplet network to a system formed by more homogeneous and separate clusters as the amount of alginate polymer chains over oleosome droplets increases, as previously observed in Fig. 5.3 d-e. This transition is caused by the alginate polymer chains that start to coat the oleosomes surface completely as discussed extensively in our previous publication. Carrageenan, however, displays more uniform and distinct clusters at 0.005 g/g, where its bridging effectiveness is lower, and on the other hand, 0.01 g/g carrageenan present more interconnected and heterogeneous, confirming that optimum bridging in carrageenan occurs at a higher concentration than alginate.

5.4.6 Final discussion

To better understand the structural details, it appears helpful to summarize the results obtained in physical models based on Fig. 5.5 and 5.6 and now extended in Fig. 5.13. Adsorption and bridging of the different hydrocolloids are responsible for the distinct mechanical behavior. This is shown in Fig. 5.13. Once oleosomes become connected by different chains, a network with embedded oleosomes emerges. The shear

modulus is defined roughly by the number of electrostatic connections between charged alginate blocks and oleosomes and the number of entanglements, which contribute as topological constraints (slip-links) to the shear modulus [170]. The flexible parts of alginate chains in between oleosomes define thus a large part of the (entropic) elasticity, very similar to conventional gels, filled with nanoparticles.

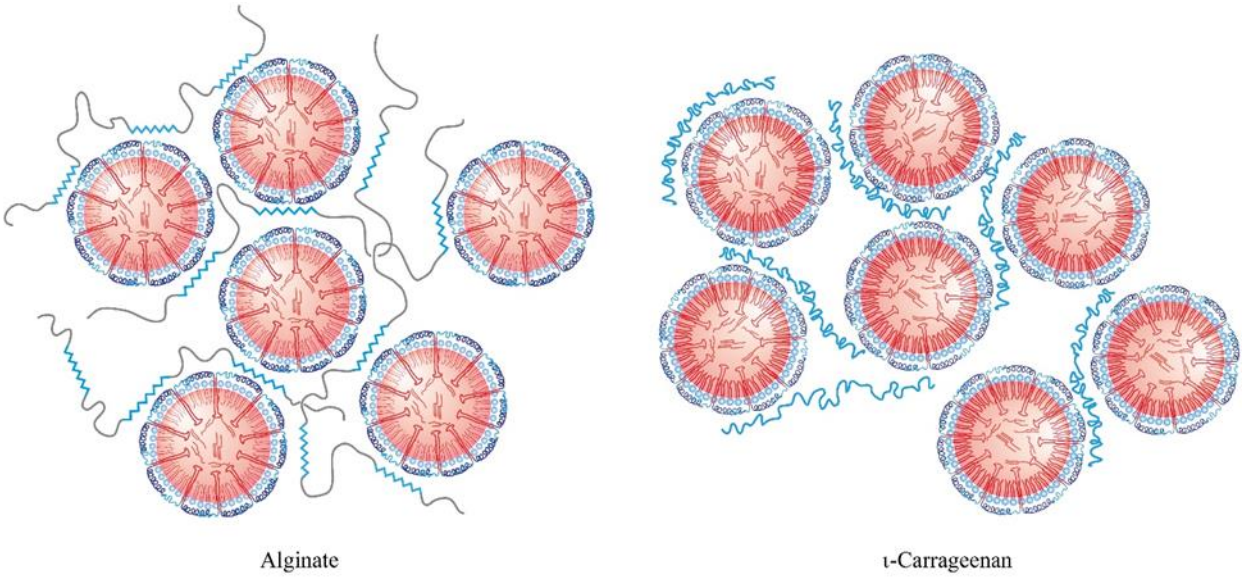

Fig. 5. 13 Schematics of typical oleosome clusters. Alginate binds oleosomes very differently as Carrageenan.

On the other hand, the negatively charged carrageenan chains bind with more monomers to the positively charged surfaces of the oleosomes. The chain of blobs can easily adjust to the oleosome curvature, making the adsorption of the individual chains on the surface stronger. Carrageenan chains interconnect oleosomes less effectively (Fig. 5.13) and cannot form entangled conformations. Clusters grow only to limited sizes, as seen in the confocal micrographs Fig. 5.12 for the concentrations of 5 % Oleosomes with 0.005 and 0.01 g/g polymer. Whereas alginate forms large interconnected clusters at 0.005 g/g, the carrageenan samples show smaller separated clusters at 0.005 g/g and 0.01 g/g. This is not surprising since carrageenan effectively coats the oleosomes, which prevents the adsorption of inter-oleosome connecting chains. Free, non-connected chains remain unattached and contribute to the bulk (compression) modulus. The flexible chains of alginate can even connect clusters of oleosomes.

The moduli in the linear viscoelastic range (LVR) are of the same order of magnitude (see Fig. 5.10) for alginate and carrageenan-oleosome mixtures, which are mainly determined by the density of oleosomes and clusters in both cases. However, the differences between the hydrocolloids become more pronounced at larger deformations. The main reason is given by the different arrangements and structures of the clusters. At local scales, the properties of the hydrocolloids come into play. For an illustration, it is helpful to have a closer view of the cluster distribution in both cases, shown in Fig. 5.14.

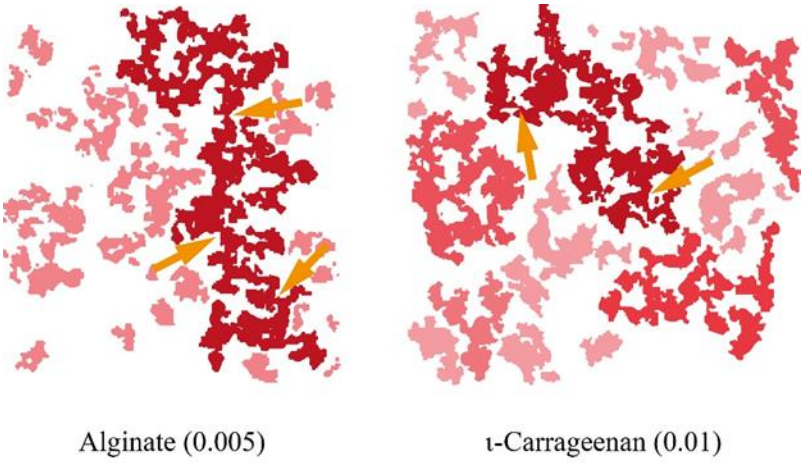

Fig. 5. 14 Comparison of the cluster distribution between the samples containing alginate (at 0.005 g/g) and ι-carrageenan (at 0.01 g/g). The different color intensities indicate as guide to the eye the cluster size. The clusters have been extracted from the corresponding CLSM results, Fig. 5.12. Representative weak links are indicated by arrows.

Alginate connects oleosomes into large, percolating clusters of irregular shapes, surrounded by small clusters of similar shapes. Carrageenan also forms (at higher polymer concentrations) larger clusters but with less connectivity. During the LVR, the clusters support shear stresses up to 2 - 5 % strain for both systems.

At the optimum bridging ratio for alginate, 0.005 g/g, both moduli present a sharp decrease, as observed in the slopes in Table 5.2, which are higher than 0.005 g/g carrageenan slope values. In comparison, at 0.01 g/g, carrageenan presents a steeper moduli decrease than 0.01 g/g alginate, which, as previously observed, corresponds to the optimum bridging ratio for carrageenan. This is shown already in Fig. 5.6 and 5.13. This

behavior has been observed elsewhere, too [89, 171]. Steeper slopes indicate sudden microstructure fracture, typical for bridging flocculated systems that have heterogeneous structures. This is caused by local stresses and strains, which are highest near the weakest links between the oleosomes and allows fractures quickly propagate through the largest clusters. The breaking of the links finally involves the polymers themselves. The shear energy needs to be larger than the electrostatic binding of the charged parts of the polymers at the oleosome surfaces. In the case of carrageenan, this is easier and even reversible. Under shear, some of the oleosomes at the weak links lose some chains, but the dissolved chains quickly coat the free surface. For alginate, the topological, transient network needs to disentangle. Since there is no longer a possibility of rearrangement of the entanglement network, the decay slope is steeper.

5.5 Conclusions

This study aimed to determine the effect of the type and ratio of polysaccharides on the gelation of soybean oleosomes using a polymer bridging mechanism. It was shown that negatively charged polysaccharides with flexible polymer chains, such as sodium alginate and ι-carrageenan, can bridge oleosome droplets, via electrostatic attractions, into a particle gel network. However, structural differences between alginate and carrageenan, such as charge distribution along its backbone, account for differences in adsorption behavior to the oleosome surface. Alginate adsorbs block-wise due to its charged units arranged in blocks along its backbone, whereas carrageenan chains adsorb uniformly due to its uniformly distributed charges. This difference will influence bridging efficiency, where alginate presented greater bridging efficiency (0.4 mg/m^2) than carrageenan (0.8 mg/m^2). Alginate flexible chains allow for more freedom, enabling interconnecting of multiple oleosome droplets into a percolated network.

On the other hand, carrageenan will be more efficient for completely coating the oleosome surface but less efficient for bridging since more charged monomers are adsorbed on the oleosome surface, thus preventing chains from interconnecting further oleosome droplets. This difference in bridging efficiency will influence microstructural properties. Alginate forms more heterogeneous and interconnected clusters, while carrageenan forms smaller and less interconnected clusters. These microstructural differences will influence

rheological response upon larger deformations where steeper slopes in *G',* indicating fracture behavior, are caused by quick stress propagation from weak links within the clusters. Therefore it is concluded that sodium alginate is an efficient polysaccharide to produce oleogels based on oleosome emulsions via a polymer bridging mechanism.

6 Compacted polymer bridging gels. Mechanical properties at large deformations

This chapter is based on the following manuscript:

Soybean oleosome-based oleogels via polymer-bridging based structuring. Mechanical properties at large deformations

Juan Carlos Zambrano S., Thomas A. Vilgis

Oilseeds & fats Crops and Lipids, (2023), 30,6

6.1 Summary

In this chapter we use polymer bridging to produce soft, malleable gels by centrifuging the bridged droplet network resulting in a compacted self-supporting gel. We compared again two bridging polysaccharides, sodium alginate and ι-carrageenan, at different polysaccharide/oleosome ratios and different oleosome contents. We investigated the viscoelastic properties of compacted polymer bridged gels by oscillatory rheological measurements. We found specific rheological features depending on the shear strain. One yielding step at a medium strains ($\sim\gamma_1$ = 20%) indicates the breaking of polysaccharide bridging bonds and was visible in all samples. A two-step yielding process was observed at large deformations (γ_2= 200-300 %) which varied depending on the type of polysaccharide and polysaccharide/oleosome ratio. This two-step yielding indicative of *caging* effect was present at polysaccharide/oleosome ratios where optimum bridging occurs for alginate and carrageenan, 0.005 g/g, 0.01 g/g, respectively. Nonetheless, the overshoots corresponding to the second yielding point were more prominent in alginate gels than in carrageenan gels due to the greater bridging ability of alginate. Identifying these rheological hallmarks could provide new ideas towards the improved design of plant-based fatty food products, e.g., cream cheeses and vegan sausages surrogates.

6.2 Introduction

Polymer bridging has been proposed as a structuring method for natural oil-in-water emulsions, so-called oleosomes. Polymer bridging requires that polymeric chains adsorb simultaneously on multiple oil droplets to create a percolated gel network [65]. Previous findings showed that bridging flocculation, induced by negatively charged polysaccharides, formed a heterogeneous and interconnected network of oleosome droplets [151, 152]. Sodium alginate proved to be a very effective polysaccharide for inducing bridging flocculation of oleosome droplets where its optimum bridging coverage occurs at 0.005 g/g [151]. In comparison, the optimum bridging coverage of ι-carrageenan occurs at 0.01 g/g [172]—this difference in bridging ability between alginate and carrageenan results from structural conformations. Alginate polymer chains are organized in a co-block arrangement of charged and uncharged units of mannuronic acid and guluronic acids groups [161], thus enabling flexible polymeric chains to interconnect multiple oleosome droplets. The charges in the carrageenan chain are organized uniformly along its chain [173], which makes it more efficient for complete surface coating of the oleosome surface. However, polymer chains are less available to interconnect multiple oleosome droplets into a percolated network.

The structural differences between both polysaccharides will also influence the microstructure of the gel network. Polymer bridging gels induced by alginate presented large and interconnected clusters, resulting in a gel network with large pores where water can easily migrate. On the other hand, ι-carrageenan-induced gels presented smaller and less interconnected clusters with smaller pores. Thus, water is less available to be separated, so the bridging efficiency decreases. Therefore, the gel microstructure will determine the extent of water separation from the droplet network. Centrifugation can quickly accelerate the network contraction and water separation process. As a result of bridging flocculation, the droplet network contracts upwards due to the relatively higher density of the oil droplet network than the water phase in which they are dispersed. Centrifugation allows the flocculated emulsions to form a continuous mass in which the water is easily removed, resulting in a low-moisture soft, malleable gel. This separation process is analogous to other processes in the food industry, such as the production of cream cheese in which the fat-containing

curd is separated from a liquid phase using a cream-type separator or a quark-type separator by application of centrifugal force.

Therefore, the physical properties of the oleogels can be systematically altered by changing process conditions, or changing preparation conditions, such as oleosome content, polymer type and polymer/oleosome ratio. This interplay of conditions can result in soft gels with different shapes or volumes, which could be efficiently designed to produce food products with different textural attributes. The current study builds on the previous chapter on polymer bridging emulsions induced by sodium alginate and ι-carrageenan [172]. Here it was also shown that differences in gel microstructure will influence the viscoelastic properties of the resulting gel material. Bridging flocculated emulsions at the optimum bridging ratio presented fracture-like behavior at deformations larger than the Linear viscoelastic range (~ 3%). This is due to the strong and irreversibly bonds in the microstructural elements formed at the optimum bridging ratio. In addition, polymer bridging gels presented a characteristic overshoot in the modulus at larger deformations (~ 200%) which needs to be further elucidated. Therefore, this study investigates the rheological properties of compacted oleosome-based gels formed by polymer bridging. For this purpose, the effect of polysaccharide/oleosome ratio between sodium alginate and ι-carrageenan are compared to analyze the effect on the mechanical properties at large deformation as determined by oscillatory rheological measurements.

6.3 Materials and methods

6.3.1 Materials

Commercially available soybeans were purchased from Rapunzel Naturkost GmbH (Legau, Germany) and were used to extract oleosomes. Sodium alginate (TICA-algin 400 Powder) was provided by TIC Gums, Inc. (Belkamp, Md., USA). Iota carrageenan was provided by Carl Roth (Karlsruhe, Germany). Distilled water was used for the preparation of all solutions.

6.3.2 Sample preparation

Soybean oleosomes extraction is based on the method by Waschatko et al. 2012[46]. Soybeans were soaked in distilled water at 4°C for at least 20 h. Then water was added to obtain a 10% soybean-to-water ratio, ground in a Vorwerk Thermomix TM31 at 10,200 rpm for 90 s. The resulting slurry was filtered through two layers of Kimtech wipes 21 x 11 cm (Kimberly Clark) to obtain raw milk. 25 wt% Sucrose was added to the raw milk, and the pH was adjusted to 11.0 with 1 N NaOH (VWR Chemicals) solution. The solution was filled into 50 ml centrifuge tubes (Roth) and centrifuged at 15000xg at 4°C for at least 5 h. The resulting floating fractions (cream layer) were collected with a small spoon and resuspended in a new centrifuge tube in 20 wt% Sucrose in distilled water (pH 11.00). A new washing and centrifugation step (15000xg, 4°C, 5 h) was repeated, and the resulting oleosome cream was collected in a centrifuge tube. This method removes unspecific bounded soybean storage proteins (glycinin and β-conglycinin) and other allergenic proteins (Gly m BD 30K) from the surface of the oleosomes [77]. The extracted oleosome cream had a 50- 40 % water content as measured by a halogen dryer. The dry weight of the cream is assumed as the oleosome content. Since the precise composition of oleosomes is unknown, theoretical values of the three major components of soybean oleosome were used according to Huang's [27]. This author calculated theoretical values of oleosome components according to the oleosome diameter size. As determined by laser diffraction analysis in Chapter 4, soybean oleosomes referred to the current extraction method resulted in a particle size of 0.350 µm. This model calculates the amounts of approximately 3.3% (w/w) phospholipids, 5.2% (w/w) protein, and 91.5% (w/w) triglycerides for an oleosome with a 0.350 µm diameter.

6.3.3 Preparation of bridging flocculated gels

The initial pH of the oleosome emulsion was adjusted to 7.0 with 1 NaOH. Dried sodium alginate and carrageenan samples were added directly to the oleosome emulsion at different concentrations to form different mass ratios (g polysaccharide/g oleosome). Polysaccharides-oleosome mixtures were stirred for a minimum of 20 h to ensure proper hydration. Afterward, polysaccharides-oleosome mixtures were slowly adjusted to pH 4.0 via dropwise addition of HCl with varying concentrations (1.0, 0.5, 0.1, 0.01 N) at a constant stirring speed of 450 rpm. Bridging flocculated polysaccharide-oleosome mixtures were

centrifuged (5000 x*g*, 4°C, 20 min) in 50 ml centrifuges tubes. The supernatant was decanted, and the compacted gels were then carefully collected.

6.3.4 Rheological measurements

Oscillatory rheology was performed on compacted gels in order to investigate their resulting viscoelastic properties. Measurements were performed with a Bohlin Instruments Gemini 200 rheometer (Malvern Panalytical Ltd., Malvern, UK) equipped with a 25-mm parallel plate geometry. The gap size was adjusted stepwise to the thickness of the gels until the load in the normal force was detected, leading to gap sizes between 1000 – 1500 µm. Wall slip effect was discarded by measuring at different gaps while keeping other measuring conditions constant. After loading, a 5-minute waiting period at 25°C was used to allow the sample's structure to relax before the measuring process began. Oscillatory amplitude sweeps were performed by increasing the strain logarithmically from 0.01 to 1000% at 1 Hz. All measurements were performed in triplicate from different batches of gels and all samples were prepared individually.

6.3.5 Microstructural observation

The microstructure of the compacted gels was observed by scanning electron microscopy (LEO Gemini 1530) under a suitable accelerating voltage. Upon centrifugation, concentrated gels were plunged into liquid nitrogen before being placed in a freeze dryer (Christ Alpha 1-2 LD plus). Samples were left to dry overnight, and afterward, the samples were stored in a sealed glass container at room temperature. Subsequently, the dried samples were carefully placed on standard aluminum stubs (Plano GmbH; Wetzlar, Germany), attached with double-sided carbon tapes, and transferred to the microscope under vacuum.

6.4 Results and discussions

6.4.1 Visual appearance of polymer bridged gels

The visual appearance of polymer bridging gels before and after centrifugation containing increasing concentrations of oleosome and alginate and ι-carrageenan are shown in Fig. 6.1. As previously observed in Chapter 4, self-standing compact gels were obtained upon centrifugation in which the resulting concentration will increase as the initial oleosome content increases. As previously discussed, droplet

networks flocculated by the polymer bridging mechanism will contract upwards due to the density difference between the oil and the continuous water phase. By accelerating this separation, the droplet network can be easily concentrated, resulting in a compact gel in which the viscoelastic properties can be expanded.

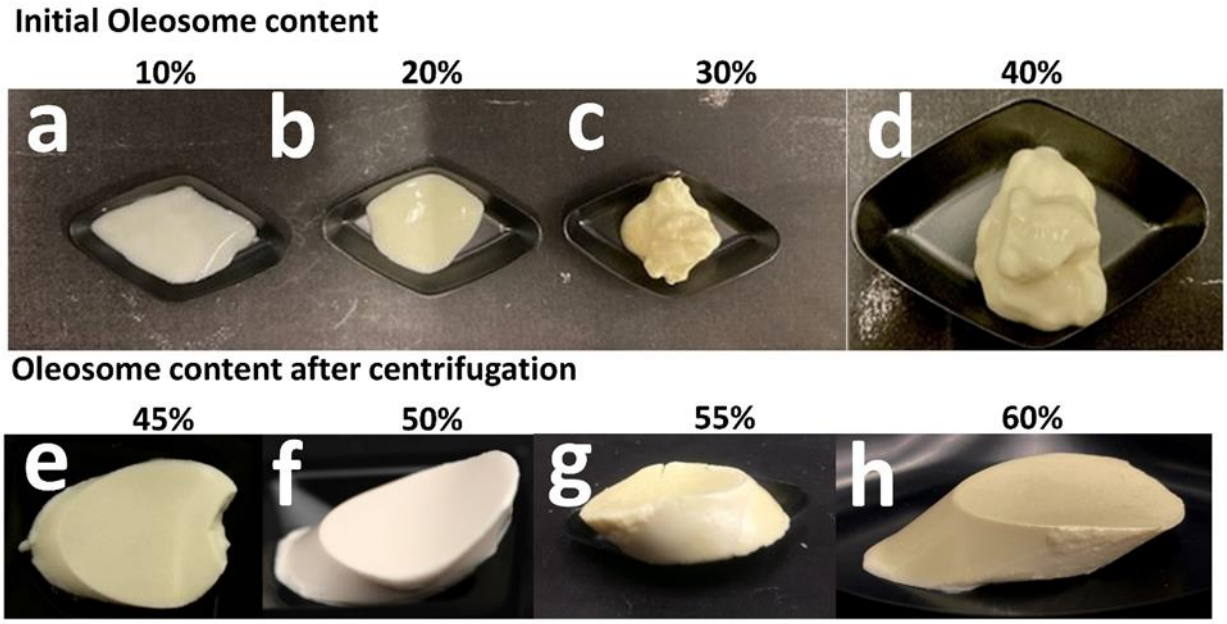

Fig. 6. 1 Visual appearance of polymer bridged gels of alginate and carrageenan-oleosome mixtures. Samples from the top correspond to samples before centrifugation, and samples from the bottom correspond to the same samples after centrifugation. a, c, e, g, corresponded to carrageenan, and b, f, d, h corresponded to alginate.

6.4.2 Microstructure of polymer bridged gels

Fig. 6.2 shows SEM images depicting the microstructure of the compacted gels by alginate and carrageenan. Carrageenan gels (Fig. 6.2 a, c) present a rougher microstructure, while alginate presents a smoother microstructure (Fig. 6.2 b,d). A rougher microstructure is likely due to loops of chains from carrageenan, which may be dangling, whereas alginate, due to more efficient use of its polymer chains, is less likely to present dangling loops around its microstructure.

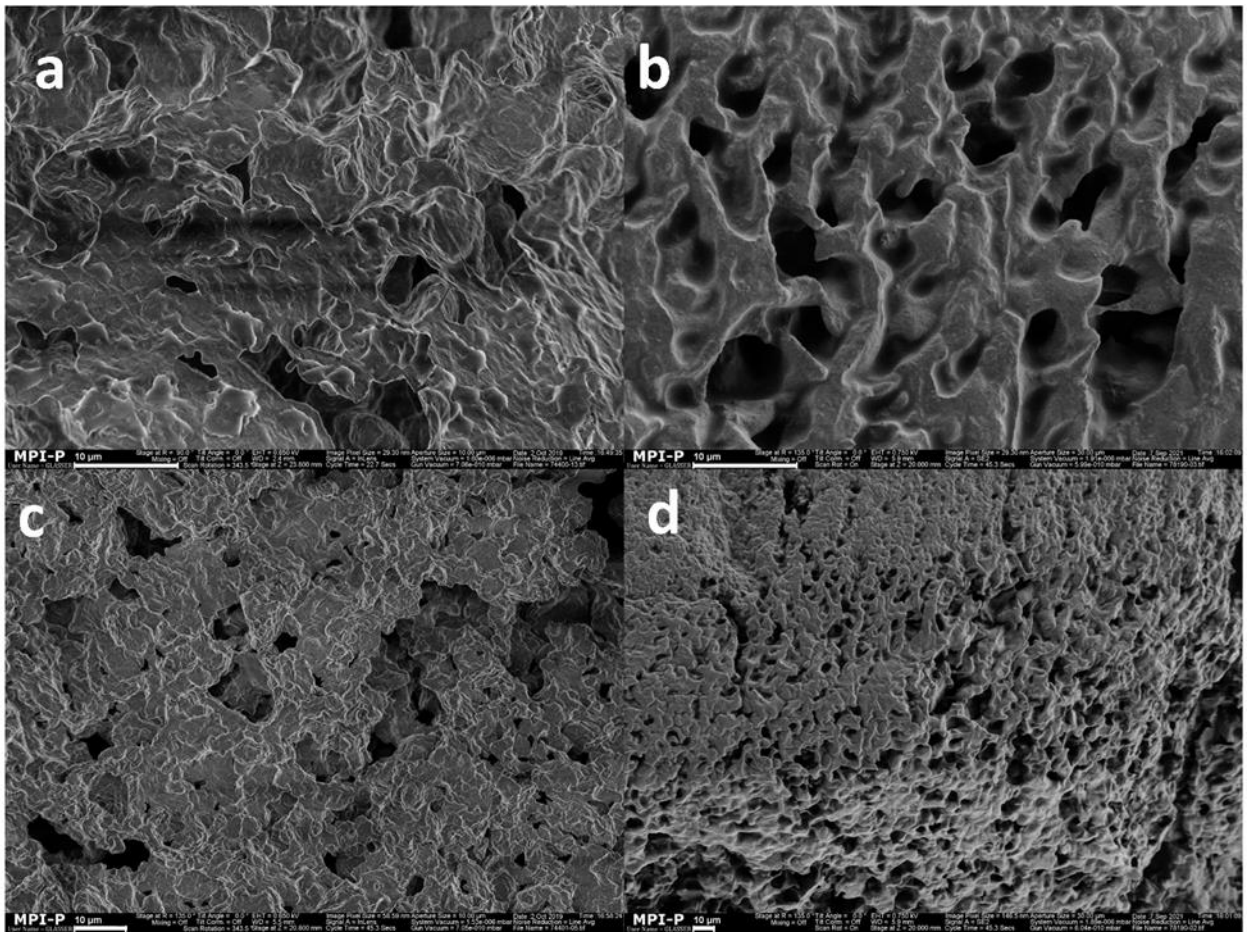

Fig. 6. 2 SEM images of polymer-bridged gels upon densification 45 wt% Oleosome fixed at 0.005 g /g. a-c) carrageenan b-d) alginate. Scale bars: 10 µm.

6.4.3 Rheological characterization of polymer-bridged gels

The results of oscillatory strain sweeps of the polymer-bridged gels upon densification are shown in Fig. 6.3. Overall *G'* values (10^3-10^4 Pa) in the linear viscoelastic region (LVR) were higher than those previously reported [172]of non-centrifuged bridging flocculated oleosomes. This shows that the high density of the oleosome clusters upon centrifugation determines the bulk modulus in the LVR. The effect of cluster density is more clearly observed in 0.005 g/g alginate (Fig. 6.3b), where *G'* values in the LVR are almost the same order of magnitude for all oleosome concentrations. At this ratio, alginate presents its optimum bridging ratio in which alginate chains effectively bridge all oleosome droplets. Thus, dense interconnected clusters determine the high density at the different oleosome concentrations.

Similarly, for 0.01 g/g carrageenan (Fig. 6.3c), the moduli in the LVR do not vary significantly, at least for oleosome concentrations > 10 wt%. As previously reported [172], the optimum bridging ratio in carrageenan occurs at 0.01 g/g where, as observed for 0.005 g/ alginate, dense clusters determine the bulk modulus in the LVR. On the other hand, the moduli values in the LVR differed across the various oleosome contents at ratios further from the optimal bridging ratio for alginate and carrageenan (0.01 g/g and 0.005 g/g, respectively) (Fig. 6.3 a,d). As the ratio between polymer and droplets are farther from the optimum ratio for efficient bridging flocculation to occur, polymer bridges between droplets start to disappear [151]. As a result, clusters upon centrifugation will be less interconnected and thus less dense at these ratios [172], causing bulk density not to be relevant anymore for the modulus in the LVR.

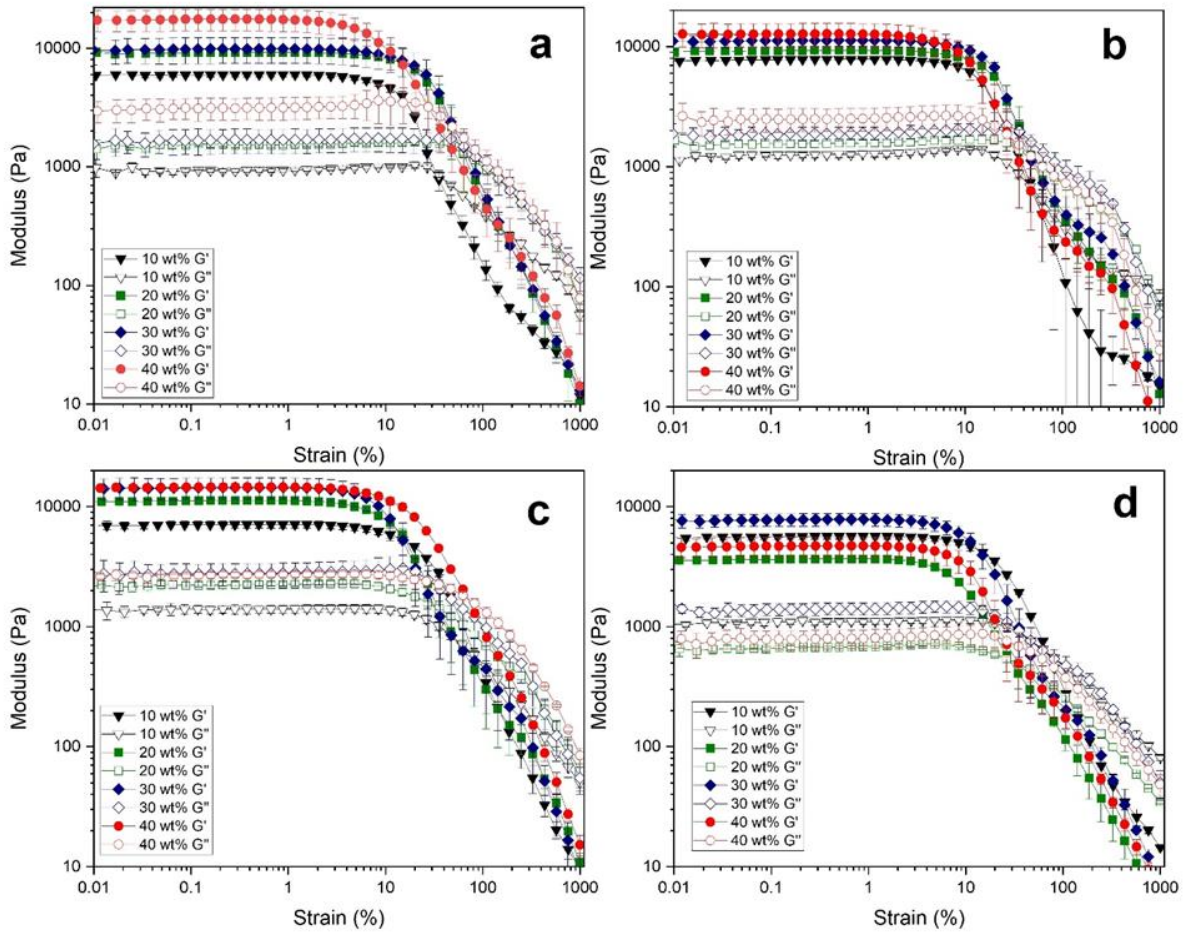

Fig. 6. 3 Oscillatory strain sweeps of polymer-bridged gels after centrifugation at different oleosome contents and fixed at two polysaccharide/oleosome ratios. a) 0.005 g carrageenan /g oleosome, b) 0.005 g alginate/g oleosome, c) 0.01 g carrageenan /g oleosome, d) 0.01 g alginate/g oleosome.

6.4.3.1 Focus on the effects of large deformations

The most remarkable difference among the samples occurs at strains around γ = 300 %, with a small hump in G' and G'' appearing. As previously observed [172], a strain overshoot is visible at higher strains, confirming a two-step yielding behavior. In order to present this yielding behavior more clearly, from the same oscillatory measurements, the stress (σ) is plotted against strain (γ) in Fig. 6.4.

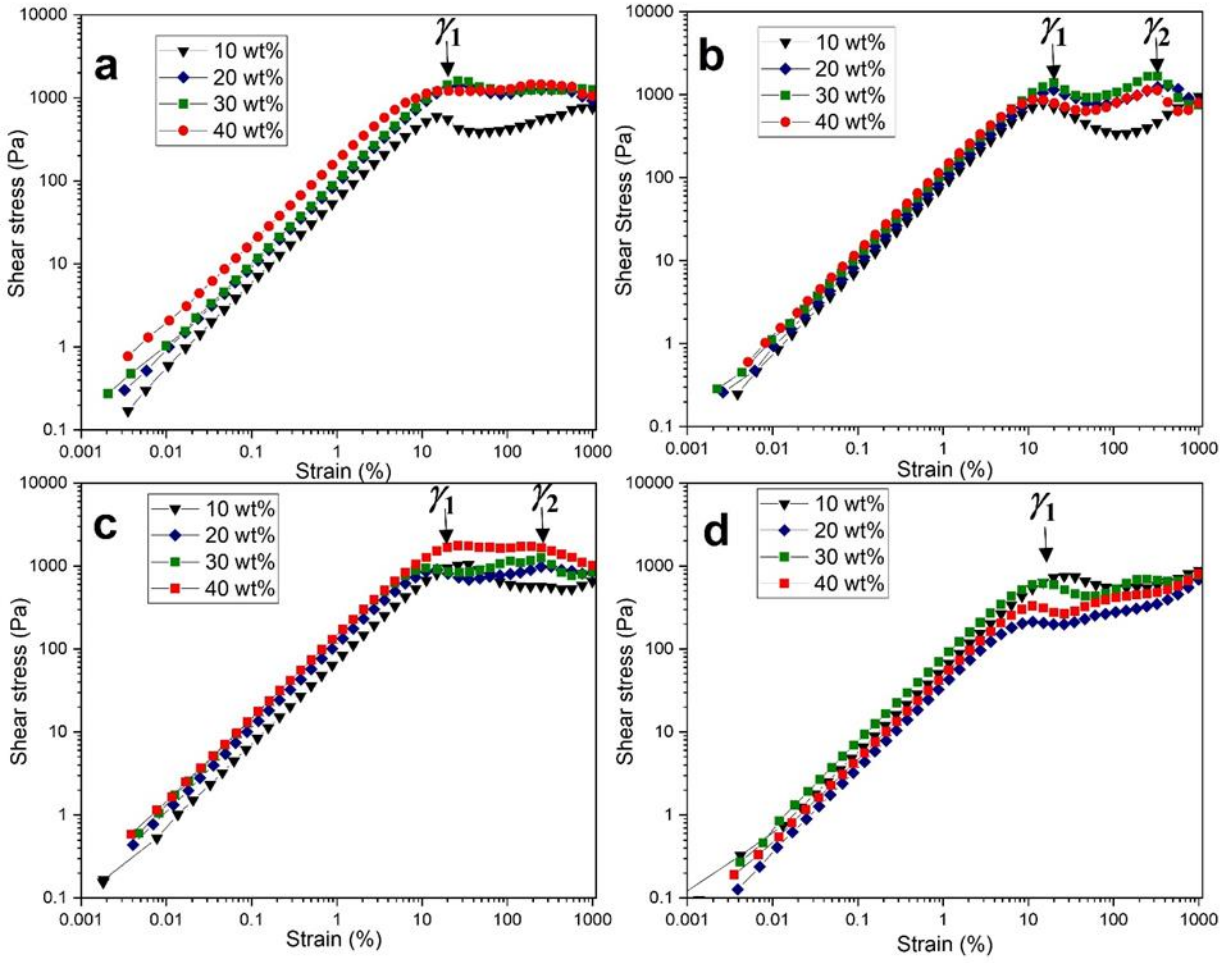

Fig. 6. 4 Oscillatory strain sweeps of same samples as Fig.6.3 but expressed as shear stress, σ, as a function of strain (%). Black arrows highlight the first yielding γ_1 and the second yielding point γ_2, which represents the stress overshoot at large strains that is clearly prominent across the different oleosome contents. a) 0.005 g carrageenan/g oleosome, b) 0.005 g alginate/g oleosome, c) 0.01 g carrageenan/g oleosome, d) 0.01 g alginate/g oleosome.

First, it is observed that stress response is linearly dependent on strain, indicating stress behaves elastically at strains up to 20%, which is followed by a first yielding point (γ_1) that seems to be independent of oleosome content (Fig. 6.5). The first yielding point (γ_1) is likely to indicate the confinement by density plus polysaccharide bridging breakage between the oil droplets. As the polysaccharide concentration is fixed at two ratios, 0.005 g/g and 0.01 g/g, the bridging bonds can be assumed the same for the different oleosome concentrations. This is supported in Fig. 6.5, where the values of the first yielding strain γ_1 among the samples do not significantly change for the different oleosome concentrations. Only small variations, however, can be depicted for carrageenan (Fig. 6.4 a,c). At 0.005 g/g and 0.01 g/g carrageenan, γ_1 slightly varies with oleosome content, albeit not significantly to the point of showing any dependence with oleosome content, as observed in Fig. 6.5. These slight variations can be explained by the weaker bridging ability of carrageenan, which fails to form tighter bridging bonds in contrast to alginate (see Fig. 6.6 below). This contrasts with 0.005 g/g alginate (Fig. 6.4b), where γ_1 does not change with oleosome content. Similar as carrageenan, for 0.01 g/g alginate (Fig. 6.4d), γ_1 slightly varies with oleosome content due to the decreased bridging ability of alginate at this ratio. Consequently, the first yield point describes the rupture of weakest links within oleosome clusters, hold together by electrostatic bridging [172].

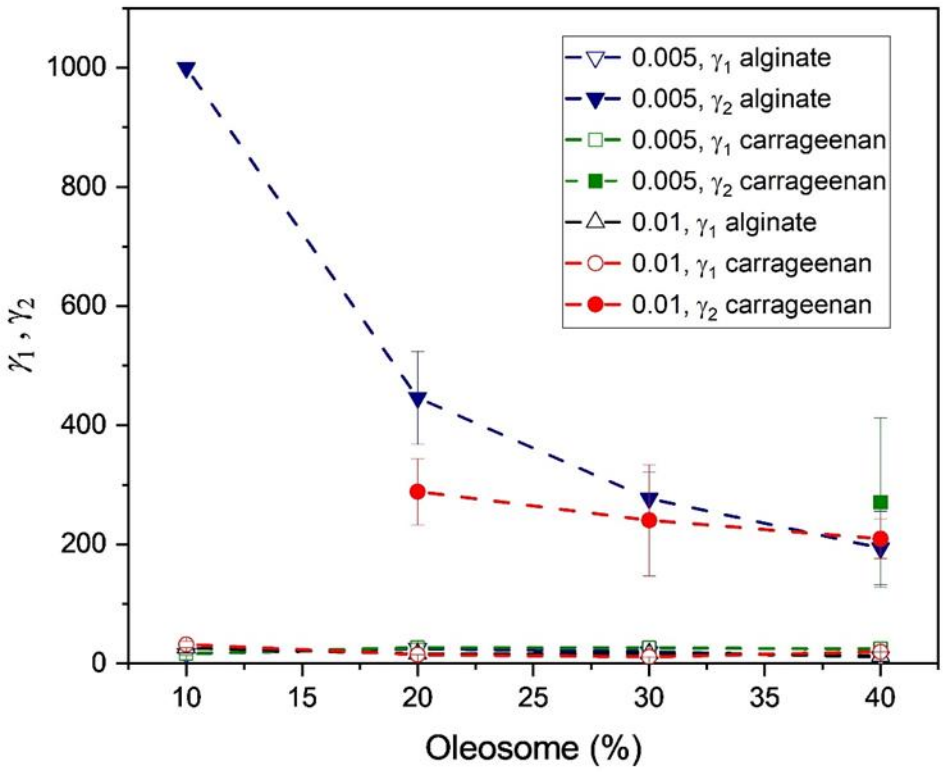

Fig. 6. 5 Plots of γ_1 and γ_2 as a function of oleosome content (wt%) of alginate and carrageenan at two fixed polysaccharide/oleosome rations. γ_1 and γ_2 were extracted from Fig. 6.4 as indicated by black arrows. Lines are guide for the eye.

Beyond the first yielding point (γ_1), 0.005 g/g alginate (Fig. 6.4b) starts deforming plastically, first showing a slight decrease in stress followed before a second hump (γ_2) at higher strains appears. The position of γ_2 becomes more prominent as oleosome content increases (> 20 wt%), as its position shifts to smaller values γ_2 as observed in Fig. 6.5. Second-step yielding is likely reminiscent of the so-called cage effect, which relates to the difficulty of a droplet to move due to the crowd of surrounding droplets [174]. Following deformation, droplets pack each other and restrict their movement resulting in an increase of stress, which upon deformation leads to a further release of each droplet. The cage effect may result from breaking bridging bonds and droplet rearrangements, which cause oleosomes to be trapped inside a cage while still interacting with the hydrocolloids, which partially coat the oleosomes. However, due to structural

differences, the polysaccharides adsorb differently on the oleosome surface, influencing the cage effect. This effect will be discussed in a more detailed manner in the following sections.

As the oleosome content decreases (< 20 wt%), droplet particles movement is less restricted thus they have a more accessible free volume to rearrange. This is reflected in the increase of the position of γ_2 as the oleosome content decreases (Fig. 6.5). Nevertheless, the different structural arrangement of alginate and carrageenan rules the concentration dependence of γ_2, which determines the final breaking of the confinement by the density-determined cage. Similar confining and caging effects were also observed by Zhao et al. [171] in macrogels produced by bridging mechanism. Although the study above corresponds to a different silica particle system and microgels, it still shows similar (universal) physics. The caging effect is most likely to occur the denser the system is, i.e., higher volume fractions, where rearrangements are less likely to occur, leading to dynamic arresting of oleosome droplets.

The second-step yielding transition is also observed among the different oleosome contents at 0.01 g/g carrageenan (Fig. 6.4c), where carrageenan presents its optimum bridging ratio [172]. However, the bumps corresponding to γ_2 do not appear as pronounced and sharp as 0.005 g/g alginate (Fig. 6.4b). This may be due to the weaker binding ability of carrageenan to oleosome surfaces compared to alginate, as suggested in a previous study [172]. Similar observations were reported elsewhere where two-step yielding behavior was present in particle gel networks formed by high interparticle attraction [175, 176]. In these systems, the overshoot on the yielding points becomes most pronounced in the samples with the strongest attraction. On the contrary, 0.005 g/g carrageenan and 0.01 g/g alginate do not present a pronounced two-step yielding behavior. Instead, it is worth observing the deformation behavior upon γ_1. For 0.01 g/g alginate (Fig. 6.4d) at oleosome contents > 10 wt%, the stress response follows a slight shear thickening which may indicate single droplet and droplet clusters flowing around each other.

The previous study in bridging flocculated gels [151] indicated that at 0.01 g/g, the bridging ability of alginate is reduced, and instead, re-stabilization of oleosome droplets is taking place. However, due to the flexible confirmation of alginate polymer chains, alginate chains can still interconnect separate clusters.

This might indicate that a transition between separate bridged clusters and stabilized single droplets is occurring.

On the contrary, the stress response in 0.005 g/g carrageenan upon γ_1 (Fig. 6.4a), at oleosome contents > 10wt%, follows a plateau indicating the presence of single droplets which do not rearrange upon further deformation upon yielding of bridging bonds. It was previously demonstrated [172] that the chain conformation of ι-carrageenan is more effective for complete surface coating of oleosome droplets than for polymer bridging. As a result, it is more likely that upon deformation, γ_1, carrageenan chains will coat free single droplets than bridging other droplets. Due to this characteristic, clusters in carrageenan-oleosome mixtures grow only until limited sizes. Similar transitions in bridging flocculated emulsions were found elsewhere [108]. The flocculation transitions can range from a dispersion of separate clusters to a network of completely bridged droplets or stabilized-coated droplets plus separate clusters. As previously suggested, these transitions will depend on the type of polysaccharide and the ratio between polysaccharide chains and droplets.

Based on a previous study [151], the strong binding between alginate polymer chains and oleosome droplets at 0.005 g/g led to denser and more compacted clusters among the conditions evaluated. Polymer bridging will thus produce clusters, which depending on the strength of binding between polymer chains and the oleosome surface, will result in more compact or less compact structures. These will influence how it responds to deformation on a microstructural level. Deformation will yield either in one stage only: bridging bonds that are broken at a lower strain, or in two stages: bridging bonds that are broken at a lower strain; then, at a higher strain, cages are opened, and then the structure breaks up into before rearranged under given shear.

It is clear from comparing the structures of alginate and carrageenan that alginate can function as a bridging agent more effectively than the latter. Both polysaccharides consist of a structural backbone with flexible polymer chains. However, they differ in how their charges are distributed along the chain. Alginate backbone consists of mannuronic acid and guluronic acid groups arranged in blocks, whereas carrageenan

presents a repeating galactose unit along its chain. Charge groups concentrated in blocks can promote stronger adsorption onto the surface of the oleosome droplets, as opposed to uniformly distributed charges along the carrageenan chain, which may lead to the less efficient use of some charges for interconnecting other droplets.

6.4.4 Final discussion

The experimental observations and interpretations propose a deeper understanding by using physical principles. Indeed, the behavior at larger strains is ruled by the different architecture of the two hydrocolloids [152, 172]. As mentioned, ι-carrageenan can be viewed as a weak but uniformly negatively charged polyelectrolyte, whereas alginate consists of (stiff) charged and uncharged flexible blocks. Therefore, alginate chains can form topological restrictions, e.g., entanglements between the uncharged flexible blocks, as shown in Fig. 6.6, which give rise to additional contributions to the viscoelastic behavior and the non-linear shear behavior. Uniformly charged polyelectrolytes such as carrageenans repel each other intensely and cannot form entanglements under these experimental conditions [158] but are rather tightly adsorbed on the positively charged oleosome surfaces. The main differences are depicted in Fig. 6.6.

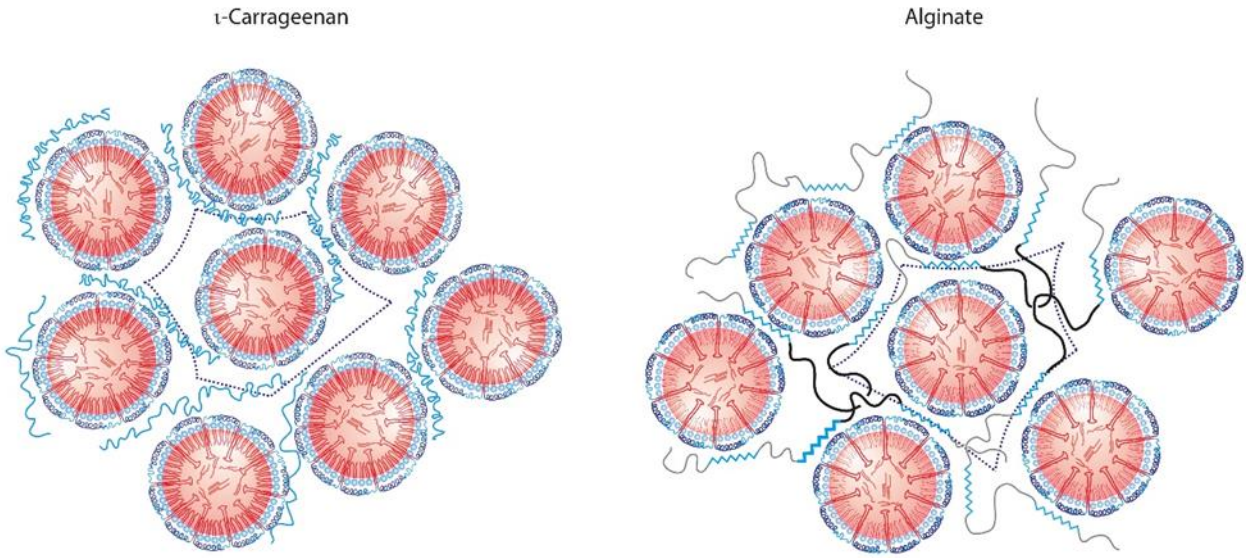

Fig. 6. 6 Schemes representing the different structures of oleosomes at high densities. The cages (polygons in dashed lines) limits motion, in addition alginate chains form entanglements (shown in black color).

From this model, it is reasonable to suggest that the chains can be easily exchanged between oleosomes under nonlinear shear at large deformations without changing much of the (free) energy of the system. On average, a similar number of monomers will be adsorbed on the oleosomes. For ι-carrageenan, it appears sufficient to describe the restriction of motion of the oleosomes by a simple cage, which opens with hardly noticeable concentration dependency.

For higher carrageenan concentrations (0.01g/g), a more pronounced second yield point becomes visible, which can be addressed to the higher repulsions of the chains which cannot adsorb at the time scales of the applied shear frequency (6.28 rad/s). When the cage opens by shear, a plastic regime starts to show up, where the stress remains roughly constant by increasing deformation (see Fig. 6.7).

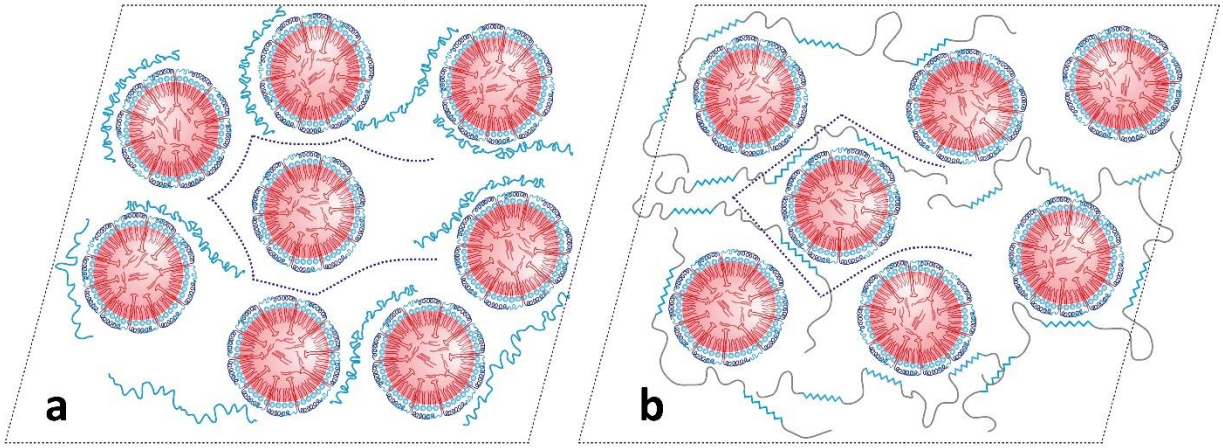

Fig. 6. 7 Schematic representing oleogels cage under shear. a) ι-Carrageenan-oleosomes b) Alginate-oleosomes.

The pronounced second yield point in 0.005 g/g alginate can be assigned to the entanglement network of the alginate (see Fig. 6.6). The cage, defined by the mean distance of the oleosomes in the corresponding matrix opens, but the charged blocks of the alginates are still strongly adsorbed at the surfaces of the oleosomes. Larger deformations increase the shear energy, which needs to be taken by the electrostatic energy by adsorption and the deformation of the entanglement network of the alginate. When the shear energy becomes larger than the energy gain by adsorption, chains become removed from the surface, the shear stress gets lower, but the entanglement network still resist stress. Only when the network disentangles,

the flow of the oleosomes enter a (short) plastic regime. These processes are expressed by the clear appearance of two concentration dependence yield points, γ_1 and γ_2. Only after complete disentanglement of the alginate network, both systems flow similarly at these high shear deformations, as can for example seen in Fig. 6.4 b and c.

6.5 Conclusion

This study investigated the mechanical properties of oleogels created by a polymer bridging mechanism using soybean oleosomes as templates and polysaccharides as structuring agents. Compact self-supporting gels can be prepared upon centrifuging bridging flocculated oleosome emulsions induced by sodium alginate and ι-carrageenan. Moduli in the LVR are determined by the bulk density of the bridged clusters and are not significantly different among the samples. However, the rheological behavior at larger deformations showed a more distinctive pattern among the different samples. Deformation will yield either in one single yielding point, γ_1 representing breakage of weak bridging bonds at lower strains, or in a two-step yielding point, γ_2, which indicates oleosome droplets are trapped into a cage that immobilizes the movement of oleosome droplets; thus, causes shear stress to increase. This second-yielding point becomes more prominent depending on whether the different sample conditions lead to compact and dense clusters and expresses the different molecular structure of the hydrocolloids. The compactness of the gel depends on the different molecular structure difference of alginate and ι-carrageenan and on the optimum bridging ratio determined by ratio of polysaccharide and olesome concentrations. In addition, to yield the most compact and dense microstructures at its optimum bridging ratio, 0.005 g/g, alginate yielded the most prominent γ_2 because the entanglement network given by its flexible chains resist deformation, causing the shear stress to increase significantly compared to the other samples. At its optimum bridging ratio, 0.01 g/g, ι-carrageenan showed a pronounced γ_2, albeit not as pronounced as alginate. This can be attributed to its decreased bridging efficiency compared to alginate, which results in less compacted microstructures. Clearly, these experiments provide different directions on how the molecular architecture of hydrocolloids (and proteins) provide ways to design macroscopic functional properties of oleogels according to their use.

Polymer bridging offers the potential for efficient use of resources by using relatively low amounts of polysaccharides and oleosome emulsion while resulting in a high yield of gels using low centrifugal forces. Furthermore, polymer bridging as a gelation mechanism can be expanded to a wide range of polymers, including those with different structural conformations, sizes, and even emulsion droplets with a wide range of diameters and interfacial compositions. However, a more thorough fundamental understanding is needed to fully benefit from this method, for instance, the dynamics of bridging flocculation, such as the impact of polymer chain relaxation as a function of stirring speed or the mechanisms that underlie the optimum bridging ratio between polymer and droplets.

7 Outlook and recommendations

This thesis showed that the polymer-bridging mechanism could be exploited to structure oleogels materials. A wide diversity of structures can be obtained using food-grade polysaccharides as a structuring agent for natural emulsions, so-called oleosomes. The rheological properties of the resulting oleogels can be fine-tuned by a careful interplay of different conditions: polysaccharide/oleosome ratio, oleosome content, or by using centrifugal forces to produce compact semi-soft gels. Also, by manipulating and controlling the conditions at which electrostatic interactions between polysaccharides and oleosomes occur, such as pH and ionic strength, the extent of bridging flocculation can be smartly controlled to design oleogels with specific rheological characteristics.

In the current work, only three polysaccharide sources and one oleosome source were tested for their suitability to form oleogels. It would be interesting to investigate the use of polysaccharides and oleosomes from different sources. Food-grade polysaccharides are widely commercially available. The wide range of available sources for oleosome in nuts and seeds gives many opportunities to expand the application of polymer bridging for oleogel production. Polysaccharides with different structural properties are abundant in nature. They can be explored for polymer bridging, including molecular weights, chain flexibility, polymer branching, or polymers with functional groups attached to their backbones. Similarly, oleosomes from different vegetable sources can provide different opportunities, such as a wide range of droplet sizes and different interfacial compositions.

Polymer bridging may represent an advantage over other oleogelation methods in terms of the efficient use of resources. 1) The concentration of polysaccharides needed for polymer bridging is relatively low (0.05 – 0.20 %) especially compared to the concentration of polysaccharides that are typically used in typical food applications such as thickening or encapsulation (> 1.5 %). 2) High yield of oleogel production. Chapters 4 and 5 show that oleogels of approximately 45% oleosome can be formed starting from 5% oleosome due to concentration by centrifugal forces. These centrifugal forces are very low (5000*g*) because the bridging flocculated emulsions start slowly creaming upward as a product of the density difference

between oil and water and due to the formation of large flocs. Centrifugation only accelerates the creaming process. 3) The simplicity of preparation. Our project's steps for inducing bridging flocculation involved only mixing and pH adjustment. In addition to using naturally available oleosomes, which serve as the perfect template for oleogel production instead of manufacturing oil-in-water emulsions, where highly energy-consuming processes are generally required for its production. Nevertheless, a more detailed study of the economic feasibility of using oleosomes vs. manufactured emulsions would be necessary to conclude the above since the process of oleosome extraction requires several centrifugation steps, which also require high-energy consumption.

Due to the flexibility to tune the texture of polymer bridging oleogels, their use as a plant fat alternative in real food applications has enormous potential. Polymer bridging oleogels resemble the visual appearance of typical dairy products such as cottage cheese, quark, and cream cheese. However, significant changes need to be made to prepare food-grade products. Distilled water would need to be replaced with regular tap water, and acetic acid instead of HCl could be used for pH adjustment. Glucono delta lactone (GdL), a food-grade acidifier used as a coagulant in products such as tofu, could also be applied in polymer bridging for a slow and progressive pH decrease. GdL could mimic dairy production processes, which use lactic acid bacteria to acidify the milk and produce curds for cheese production.

Compacted polymer bridging oleogels resemble feta cheese's compactness and slightly grainy texture and other crumbly cheeses such as goat cheese. They could be applied as their plant version. The final texture (soft, semi-hard, hard) and moisture content of the compacted gels could be fine-tuned with special molds and cloth bags that allow supernatant to drain more easily. Flavored and cured brines could be applied to resemble the typical dairy aroma. The final fat content could also be easily altered by using different initial oleosome contents.

Although the versatility of polymer bridging for designing oleogels with different rheological properties has great potential, a more thorough fundamental understanding of the bridging flocculation process is required for future potential applications. Of particular interest is understanding the dynamics of polymer

chain relaxation as a function of mixing speed or acidification rate, as this will also influence the final gel structure. Techniques that monitor the structural changes with time include scattering tools such as Diffusing Wave Spectroscopy (DWV) and Photon Density Wave Spectroscopy (PDW). Advanced microscopy techniques such as super-resolution microscopy (SRM) can also probe the structural evolution of aggregates as the effect of changes with time. This technique offers high spatial resolutions to examine the impact of pH on the formation and arrangements of the aggregates. SRM could also provide the opportunity to visualize the location of the polysaccharide chain within the gel network by fluorescent labeling.

In addition, the mechanisms that underlie the optimum bridging ratio between polysaccharide and droplet will also lead to interesting insights in this area, which would enable to design more interesting gel structures. This may require though a more fundamental approach such as a simulation framework, which can target specific properties in polymers and its interaction with particles.

Bibliography

1. Lunn, J. and H. Theobald, *The health effects of dietary unsaturated fatty acids.* Nutrition Bulletin, 2006. **31**(3): p. 178-224.
2. Hu, F.B. and W.C. Willett, *Optimal diets for prevention of coronary heart disease.* Jama, 2002. **288**(20): p. 2569-2578.
3. Patel, A.R. and K. Dewettinck, *Edible oil structuring: an overview and recent updates.* Food & function, 2016. **7**(1): p. 20-29.
4. Marangoni, A.G., *Organogels: An alternative edible oil-structuring method.* Journal of the American Oil Chemists' Society, 2012. **89**(5): p. 749-780.
5. Schaink, H., et al., *Crystal network for edible oil organogels: possibilities and limitations of the fatty acid and fatty alcohol systems.* Food Research International, 2007. **40**(9): p. 1185-1193.
6. Palla, C.A., M. Dominguez, and M.E. Carrín, *An overview of structure engineering to tailor the functionality of monoglyceride oleogels.* Comprehensive Reviews in Food Science and Food Safety, 2022.
7. Brykczynski, H., T. Wettlaufer, and E. Flöter, *Revisiting pure component wax esters as basis of wax-based oleogels.* Journal of the American Oil Chemists' Society, 2021.
8. Bot, A. and W.G. Agterof, *Structuring of edible oils by mixtures of γ-oryzanol with β-sitosterol or related phytosterols.* Journal of the American Oil Chemists' Society, 2006. **83**(6): p. 513-521.
9. Bodennec, M., Q. Guo, and D. Rousseau, *Molecular and microstructural characterization of lecithin-based oleogels made with vegetable oil.* RSC advances, 2016. **6**(53): p. 47373-47381.
10. Truong, T., S. Prakash, and B. Bhandari, *Effects of crystallisation of native phytosterols and monoacylglycerols on foaming properties of whipped oleogels.* Food chemistry, 2019. **285**: p. 86-93.
11. Okuro, P.K., et al., *Synergistic interactions between lecithin and fruit wax in oleogel formation.* Food & function, 2018. **9**(3): p. 1755-1767.
12. Gandolfo, F.G., A. Bot, and E. Flöter, *Structuring of edible oils by long-chain FA, fatty alcohols, and their mixtures.* Journal of the American Oil Chemists' Society, 2004. **81**(1): p. 1-6.
13. Nikiforidis, C.V. and E. Scholten, *High internal phase emulsion gels (HIPE-gels) created through assembly of natural oil bodies.* Food Hydrocolloids, 2015. **43**: p. 283-289.
14. Kirimlidou, M., et al., *Composite gels structured by a gelatin protein matrix filled with oil bodies.* Food Structure, 2017. **14**: p. 46-51.
15. Yang, N., et al., *Structure and tribology of κ-carrageenan gels filled with natural oil bodies.* Food Hydrocolloids, 2020. **107**: p. 105945.
16. Farooq, S., et al., *Preparation, characterization and digestive mechanism of plant-derived oil bodies-based oleogels structured by chitosan and vanillin.* Food Hydrocolloids, 2023. **136**: p. 108247.
17. Mert, B. and T.A. Vilgis, *Hydrocolloid coated oleosomes for development of oleogels.* Food Hydrocolloids, 2021. **119**: p. 106832.
18. Salunkhe, D.K., et al., *World oilseeds*. 1992: Springer Science & Business Media.
19. Williams, M.A., *Recovery of oils and fats from oilseeds and fatty materials.* Bailey's industrial oil and fat products, 2005.
20. Dunn, P.J., A.S. Wells, and M.T. Williams, *Future trends for green chemistry in the pharmaceutical industry.* Green Chemistry in the Pharmaceutical Industry, 2010: p. 333-355.
21. Bergfeld, R., et al., *Formation of oleosomes (storage lipid bodies) during embryogenesis and their breakdown during seedling development in cotyledons of Sinapis alba L.* Planta, 1978. **143**(3): p. 297-307.
22. Fisk, I.D., et al., *Oxidative stability of sunflower oil bodies.* European journal of lipid science and technology, 2008. **110**(10): p. 962-968.

23. Iwanaga, D., et al., *Extraction and characterization of oil bodies from soy beans: a natural source of pre-emulsified soybean oil.* Journal of agricultural and food chemistry, 2007. **55**(21): p. 8711-8716.
24. Platt-Aloia, K. and W. Thomson, *Ultrastructure of the mesocarp of mature avocado fruit and changes associated with ripening.* Annals of Botany, 1981. **48**(4): p. 451-466.
25. Mohankumar, C., C. Arumughan, and R. Kaleysa Raj, *Histological localization of oil palm fruit lipase.* Journal of the American Oil Chemists' Society, 1990. **67**(10): p. 665-669.
26. Tzen, J.T., et al., *Lipids, proteins, and structure of seed oil bodies from diverse species.* Plant physiology, 1993. **101**(1): p. 267-276.
27. Huang, A.H., *Oil bodies and oleosins in seeds.* Annual Review of Plant Physiology and Plant Molecular Biology, 1992. **43**(1): p. 177-200.
28. Chen, Y., et al., *Macronutrients and micronutrients of soybean oil bodies extracted at different pH.* Journal of Food Science, 2014. **79**(7): p. C1285-C1291.
29. Nikiforidis, C.V., S. Donsouzi, and V. Kiosseoglou, *The interplay between diverse oil body extracts and exogenous biopolymers or surfactants.* Food Research International, 2016. **83**: p. 14-24.
30. Zielbauer, B.I., et al., *Soybean oleosomes studied by small angle neutron scattering (SANS).* Journal of colloid and interface science, 2018. **529**: p. 197-204.
31. Nikiforidis, C.V., *Structure and functions of oleosomes (oil bodies).* Advances in Colloid and Interface Science, 2019. **274**: p. 102039.
32. Waschatko, G., *Oleosome. Natürliche Emulgatoren und deren Verhalten an lebensmittelrelevanten Grenzflächen*, in *Chemie, Pharmazie und Geowissenschaften*. 2013, Johannes Gutenberg Universität Mainz. p. 124.
33. Purkrtova, Z., et al., *Structure and function of seed lipid body-associated proteins.* Comptes rendus biologies, 2008. **331**(10): p. 746-754.
34. LACEY, D.J., et al., *Secondary structure of oleosins in oil bodies isolated from seeds of safflower (Carthamus tinctorius L.) and sunflower (Helianthus annuus L.).* Biochemical Journal, 1998. **334**(2): p. 469-477.
35. Li, M., et al., *Purification and structural characterization of the central hydrophobic domain of oleosin.* Journal of Biological Chemistry, 2002. **277**(40): p. 37888-37895.
36. Kim, H.U., et al., *A novel group of Oleosins is present inside the pollen ofArabidopsis.* Journal of Biological Chemistry, 2002. **277**(25): p. 22677-22684.
37. Frandsen, G.I., J. Mundy, and J.T. Tzen, *Oil bodies and their associated proteins, oleosin and caleosin.* Physiologia plantarum, 2001. **112**(3): p. 301-307.
38. Chen, J.C., C.C. Tsai, and J.T. Tzen, *Cloning and secondary structure analysis of caleosin, a unique calcium-binding protein in oil bodies of plant seeds.* Plant and Cell Physiology, 1999. **40**(10): p. 1079-1086.
39. Chen, M.C., et al., *Constitution of stable artificial oil bodies with triacylglycerol, phospholipid, and caleosin.* Journal of Agricultural and Food Chemistry, 2004. **52**(12): p. 3982-3987.
40. Lin, L.-J., et al., *Steroleosin, a sterol-binding dehydrogenase in seed oil bodies.* Plant physiology, 2002. **128**(4): p. 1200-1211.
41. Wang, Q.L., et al., *Oil Bodies Extracted from High-Fat and Low-Fat Soybeans: Stability and Composition During Storage.* Journal of food science, 2017. **82**(6): p. 1319-1325.
42. Chen, Y. and T. Ono, *Simple extraction method of non-allergenic intact soybean oil bodies that are thermally stable in an aqueous medium.* Journal of agricultural and food chemistry, 2010. **58**(12): p. 7402-7407.
43. Kapchie, V.N., et al., *Evaluation of enzyme efficiency for soy oleosome isolation and ultrastructural aspects.* Food research international, 2010. **43**(1): p. 241-247.
44. Towa, L.T., et al., *Enzyme-assisted aqueous extraction of oil from isolated oleosomes of soybean flour.* Journal of the American Oil Chemists' Society, 2010. **87**(3): p. 347-354.

45. Zhao, Q., Y. Xu, and Y. Liu, *Soybean oil bodies: A review on composition, properties, food applications, and future research aspects.* Food Hydrocolloids, 2022. **124**: p. 107296.
46. Waschatko, G., A. Junghans, and T.A. Vilgis, *Soy milk oleosome behaviour at the air–water interface.* Faraday discussions, 2012. **158**: p. 157-169.
47. Zhao, L., et al., *Physicochemical and rheological properties and oxidative stability of oil bodies recovered from soybean aqueous extract at different pHs.* Food Hydrocolloids, 2016. **61**: p. 685-694.
48. Wu, N., et al., *Analysis of stability and rheology of soybean oil body emulsions.* Transactions of the Chinese Society of Agricultural Engineering, 2012. **28**(1): p. 369-374.
49. Stephen, A.M. and G.O. Phillips, *Food polysaccharides and their applications*. 2006: CRC press.
50. Whistler, R. and J. BeMiller, *Industrial gums*. Polysaccharides and their Derivatives, ed. 3rd. 1993, London: Academic Press Limited.
51. Imeson, A., *Food stabilisers, thickeners and gelling agents*. 2011: John Wiley & Sons.
52. Draget, K.I., et al., *Effects of molecular weight and elastic segment flexibility on syneresis in Ca-alginate gels.* Food Hydrocolloids, 2001. **15**(4-6): p. 485-490.
53. Vilgis, T.A., *Gels: Model systems for soft matter food physics.* Current Opinion in Food Science, 2015. **3**: p. 71-84.
54. Vreeman, H., T. Snoeren, and T. Payens, *Physicochemical investigation of k-carrageenan in the random state.* Biopolymers: Original Research on Biomolecules, 1980. **19**(7): p. 1357-1374.
55. Ogawa, S., E.A. Decker, and D.J. McClements, *Influence of environmental conditions on the stability of oil in water emulsions containing droplets stabilized by lecithin− chitosan membranes.* Journal of Agricultural and Food Chemistry, 2003. **51**(18): p. 5522-5527.
56. Souza, S.F., et al., *Effect of depletion forces on the morphological structure of carboxymethyl cellulose and micro/nano cellulose fiber suspensions.* Journal of colloid and interface science, 2019. **538**: p. 228-236.
57. Tuinier, R. and C. De Kruif, *Phase separation, creaming, and network formation of oil-in-water emulsions induced by an exocellular polysaccharide.* Journal of Colloid and Interface Science, 1999. **218**(1): p. 201-210.
58. McClements, D.J., *Theoretical analysis of factors affecting the formation and stability of multilayered colloidal dispersions.* Langmuir, 2005. **21**(21): p. 9777-9785.
59. Yeung, A.K. and R. Pelton, *Micromechanics: a new approach to studying the strength and breakup of flocs.* Journal of Colloid and Interface Science, 1996. **184**(2): p. 579-585.
60. La Mer, V.K., *Filtration of colloidal dispersions flocculated by anionic and cationic polyelectrolytes.* Discussions of the Faraday Society, 1966. **42**: p. 248-254.
61. Gregory, J. and S. Barany, *Adsorption and flocculation by polymers and polymer mixtures.* Advances in colloid and interface science, 2011. **169**(1): p. 1-12.
62. Barany, S., et al., *Effect of polyelectrolyte mixtures on the electrokinetic potential and kinetics of flocculation of clay mineral particles.* Colloids and Surfaces A: Physicochemical and Engineering Aspects, 2011. **383**(1-3): p. 48-55.
63. Stoll, S. and J. Buffle, *Computer simulation of bridging flocculation processes: the role of colloid to polymer concentration ratio on aggregation kinetics.* Journal of Colloid and Interface Science, 1996. **180**(2): p. 548-563.
64. Lapointe, M. and B. Barbeau, *Understanding the roles and characterizing the intrinsic properties of synthetic vs. natural polymers to improve clarification through interparticle Bridging: A review.* Separation and Purification Technology, 2020. **231**: p. 115893.
65. Yu, X. and P. Somasundaran, *Role of polymer conformation in interparticle-bridging dominated flocculation.* Journal of Colloid and Interface Science, 1996. **177**(2): p. 283-287.
66. Gregory, J., *Polymer adsorption and flocculation in sheared suspensions.* Colloids and Surfaces, 1988. **31**: p. 231-253.
67. Napper, D.H., *Polymeric stabilization of colloidal dispersions*. Vol. 3. 1983: Academic Press.

68. Adachi, Y., *Dynamic aspects of coagulation and flocculation.* Advances in colloid and interface science, 1995. **56**: p. 1-31.
69. Dickinson, E. and S.R. Euston, *Computer simulation of bridging flocculation.* Journal of the Chemical Society, Faraday Transactions, 1991. **87**(14): p. 2193-2199.
70. Vajihinejad, V., et al., *Water soluble polymer flocculants: synthesis, characterization, and performance assessment.* Macromolecular Materials and Engineering, 2019. **304**(2): p. 1800526.
71. Chen, W., et al., *Fabricating a flocculant with controllable cationic microblock structure: characterization and sludge conditioning behavior evaluation.* Industrial & Engineering Chemistry Research, 2016. **55**(10): p. 2892-2902.
72. Koenderink, G.H., et al., *Morphology and Kinetics of Phase Separating Transparent Xanthan− Colloid Mixtures.* Biomacromolecules, 2003. **4**(1): p. 129-136.
73. Asselman, T. and G. Garnier, *Mechanism of polyelectrolyte transfer during heteroflocculation.* Langmuir, 2000. **16**(11): p. 4871-4876.
74. Fellows, C.M. and W.O. Doherty. *Insights into bridging flocculation*. in *Macromolecular symposia*. 2005. Wiley Online Library.
75. Adachi, Y., M.C. Stuart, and R. Fokkink, *Dynamic aspects of bridging flocculation studied using standardized mixing.* Journal of colloid and interface science, 1994. **167**(2): p. 346-351.
76. Blijdenstein, T., et al., *Serum separation and structure of depletion-and bridging-flocculated emulsions: a comparison.* Colloids and Surfaces A: Physicochemical and Engineering Aspects, 2004. **245**(1-3): p. 41-48.
77. Waschatko, G., et al., *Soybean oleosomes behavior at the air–water interface.* The Journal of Physical Chemistry B, 2012. **116**(35): p. 10832-10841.
78. Willenbacher, N. and K. Georgieva, *Rheology of disperse systems*. 2013, Wiley-VCH Verlag GmbH & Co. KGaA Weinheim, Germany.
79. Kavanagh, G.M., A.H. Clark, and S.B. Ross-Murphy, *Heat-induced gelation of globular proteins: 4. Gelation kinetics of low pH β-lactoglobulin gels.* Langmuir, 2000. **16**(24): p. 9584-9594.
80. van der Linden, E. and L.M. Sagis, *Isotropic force percolation in protein gels.* Langmuir, 2001. **17**(19): p. 5821-5824.
81. Mellema, M., J. Van Opheusden, and T. Van Vliet, *Categorization of rheological scaling models for particle gels applied to casein gels.* Journal of Rheology, 2002. **46**(1): p. 11-29.
82. Otsubo, Y., *Elastic percolation in suspensions flocculated by polymer bridging.* Langmuir, 1990. **6**(1): p. 114-118.
83. Pandey, R. and D. Stauffer, *Confirmation of dynamical scaling at the percolation threshold.* Physical review letters, 1983. **51**(7): p. 527.
84. Mitescu, C. and M. Musolf, *Critical exponent for 3-D percolation conductivity, revisited.* Journal de Physique Lettres, 1983. **44**(16): p. 679-683.
85. Feng, S. and P.N. Sen, *Percolation on elastic networks: new exponent and threshold.* Physical review letters, 1984. **52**(3): p. 216.
86. Kantor, Y. and I. Webman, *Elastic properties of random percolating systems.* Physical Review Letters, 1984. **52**(21): p. 1891.
87. Veerman, C., et al., *Effect of electrostatic interactions on the percolation concentration of fibrillar β-lactoglobulin gels.* Biomacromolecules, 2002. **3**(4): p. 869-873.
88. Diedericks, C.F., et al., *Extraction, gelation and microstructure of Bambara groundnut vicilins.* Food Hydrocolloids, 2019. **97**: p. 105226.
89. Blijdenstein, T.B., et al., *Scaling behavior of delayed demixing, rheology, and microstructure of emulsions flocculated by depletion and bridging.* Langmuir, 2004. **20**(26): p. 11321-11328.
90. Shannon, R.R.F., Brian J. *History of optical microscopes*. Available from: https://www.britannica.com/technology/microscope/Confocal-microscopes.
91. Holik, A., *Optical microscopy.* Encyclopedia of Materials: Science and Technology, 2001: p. 6458-6463.

92. Dickinson, E., *Strategies to control and inhibit the flocculation of protein-stabilized oil-in-water emulsions.* Food hydrocolloids, 2019. **96**: p. 209-223.
93. Fellers, T.J.D., Michael W. *Introduction to Confocal Microscopy*.
94. Ferrando, M. and W. Spiess, *Confocal scanning laser microscopy. A powerful tool in food science Revision: Microscopía láser confocal de barrido. Una potente herramienta en la ciencia de los alimentos.* Food Science and Technology International, 2000. **6**(4): p. 267-284.
95. Greenspan, P., E.P. Mayer, and S.D. Fowler, *Nile red: a selective fluorescent stain for intracellular lipid droplets.* The Journal of cell biology, 1985. **100**(3): p. 965-973.
96. Dickinson, E., *Hydrocolloids at interfaces and the influence on the properties of dispersed systems.* Food hydrocolloids, 2003. **17**(1): p. 25-39.
97. Van Dalen, G., *Determination of the water droplet size distribution of fat spreads using confocal scanning laser microscopy.* Journal of Microscopy, 2002. **208**(2): p. 116-133.
98. Brakenhoff, G., et al., *3-dimensional imaging of biological structures by high resolution confocal scanning laser microscopy.* Scanning Microscopy, 1988. **2**(1): p. 33-40.
99. Brujić, J., et al., *3D bulk measurements of the force distribution in a compressed emulsion system.* Faraday discussions, 2003. **123**: p. 207-220.
100. Zhang, X., et al., *Simultaneous scanning electron microscope imaging of topographical and chemical contrast using in-lens, in-column, and everhart–thornley detector systems.* Microscopy and Microanalysis, 2016. **22**(3): p. 565-575.
101. Griffin, B.J., *A comparison of conventional Everhart-Thornley style and in-lens secondary electron detectors—a further variable in scanning electron microscopy.* Scanning, 2011. **33**(3): p. 162-173.
102. Coulter, B., *LS 13 320 Laser Diffraction Particle Size Analyzer*

Instrument Manual. 2009.
103. Pate, K. and P. Safier, *12-Chemical metrology methods for CMP quality. Advances in Chemical Mechanical Planarization (CMP).* 2016, von S. Babu. Woodhead Publishing.
104. Delgado, A., F. González-Caballero, and J. Salcedo, *On the zeta potential of spherical polystyrene particles from electrophoresis theories.* Acta polymerica, 1986. **37**(6): p. 361-364.
105. Dalgleish, D.G., *Adsorption of protein and the stability of emulsions.* Trends in Food Science & Technology, 1997. **8**(1): p. 1-6.
106. Jiang, X., et al., *Biopolymer-based flocculants: a review of recent technologies.* Environmental Science and Pollution Research, 2021. **28**(34): p. 46934-46963.
107. Zhai, H., P. Gunness, and M.J. Gidley, *Depletion and bridging flocculation of oil droplets in the presence of β-glucan, arabinoxylan and pectin polymers: Effects on lipolysis.* Carbohydrate Polymers, 2021. **255**: p. 117491.
108. Dickinson, E. and K. Pawlowsky, *Effect of ι-carrageenan on flocculation, creaming, and rheology of a protein-stabilized emulsion.* Journal of agricultural and food chemistry, 1997. **45**(10): p. 3799-3806.
109. Zhou, Y. and G.V. Franks, *Flocculation mechanism induced by cationic polymers investigated by light scattering.* Langmuir, 2006. **22**(16): p. 6775-6786.
110. Hu, C., et al., *Ions-induced gelation of alginate: Mechanisms and applications.* International Journal of Biological Macromolecules, 2021. **177**: p. 578-588.
111. Su, C., et al., *Effect of sodium alginate on the stability of natural soybean oil body emulsions.* RSC advances, 2018. **8**(9): p. 4731-4741.
112. Payne, L., J. Rodrigues, and B. Straughan, *Effect of anisotropic permeability on Darcy's law.* Mathematical methods in the applied sciences, 2001. **24**(6): p. 427-438.
113. Eremin, Y., *Scattering: Scattering Theory*, in *Encyclopedia of Modern Optics, Five-Volume Set*. 2004. p. 326-330.

114. Qi, B., et al., *Deciphering the characteristics of soybean oleosome-associated protein in maintaining the stability of oleosomes as affected by pH.* Food Research International, 2017. **100**: p. 551-557.
115. Bastos, L.P.H., C.W.P. de Carvalho, and E.E. Garcia-Rojas, *Formation and characterization of the complex coacervates obtained between lactoferrin and sodium alginate.* International journal of biological macromolecules, 2018. **120**: p. 332-338.
116. Dickinson, E. and K. Pawlowsky, *Influence of κ-carrageenan on the properties of a protein-stabilized emulsion.* Food Hydrocolloids, 1998. **12**(4): p. 417-423.
117. Bertsch, P., et al., *Transient measurement and structure analysis of protein–polysaccharide multilayers at fluid interfaces.* Soft Matter, 2019. **15**(31): p. 6362-6368.
118. De Gennes, P.-G., *Scaling concepts in polymer physics*. 1979: Cornell university press.
119. Moschakis, T., B.S. Murray, and E. Dickinson, *Particle tracking using confocal microscopy to probe the microrheology in a phase-separating emulsion containing nonadsorbing polysaccharide.* Langmuir, 2006. **22**(10): p. 4710-4719.
120. Boonlao, N., et al., *Influence of whey protein-xanthan gum stabilized emulsion on stability and in vitro digestibility of encapsulated astaxanthin.* Journal of Food Engineering, 2020. **272**: p. 109859.
121. Sato, T., T. Kakihara, and A. Teramoto, *Isotropic-liquid crystal phase equilibrium in semiflexible polymer solutions: xanthan, a rigid polyelectrolyte.* Polymer, 1990. **31**(5): p. 824-828.
122. Wang, A. and W. Wang, *Gum-g-copolymers: synthesis, properties, and applications*, in *Polysaccharide based graft copolymers*. 2013, Springer. p. 149-203.
123. Moorhouse, R., M. Walkinshaw, and S. Arnott, *Xanthan Gumâ€" Molecular Conformation and Interactions*. 1977, ACS Publications.
124. Cheng, H. and M. Olvera de la Cruz, *Adsorption of rod-like polyelectrolytes onto weakly charged surfaces.* The Journal of chemical physics, 2003. **119**(23): p. 12635-12644.
125. Nikiforidis, C.V. and V. Kiosseoglou, *Physicochemical stability of maize germ oil body emulsions as influenced by oil body surface− xanthan gum interactions.* Journal of Agricultural and Food Chemistry, 2010. **58**(1): p. 527-532.
126. Ting, J.T., et al., *Oleosin genes in maize kernels having diverse oil contents are constitutively expressed independent of oil contents.* Planta, 1996. **199**(1): p. 158-165.
127. Martinsen, A., et al., *Comparison of different methods for determination of molecular weight and molecular weight distribution of alginates.* Carbohydrate polymers, 1991. **15**(2): p. 171-193.
128. Kong, H.J., et al., *Controlling rigidity and degradation of alginate hydrogels via molecular weight distribution.* Biomacromolecules, 2004. **5**(5): p. 1720-1727.
129. Ye, A., Y. Hemar, and H. Singh, *Enhancement of coalescence by xanthan addition to oil-in-water emulsions formed with extensively hydrolysed whey proteins.* Food Hydrocolloids, 2004. **18**(5): p. 737-746.
130. Hege, J., T. Palberg, and T.A. Vilgis, *Interactions of different hydrocolloids with milk proteins.* Journal of Physics: Materials, 2020. **3**(4): p. 044003.
131. Bressel, K., et al., *Depletion-induced flocculation of concentrated emulsions probed by photon density wave spectroscopy.* Langmuir, 2020. **36**(13): p. 3504-3513.
132. Bhat, S., R. Tuinier, and P. Schurtenberger, *Spinodal decomposition in a food colloid–biopolymer mixture: evidence for a linear regime.* Journal of Physics: Condensed Matter, 2006. **18**(26): p. L339.
133. Assenza, S. and R. Mezzenga, *Soft condensed matter physics of foods and macronutrients.* Nature Reviews Physics, 2019. **1**(9): p. 551-566.
134. Koczo, K., et al., *Flocculation of food dispersions by gums: isotropic/anisotropic dispersion separation by xanthan gum.* Food hydrocolloids, 1998. **12**(1): p. 43-53.
135. Rodd, A., D. Dunstan, and D. Boger, *Characterisation of xanthan gum solutions using dynamic light scattering and rheology.* Carbohydrate polymers, 2000. **42**(2): p. 159-174.

136. Dickinson, E. and K. Pawlowsky, *Effect of high-pressure treatment of protein on the rheology of flocculated emulsions containing protein and polysaccharide.* Journal of agricultural and food chemistry, 1996. **44**(10): p. 2992-3000.
137. Nordqvist, D. and T.A. Vilgis, *Rheological study of the gelation process of agarose-based solutions.* Food Biophysics, 2011. **6**(4): p. 450-460.
138. Taflin, D.C., T.L. Ward, and E.J. Davis, *Electrified droplet fission and the Rayleigh limit.* Langmuir, 1989. **5**(2): p. 376-384.
139. Deserno, M., *Rayleigh instability of charged droplets in the presence of counterions.* The European Physical Journal E, 2001. **6**(2): p. 163-168.
140. de Wijk, R.A., A.M. Janssen, and J.F. Prinz, *Oral movements and the perception of semi-solid foods.* Physiology & Behavior, 2011. **104**(3): p. 423-428.
141. Upadhyay, R., T. Aktar, and J. Chen, *Perception of creaminess in foods.* Journal of texture studies, 2020. **51**(3): p. 375-388.
142. Vilgis, T.A., *Texture, taste and aroma: multi-scale materials and the gastrophysics of food.* Flavour, 2013. **2**(1): p. 1-5.
143. Patel, A., et al., *Salt and pH-induced attractive interactions on the rheology of food protein-stabilized nanoemulsions.* ACS omega, 2019. **4**(7): p. 11791-11800.
144. Dickinson, E. and E.L. Parkinson, *Heat-induced aggregation of milk protein-stabilized emulsions: sensitivity to processing and composition.* International Dairy Journal, 2004. **14**(7): p. 635-645.
145. Fuhrmann, P.L., et al., *Clustering of oil droplets in o/w emulsions: Controlling cluster size and interaction strength.* Food Research International, 2019. **122**: p. 537-547.
146. Lee, H.A., S.J. Choi, and T.W. Moon, *Characteristics of sodium caseinate-and soy protein isolate-stabilized emulsion-gels formed by microbial transglutaminase.* Journal of Food Science, 2006. **71**(6): p. C352-C357.
147. Wang, X., et al., *Modulation of stability, rheological properties, and microstructure of heteroaggregated emulsion: Influence of oil content.* LWT, 2019. **109**: p. 457-466.
148. Mao, Y. and D.J. McClements, *Modulation of emulsion rheology through electrostatic heteroaggregation of oppositely charged lipid droplets: Influence of particle size and emulsifier content.* Journal of colloid and interface science, 2012. **380**(1): p. 60-66.
149. Fuhrmann, P.L., et al., *Influence of clustering of protein-stabilised oil droplets with proanthocyanidins on mechanical, tribological and sensory properties of o/w emulsions and emulsion-filled gels.* Food Hydrocolloids, 2020. **105**: p. 105856.
150. Zhao, C., et al., *Macrogel induced by microgel: Bridging and depletion mechanisms.* Soft Matter, 2012. **8**(26): p. 7036-7043.
151. Zambrano, J.C. and T.A. Vilgis, *Tunable oleosome-based oleogels: Influence of polysaccharide type for polymer bridging-based structuring.* Food Hydrocolloids, 2022. **137**: p. 108399.
152. Zambrano, J.C. and T.A. Vilgis, *Tunable oleosome-based oleogels: Influence of polysaccharide type for polymer bridging-based structuring.* Food Hydrocolloids, 2022. **In submission process**.
153. Wu, N.-n., et al., *Stabilization of soybean oil body emulsions using κ, ι, λ-carrageenan at different pH values.* Food Research International, 2011. **44**(4): p. 1059-1068.
154. Xi, Z., et al., *Rheological, structural, and microstructural properties of ethanol induced cold-set whey protein emulsion gels: Effect of oil content.* Food chemistry, 2019. **291**: p. 22-29.
155. Roullet, M., P.S. Clegg, and W.J. Frith, *Rheology of protein-stabilised emulsion gels envisioned as composite networks. 2-Framework for the study of emulsion gels.* Journal of Colloid and Interface Science, 2021. **594**: p. 92-100.
156. Veerman, C., et al., *Irreversible self-assembly of ovalbumin into fibrils and the resulting network rheology.* International Journal of Biological Macromolecules, 2003. **33**(1-3): p. 121-127.
157. Chang, C.-W. and Y.-C. Liao, *Accelerated sedimentation velocity assessment for nanowires stabilized in a non-Newtonian fluid.* Langmuir, 2016. **32**(51): p. 13620-13626.

158. Dobrynin, A.V. and M. Jacobs, *When do polyelectrolytes entangle?* Macromolecules, 2021. **54**(4): p. 1859-1869.
159. Matsumoto, A., et al., *Microrheological Approach for Probing the Entanglement Properties of Polyelectrolyte Solutions.* ACS Macro Letters, 2021. **11**(1): p. 84-90.
160. Nie, H., et al., *Effects of chain conformation and entanglement on the electrospinning of pure alginate.* Biomacromolecules, 2008. **9**(5): p. 1362-1365.
161. Ahn, Y., H. Kim, and S.-Y. Kwak, *Self-reinforcement of alginate hydrogel via conformational control.* European Polymer Journal, 2019. **116**: p. 480-487.
162. Doi, M., S.F. Edwards, and S.F. Edwards, *The theory of polymer dynamics*. Vol. 73. 1988: oxford university press.
163. Lips, A., I. Campbell, and E. Pelan, *Aggregation mechanisms in food colloids and the role of biopolymers*, in *Food polymers, gels and colloids*. 1991, Elsevier. p. 1-21.
164. Dobrynin, A.V., R.H. Colby, and M. Rubinstein, *Scaling theory of polyelectrolyte solutions.* Macromolecules, 1995. **28**(6): p. 1859-1871.
165. Segre, P., et al., *Glasslike kinetic arrest at the colloidal-gelation transition.* Physical Review Letters, 2001. **86**(26): p. 6042.
166. Kanai, H., et al., *Fragile networks and rheology of concentrated suspensions.* Rheologica acta, 1992. **31**(4): p. 333-344.
167. Trappe, V. and D. Weitz, *Scaling of the viscoelasticity of weakly attractive particles.* Physical review letters, 2000. **85**(2): p. 449.
168. Sahimi, M. and S. Arbabi, *Mechanics of disordered solids. II. Percolation on elastic networks with bond-bending forces.* Physical Review B, 1993. **47**(2): p. 703.
169. Grant, M. and W. Russel, *Volume-fraction dependence of elastic moduli and transition temperatures for colloidal silica gels.* Physical Review E, 1993. **47**(4): p. 2606.
170. Edwards, S. and T. Vilgis, *The effect of entanglements in rubber elasticity.* Polymer, 1986. **27**(4): p. 483-492.
171. Zhao, C., G. Yuan, and C.C. Han, *Bridging and caging in mixed suspensions of microsphere and adsorptive microgel.* Soft Matter, 2014. **10**(44): p. 8905-8912.
172. Zambrano, J.C. and T.A. Vilgis, *Tunable oleosome-based oleogels: effect of polysaccharide architecture on polymer-bridging based structuring.* Physics of Fluids, 2022. **In press**.
173. Piculell, L., *Gelling carrageenans*. Food polysaccharides and their applications. Vol. 239. 2006.
174. Sciortino, F. and P. Tartaglia, *Glassy colloidal systems.* Advances in Physics, 2005. **54**(6-7): p. 471-524.
175. Pham, K., et al., *Yielding behavior of repulsion-and attraction-dominated colloidal glasses.* Journal of Rheology, 2008. **52**(2): p. 649-676.
176. Koumakis, N. and G. Petekidis, *Two step yielding in attractive colloids: transition from gels to attractive glasses.* Soft Matter, 2011. **7**(6): p. 2456-2470.